GEOLOGICAL SURVEY OF CANADA

OPEN FILE 2973

Interpretation of data and presentation of results from the Ice Island 1986 and 1990 seismic refraction experiments

M. Argyle, D.A. Forsyth

1994

Natural Resources Canada Ressources naturelles Canada

Canada

Geological Survey of Canada
Open File No. 2973

Interpretation of Data and Presentation of Results from the Ice Island 1986 and 1990 Seismic Refraction Experiments

by:

M. Argyle
Argyle Geophysics, Ottawa, Ont., Canada, K1N 5B9

and

D.A. Forsyth
Geological Survey of Canada, Ottawa, Ont., Canada, K1A 0Y3

CONTENTS

EXECUTIVE SUMMARY

This report presents an integrated interpretation of the crustal structure of the northeast Sverdrup Basin and adjacent polar margin from new wide-angle seismic velocity models, newly interpreted industry reflection data, borehole data and newly compiled aeromagnetic data. The seismic information places new constraints on the crustal structure of a little known area of the polar margin and by default, on the rifting associated with the formation of the adjacent Canada Basin. The seismic data also provide the first structural calibration for the new magnetic data. The seismic analysis has directly provided:

1) A new regional velocity structure of the northeast Sverdrup Basin.
2) New crustal structure both along and across the transition from Sverdrup Basin to the adjoining continental shelf.
3) New crustal evidence beneath the continental shelf offshore of Axel Heiberg Island to document the continuity and changes in principal regional structures from those mapped onshore, and clues to the nature of these structures at depth.
4) New parameters for resource assessments of Canada's polar margin.
5) New parameters to help define Canada's Arctic margin under the internationally ratified Law of the Sea agreement.

Newly compiled aeromagnetic data for the study area provide new supporting evidence for:

1) The offshore continuation and termination of the Princess Margaret Arch.
2) A major sedimentary basin north of Meighen Island.
3) A major change in crustal structure beneath the outer continental shelf that may be related to the proximity of the Alpha Ridge.
4) The northeast continuation of a suggested major mid-Cretaceous "incipient rift" that traverses the Sverdrup Rim and extends beneath the continental shelf north of Ellef Ringnes Island.
5) New seismically documented diapiric structures in Peary Channel.
6) A complex northerly merging of structural trends offshore from the area of Sverdrup Channel. Structural trends inferred from clear linear anomaly patterns in both the magnetic and gravity data are sub-parallel to major thrusts mapped on Axel Heiberg Island.

In the area between Ellef Ringnes and western Ellesmere Island and the adjacent offshore much conjecture surrounds the formation of multiple basins during Eurekan tectogenesis. The seismic results show clear evidence of a complex network of local basins separated by basement highs both within the Sverdrup Basin in the study area and beneath the adjacent continental shelf. To better quantify these linkages, further integration of the seismic results with recently acquired magnetic data and existing gravity data is required.

Wide-angle seismic data recorded in 1986 northwest of Axel Heiberg Island, and in 1990 between Meighen Island and Ellef Ringnes Islands, together with reinterpreted industry borehole and reflection data provide new constraints on the crustal structure of Canada's northeast polar margin, including the northeast Sverdrup Basin and adjacent continental shelf. Interpretation of the 1986 wide-angle data suggests that the regional crustal structure beneath the continental shelf consists of a complex series of basement arches separating sedimentary basins containing at least 12 km of strata with velocities less than 5.2 km/s. Crustal thickness is generally less than 30 km

beneath the study area, but the crust thins to about 26 km beneath the outer shelf in the area of a classic elliptical gravity high. Large-scale Eurekan compressional structures, such as the Princess Margaret Arch, appear to extend offshore and are observed as major basement highs that bound sedimentary basins in the wide-angle models. A distinct velocity expression of the Cornwall Arch is not evident. Basin formation has been influenced by both structures predating the margin rifting and later compressional events. Some of the major velocity units in the refraction models for the northeast margin are similar to those observed in the hydrocarbon-rich Beaufort Sea-Mackenzie Delta area 1500 km to the southeast.

Interpretation of the 1990 wide-angle data, together with industry reflection data, between Ellef Ringnes and Meighen islands shows that sediments of the mainly Mesozoic Sverdrup Basin section are characterized by velocities generally less than 5.2 km/s and a thickness of 5-6 km. The presence of several new diapiric structures are indicated by both seismic and magnetic data in an area suggested to be evaporitic. The Sverdrup Rim - a local upper-mid crustal high, defined seismically by a 1.5 km high ridge of 5.2 km/s material overlying a 50 km wide basement high of 5.9 km/s material - is interpreted to be the northeastern boundary of the Sverdrup Basin. This Rim is imaged beneath Ellef Ringnes Island, on both the wide-angle and the reflection data, and is indicated beneath Peary Channel from the wide-angle interpretation. The structure of the Rim becomes increasingly complex to the northeast supporting an increase in regional deformation towards Axel Heiberg Island. The wide-angle model includes a sedimentary wedge, thickening offshore to 10 km, near the edge of the margin. Moho depths of less than 30 km indicate that thin continental, or transitional, crust continues beneath the shelf north of the Sverdrup Basin.

INTRODUCTION

The Canadian polar margin is considered to be a passive margin perhaps formed by the Late Jurassic-Cretaceous counterclockwise rotation and translation of Alaskan and Russian crustal blocks away from Arctic Canada (Vogt et al., 1982; Embry, 1989). As such, the Margin represents an excellent study area for the crustal velocity structure formed in the early stages of continental rifting, including the crustal thickness, dimensions and configuration of syn- to post-rift marginal basins.

The Western Canadian Arctic offshore has been relatively well studied both geologically and geophysically (eg. Dixon and Dietrich, 1990; Nassichuk, 1987), but due to the extreme climate and permanent ice cover the eastern polar margin remains one of the least studied regions in Canada, despite the suggested potential for significant hydrocarbon occurrence (Haimila et al., 1990). In 1985, in an effort to determine the configuration and structure of sedimentary basins beneath the Canadian Polar Margin, the Geological Survey of Canada, with funding from the Frontier Geoscience Program, began regional seismic refraction studies along the northeastern continental shelf, using a floating Canadian ice island as a base (see Jackson, 1989, for an overview of the Canadian Ice Island Hobson's Choice; and Jeffries, 1992, for a technical discussion of the formation of arctic ice islands). A regional grid of wide-angle seismic lines was established by three surveys completed in 1985, 1986 and 1990 (Fig. 1), yielding 2130 seismograms covering 1200 line-km. The technical aspects of the 1985, 1986 and 1990 refraction surveys are described fully in Asudeh et al. (1985), Asudeh et al. (1986), and Forsyth et al. (1990a), and the velocity modelling and interpretation of the 1985 survey are presented in Asudeh et al. (1989).

The main 1986 survey consisted of four and one-half reversed 120 km long profiles parallel and perpendicular to the polar continental margin northwest of Ellesmere and Axel Heiberg Islands (Fig. 1). The survey more than doubled the region investigated by the 1985 experiment, and additional constraints were supplied by having the two surveys intersect at several points. Modelling of the data by two-dimensional (2-D) raytracing provides velocity-depth information down to the Moho. The 1986 data were modelled using the algorithm of Spence et al. (1984), whereas the 1990 data were modelled using the more recent inversion algorithm of Zelt and Smith (1992) that automatically calculates take-off angles and provides estimates of model parameter resolution, uncertainty and non-uniqueness, among other improvements.

The 1990 survey extended from Ellef Ringnes Island to the Sverdrup Channel east of Meighen Island and south to near Amund Ringnes Island, across the northeast Sverdrup Basin and adjacent continental margin (Fig. 1). The survey consisted of two lines perpendicular to the margin and one line parallel to the margin. The results of 2-D velocity raytrace-modelling of the three lines provides information to Moho depths. Borehole information and re-interpreted industry seismic reflection data adjacent to the wide-angle lines were used to further constrain, and provide clear geological calibration for, the upper crustal structure derived from the wide-angle profiles.

Velocity models derived from the 1986 and 1990 data, as well as a regional geological and tectonic interpretation are presented here. Because the two surveys are geographically and temporally separated, and were modelled using different raytracing algorithms, they are presented in individual sections.

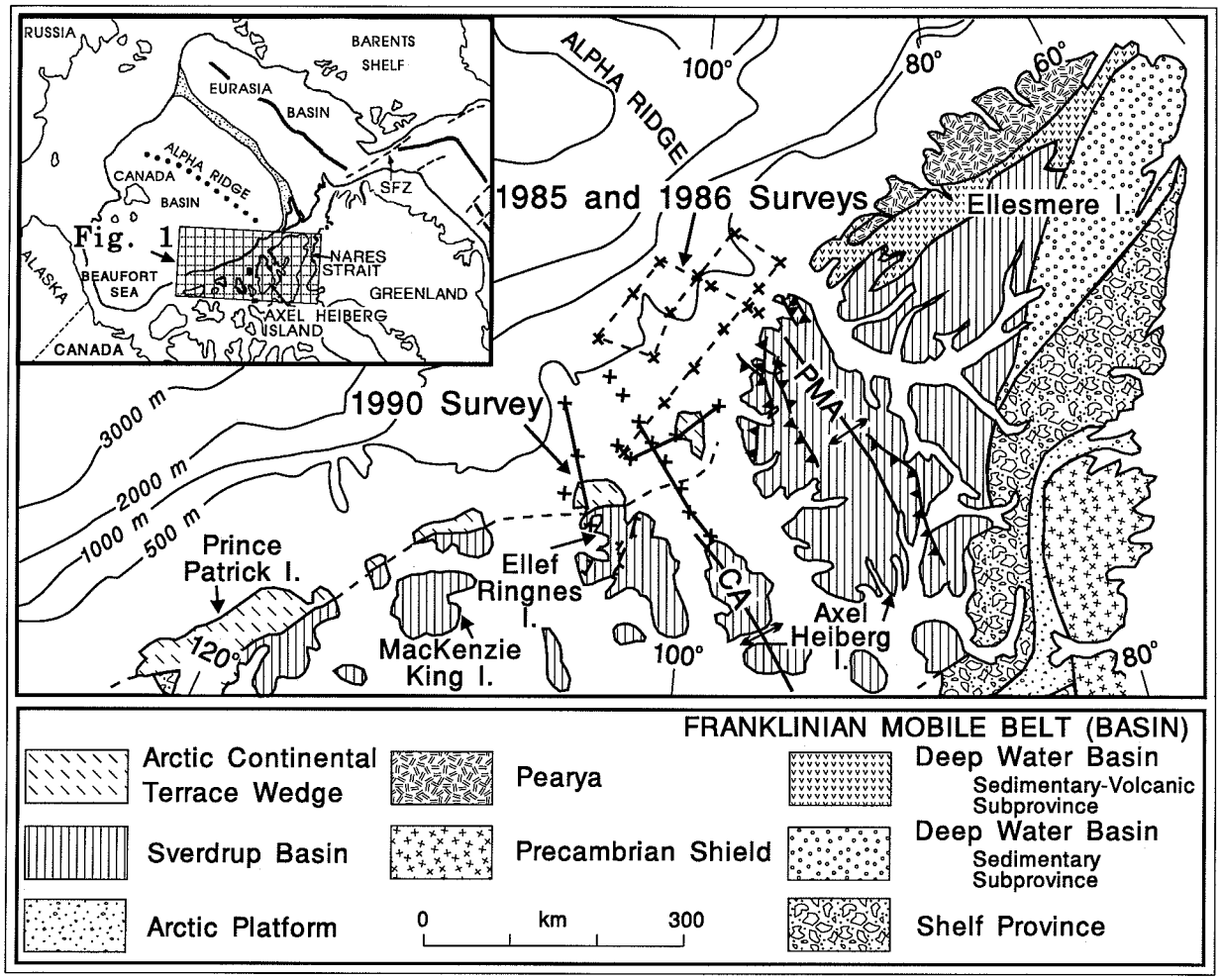

Fig. 1. Map of the eastern Canadian Arctic Margin with the location of the 1985, 1986, and 1990 wide-angle seismic surveys. The regional onshore geology and the offshore bathymetry are also shown. PMA=Princess Margaret Arch; CA=Cornwall Arch.

2. GEOLOGICAL AND TECTONIC SETTING

The regional geological framework of the northeastern Canadian polar continental shelf is provided by the known geology of the adjacent Arctic archipelago and of the contiguous Beaufort-Mackenzie basin (e.g. Overton and Embry, 1989; Embry, 1990). Harbert et al. (1990) describe the Canadian Arctic Island region as a series of large uplifted sedimentary basins separated by arches.

The Phanerozoic tectonic episodes or events that are inferred to have significantly affected the geology of the continental shelf in the study area (Fig. 1) are:

a) The development of the Lower Paleozoic Franklinian Basin, severely deformed during the late Paleozoic collisional Ellesmerian Orogeny (Trettin, 1987).

b) Continental rifting from Late Carboniferous to Early Permian, followed by thermal subsidence throughout the Mesozoic Era, resulting in the development of the Sverdrup Basin (Balkwill, 1978; Stephenson et al., 1987).

c) Continental rifting from the Middle Jurassic to Early Cretaceous, north of the Sverdrup Basin axis, leading to mildly renewed subsidence in the Sverdrup Basin (Stephenson et al., 1987); to seafloor spreading and the opening of the Amerasian part of the Arctic Ocean in the late Early Cretaceous and early Late Cretaceous (e.g. Sweeney, 1985; Embry, 1990); and to syn-rift and post-rift (thermal) sedimentary basin development on the newly formed continental margin.

d) Uplift and deformation of the northeastern portion of the Arctic Islands by the early Tertiary Eurekan Orogeny, as Greenland impinged upon Ellesmere Island (e.g., de Paor et al., 1989), and development of intramontane sedimentary basins (Miall, 1984; Ricketts, 1987).

These events are expected to have created major unconformities in the continental margin succession, as they have on land, that allow the shelf stratigraphy to be subdivided into megasequences as follows:

1) Lower Paleozoic Franklinian and associated strata.

2) Upper Paleozoic-Middle Jurassic Sverdrup Basin strata deposited during the initial Sverdrup rifting episode and its subsequent phase of thermal subsidence.

3) Middle Jurassic-Lowest Cretaceous syn-rift deposits on the developing Arctic continental margin.

4) Post-"breakup unconformity" Upper Cretaceous and Lower Tertiary strata of the Sverdrup Basin and continental margin successions.

5) Upper Tertiary strata, primarily at the continental margin, deposited after the culmination of Eurekan tectonism.

Megasequences (1) and (5) are shown on Fig. 1 as the regional geological map units Franklinian Basin-Pearya and Arctic Continental Terrace Wedge respectively; megasequences (2), (3) and (4) are mapped in Fig. 1 together as Sverdrup Basin. Beneath the present continental shelf, which formed the northern margin of the late Paleozoic-Jurassic Sverdrup Basin, the seismic evidence in this report suggests that megasequence (2) is quite variable compared to (3) and (4). In the study area, where the effects of the Eurekan Orogeny have probably extended to the continental shelf, strata of megasequences (3) and (4) are probably mildly to moderately deformed and overlain by undeformed rocks of megasequence (5).

3. HYDROCARBON POTENTIAL

Using the limited available geological and geophysical data for the Arctic continental shelf, Haimila et al. (1990) estimated the petroleum potential for the megasequences described above to be as follows. Within the study area, which falls within the regional "central sector" of the Canadian Arctic shelf, the lower Paleozoic strata are too highly deformed and thermally altered to have petroleum potential. The Upper Paleozoic to Lower Jurassic units are considered to be fair to good for petroleum potential within the Sverdrup Basin, with a thermal maturity level of mature, which would allow for the presence of oil and gas, but the potential of this interval on the continental shelf is unknown. The potential of Middle Jurassic to Lower Cretaceous strata, where present, is difficult to predict due to lack of data. The thick Upper Cretaceous to lower Tertiary successions, such as the Kanguk and Eureka Sound Formations, are rated as having good petroleum potential, with some depositional sequences probably similar to those identified in the Beaufort Sea. The southwestern portion of the study area is probably the area of greatest potential along the northeastern margin as it is only mildly deformed, is free of volcanic rocks, and contains a thick enough sequence to create a mature source rock. The Miocene to Holocene strata probably have a very low petroleum potential due to the low thermal maturity and lack of source rock.

Along the Arctic coastal plain a more detailed analysis of the hydrocarbon potential can be made. The first exploratory well in the Canadian Arctic Archipelago was drilled in 1960, but by 1977, 125 wells had been drilled and three-fourths of those had prospective reservoir targets in upper Paleozoic and Mesozoic rocks of the Sverdrup Basin (Balkwill, 1978). The western part of the basin is considered by Balkwill (1978) to be more conducive to hydrocarbon presence due to less mafic intrusion and shallower burial than in the central and eastern portions, and due to the preservation of suitable trap structures. The Mesozoic rocks of the basin have yielded major gas fields at Melville Island, King Christian Island, and western Ellef Ringnes Island, with a calculated 425 billion m^3 (15 TCF) of predominantly methane gas, and 80 million m^3 (500 million barrels) of oil (Haimila et al., 1990). It is suggested by Stuart Smith and Wennekers (1977) that as a result of topographic inversion and selective erosion of anticlinal or structurally high features, the majority of the potential reserves lie between the islands in Upper Carboniferous and Permian rocks. These potential reserves have been estimated by Haimila et al. (1990) to be 2.2 trillion m^3 (78 TCF) of gas and 685 million m^3 (4.3 billion barrels) of oil.

The seismic indications (this study) of increasingly complex structure towards Axel Heiberg Island, and the Mesozoic or younger basins containing some 12 km of strata immediately offshore, offer favourable structural criteria for hydrocarbon occurence, and good oil and gas shows were encountered on western Ellesmere Island (Embry et al., 1991). Although data from south of Ellef Ringnes Island suggest that rocks in the southern part of the study area are overmature, hydrocarbon potential to the northeast is relatively unknown.

4. PREVIOUS SEISMIC EXPLORATION

Pioneering seismic refraction surveys were carried out in the Ellef Ringnes-Melville Island area by Sander, Hobson and Overton in the 1960's (Hobson, 1962; Sander and Overton, 1965; Overton, 1970) and simple traveltime-distance curves were plotted to estimate layer velocities and thicknesses. Later, time-term analysis was used to interpret wide-angle surveys across the central Sverdrup Basin (Forsyth et al., 1979). In the 1970's industry reflection data was recorded, but it was mostly on land and structural resolution is limited to depths less than about 8 km. The 1985 wide-angle survey (Asudeh et al., 1986) was the first well located survey to provide information to upper mantle depths. The nearest offshore seismic studies include wide-angle surveys carried out near the north pole, across the Alpha and Lomonosov ridges, (Forsyth et al., 1986; Forsyth and Mair, 1984), and a wide-angle line that was recorded in 1992 approximately 500 km northeast of the study area, off northern Ellesmere Island (Argyle et al., 1994).

5. 1986 SEISMIC REFRACTION SURVEY

The 1986 refraction survey was carried out as 60 km-long reversed profiles with receivers deployed at 5 km intervals on the sea ice by helicopter (Fig. 2). The seismographs were programmed to digitally record the output of a seismometer array (Mair and Lyons, 1981) of 4.5 Hz geophones in pre-determined 2 to 3 minute time windows. At both ends of the 60 km profiles two shots were detonated at a spacing of 2.5 km and the resulting seismic sections were combined to produce a composite section with an apparent recorder spacing of 2.5 km. In addition to these shots, shots were detonated at offset distances of 60, 120, 180 and, when possible, 240 km from both ends of each recording spread to provide reversed coverage to Moho depths as the profile grid in Fig. 2 was established.

For distance ranges of 0-60, 60-120, 120-180, and 180-240 km shots of 136, 217.6, 435.2 and 652.8 kg respectively were detonated while suspended at a depth of 100 m below the sea ice. "Fan" shots were also fired from selected offshore shotpoints broadside into nearshore spreads, to provide additional control on structure and Moho depth beneath the continental shelf. In total, the 1986 seismic refraction survey involved 35 shots fired into 23 recorders producing 805 seismograms.

Survey positioning was provided by four Ultra High Frequency pulse positioning beacons established on elevated sites along the costs of Ellesmere, Axel Heiberg, and Meighen islands (Dearnley-Davison and Forsyth, 1989). Mobile units aboard the helicopters were used to fix signals transmitted from the onshore beacons to navigate to planned survey sites. Coordinates of the beacons were obtained using the Global Positioning System (GPS) in non-differential mode. Four satellite doppler receivers were used to position shotpoints and fuel caches outside the range of the beacon network (about 150 km).

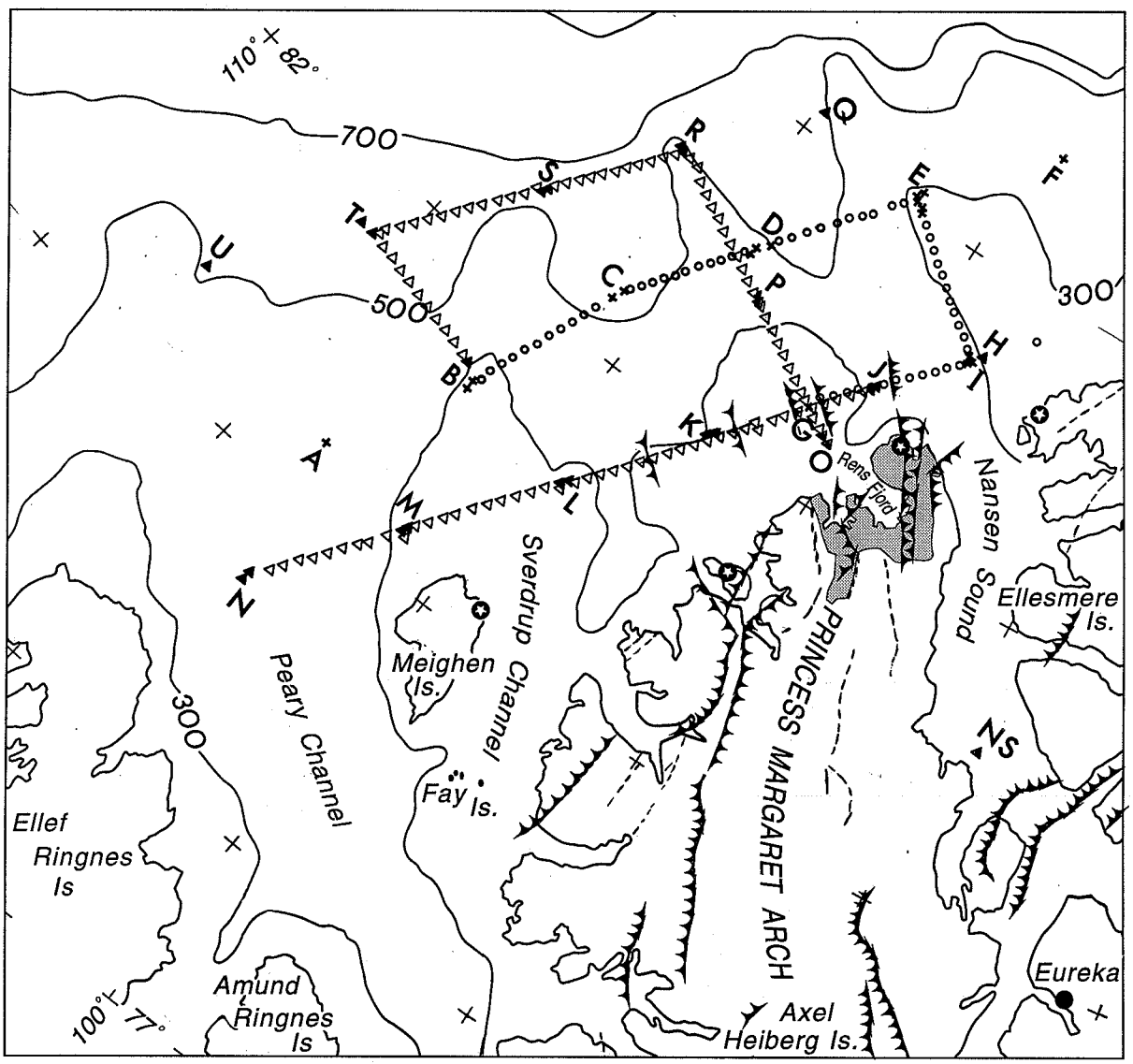

Fig. 2. Location of the 1985 (circles) and 1986 (triangles) survey lines. Shotpoints are filled triangles and x's. Major thrust faults and structural trends are indicated on Axel Heiberg and adjacent Ellesmere Island. Paleozoic rocks in the core of the Princess Margaret Arch are shaded. Dip symbols on nearshore seismic line are from seismic model. Stars are navigation transmitter sites.

5.1. SEISMIC REFRACTION RESULTS

Continental Margin Velocity Model

The 1986 seismic refraction data were modelled with the ray-trace program of Spence et al. (1984), based on asymptotic ray theory (Cerveny et al., 1977), in which observed seismic phase traveltimes and amplitudes are synthetically replicated using a 2-D crustal velocity model. The model is specified by the coordinates of the upper boundaries of a number of blocks and by the velocities and velocity gradients normal to the upper boundaries of the specified blocks. The crustal velocity model is developed by beginning with the interpretation of the nearest observations (the shallowest depths) from reversed 60 - km long spreads and moving to observations from greater distances and deeper depths. At each step, reversed first arrival and prominent later arrival reflections are modelled. Greater emphasis was placed on fitting traveltimes due to the sensitivity of amplitudes to small scale heterogeneities, differences in seismometer placements or shotpoints, and the limitation of ray theory (see eg. Mooney 1983; Cerveny, 1985). At the points where lines intersect, deriving a model compatible with both lines provides additional constraint. The results of the 1986 survey alone are based on the modelling of 19 pairs of reversed profiles.

Seismic Velocity Units and Stratigraphic Sequences

An overview of the seismo-stratigraphic interpretation (Fig. 3) is presented here; additional evidence will accompany the detailed description of crustal features from both 1986 and 1990 surveys that follows. The interpretation of the seismic velocity units are related to the geological sequences described earlier. The lowermost unit 1/unit 2 boundary is clearly the crust-mantle transition, or Moho, underlain by a velocity >8 km/s. The crustal thickness of generally less than 30 km indicates that the shelf is underlain by thin continental crust. Units 2 and 3 together represent basement, consisting of metamorphosed Franklinian strata overlying older cratonic rocks. Together, these layers would have been thinned to their present combined thickness during at least two extensional phases, prior to deposition of the Sverdrup Basin and prior to the development of the present continental margin. The overlying units 4 and 5 are interpreted to consist of essentially undeformed and unmetamorphosed Mesozoic and Tertiary sedimentary rocks. Apparent structural changes along the unit4/unit 5 boundary may have resulted from Eurekan tectonism. The complicated disposition of the unit4/unit 5 boundary is interpreted to be at, or close to, the base of the Mesozoic succession.

A number of representative modelled seismic sections are presented to illustrate the regional geometry of the velocity structure beneath the continental shelf (Figs. 3-9). The results of all the modelling are summarized as a fence diagram in Fig. 10.

Nearshore Line N-I

From southwest to northeast, the principal features along the nearshore line N-I are a major basin with internal structures from shotpoints M to K, a basement high which appears near surface between K and G and a smaller basin northeast of shotpoint G (Fig. 4).

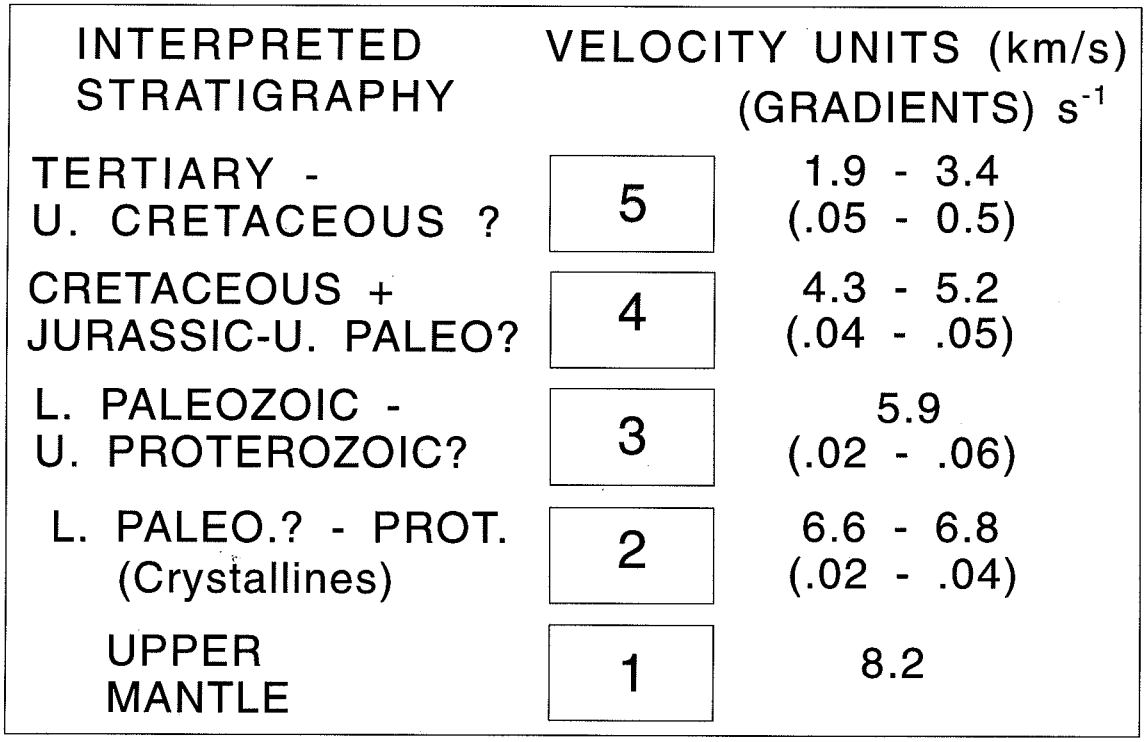

Fig. 3. Seismic velocity units and interpreted stratigraphy.

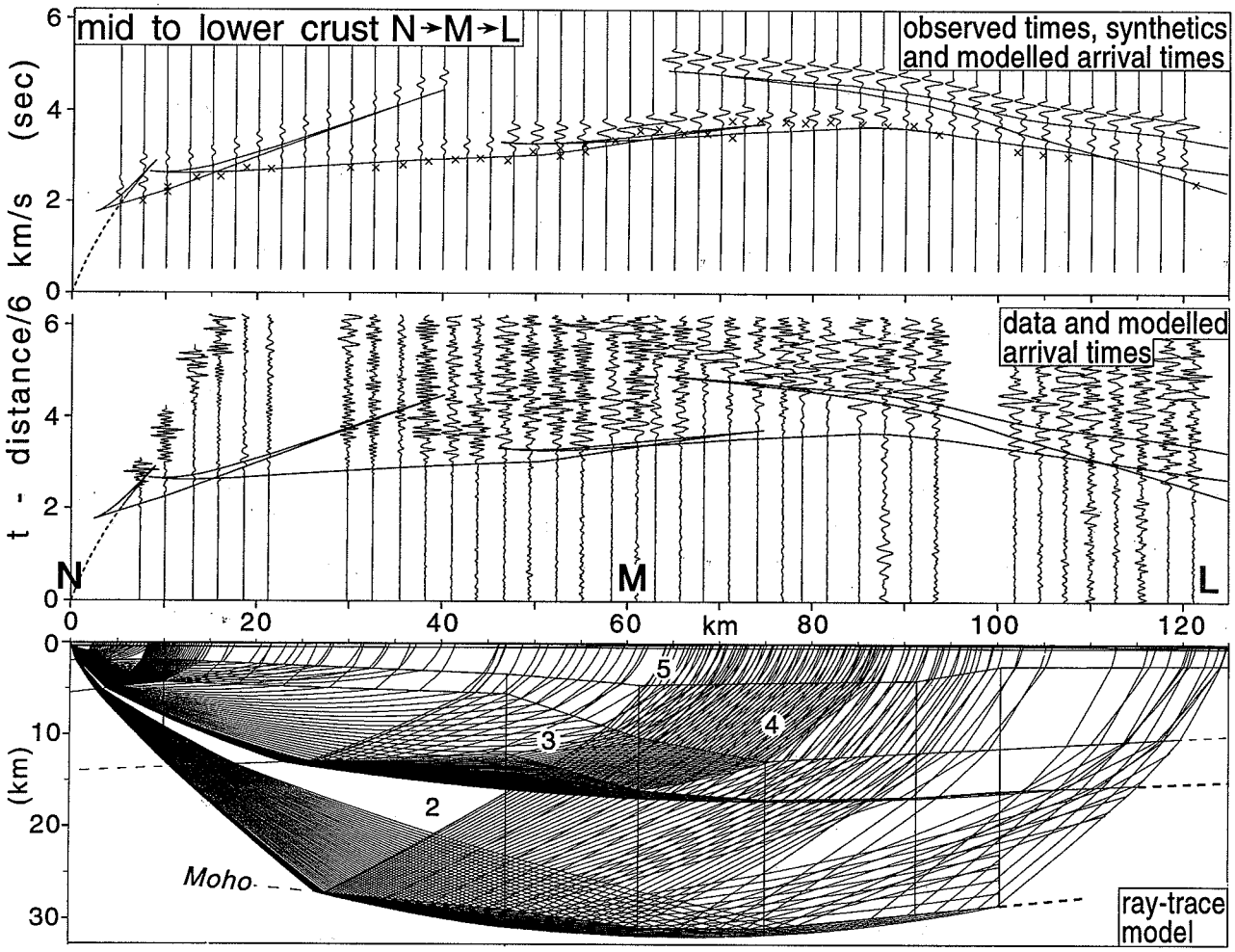

Fig. 4. Geometry of velocity units to lower crustal depths beneath N-L. Moho depths are generally less than 30 km. Upper crustal basin of units 5 and 4 contain over 10 km of Tertiary-Mesozoic strata.

North of Meighen Island

Immediately northeast of shotpoint N the thickness of the combined Tertiary-Mesozoic strata increases from about 4 km beneath northern Peary Channel to a large basin containing 4-5 km of Tertiary-Cretaceous (unit 5) sediment and some 7 km of mainly Mesozoic unit 4 material (Fig. 4). The basin lies north of Meighen Island and extends for about 100 km to midway between L and K (Fig. 2). A general thickening of the Tertiary-Cretaceous section beneath the shelf is supported by data to the south. A borehole on Meighen Island (near the star in Fig. 2) shows 3 km of Tertiary-Cretaceous strata while this section is completely missing on the Fay islands 60 km to the south of the borehole. Structural disruption within the Tertiary-Mesozoic sequences is suggested by the basin margin southwest of M, thinning of the Tertiary-Cretaceous material to about 2 km southwest of shotpoint L and the abrupt juxtaposition of unit 5 and unit 4 at a structure with apparent southwest dip about 25 km southwest of K (Fig. 5).

Offshore Extension of the Princess Margaret Arch

Both units 5 and 4 abut a major basement high northeast of shotpoint K. The shallowest part of the basement high about 20 km northeast of K (Fig. 5) lies directly offshore of the exposed Paleozoic rocks in the core of the Princess Margaret Arch around Rens Fiord, and is represented by minimal sediment cover overlying material with a velocity of 5.9 km/s. We therefore interpret the 5.9 km/s material (velocity unit 3) as Lower Paleozoic and possibly some Upper Proterozoic material within an offshore extension of the Princess Margaret Arch. The apparent southwest dips from seismic models of the western limb of the Princess Margaret Arch are consistent with the attitudes of major thrusts mapped on northwestern Axel Heiberg Island (Fig.2). Several velocity structures were modelled to place limits on the internal geometry of the arch. The clear reflected event 20-35 km northeast of K (Fig. 5 lower section) is interpreted as a reflection from the top of unit 2 at a depth of 6 km. The structure also fits the reversed coda observed from shotpoint J (Fig. 5 upper section). The complex variations in first arrival amplitudes and, to a lesser extent, arrival times across this structure indicate that the velocity structure model is a simplified form of the true structure. The presence of the basement high and the associated non-horizontal structure help explain why the reflection data from the ice island in this area could not clearly delineate features (Hajnal et al., 1990). Computed model iterations indicate that as the depth to the top of unit 2 increases, the fit to the data becomes worse. Fig. 6 shows a deeper top to unit 2 at 11 km, however the modelled reflections (R in Figs. 5 and 6) from shotpoints K and J are a much less satisfactory fit to the data for the deeper unit 2 model.

Fig 7. shows reversed ray-traced solutions emphasizing the velocity structure of the lower crust and Moho. The crust-mantle transition is at a depth of 26 km. The coincidence of the slightly thinner crust with the overlying westerly dipping crustal geometry suggests the entire crust has been involved in the (Eurekan?) formation of the western limb of the Princess Margaret Arch.

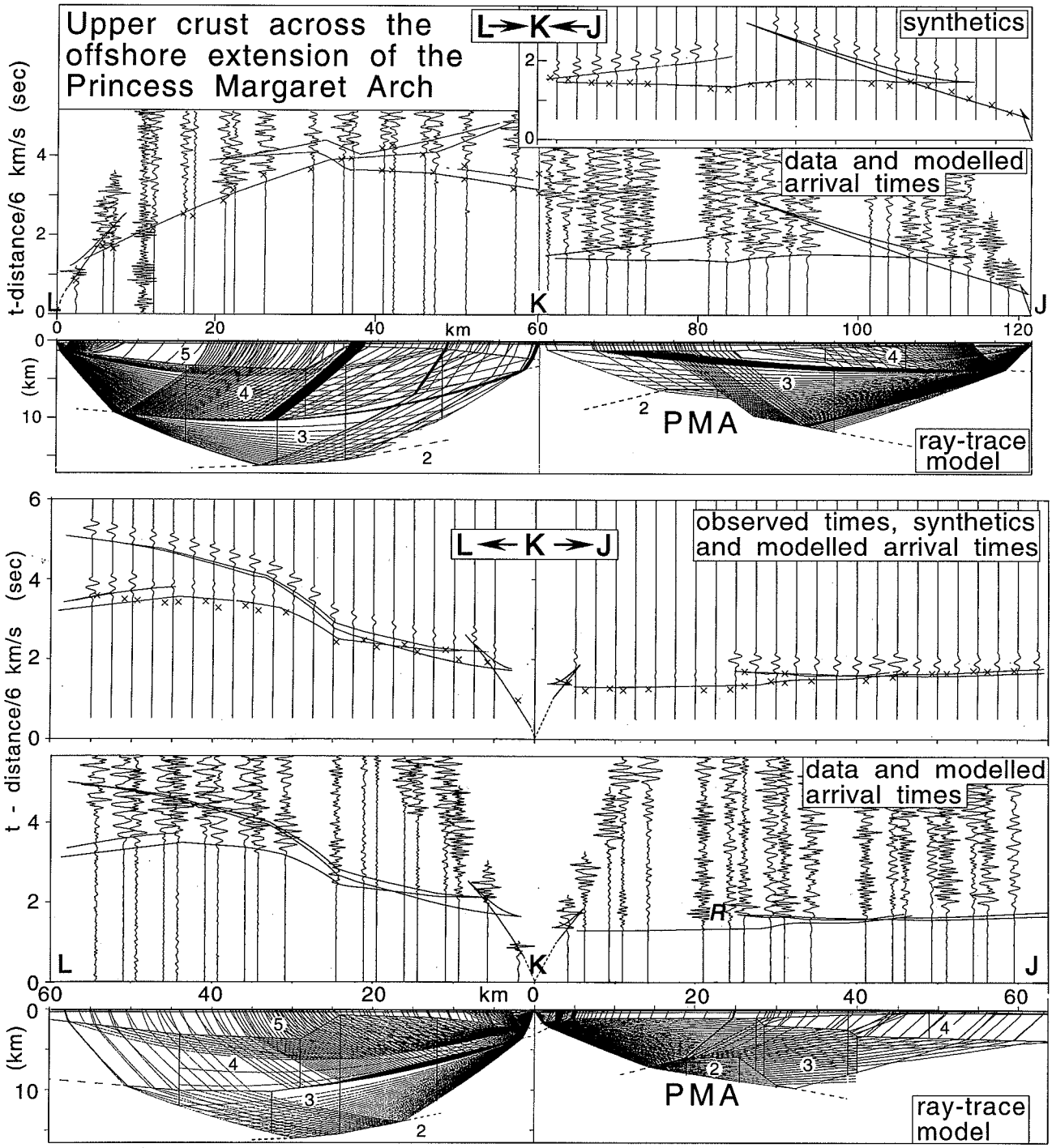

Fig. 5. Upper crustal velocity structure across the offshore extension of the Princess Margaret Arch (PMA) shows minimal sedimentary cover over unit 3 (5.9km/s). The basement high is adjacent to the exposed Paleozoic core of the PMA mapped around Rens Fjord (see Fig. 2). The reflection "R" (20-35 km from K) suggests the top of unit 2 (6.6 km/s) lies at 6 km depth in the core of the PMA.

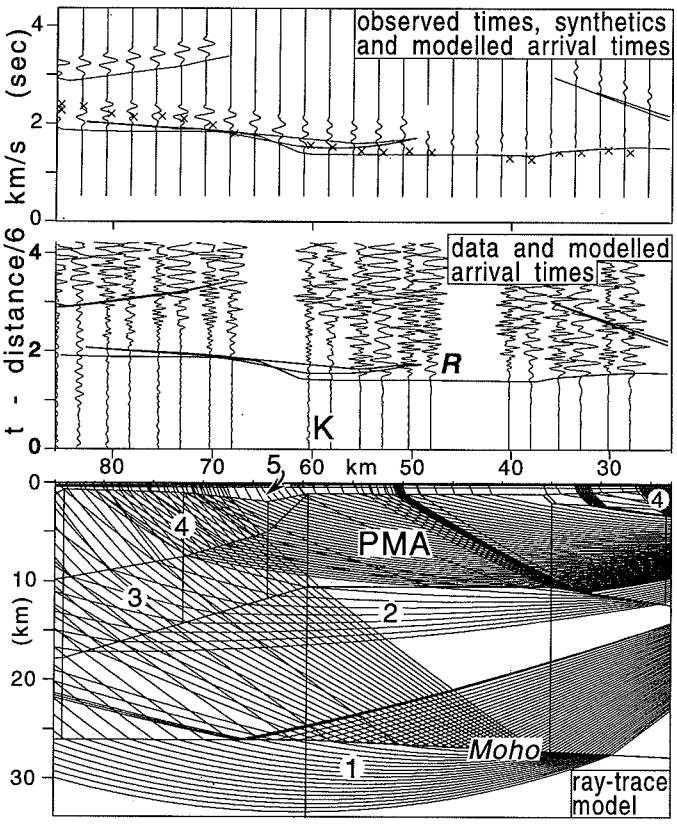

Fig. 6. Minimum Princess Margaret Arch model from shotpoint J with top of unit 2 (6.6 km/s) at 11 km. The fit to the observed large amplitude reflection "R" following first arrival in distance range 45-57 km from J is less satisfactory than our preferred model with top at a depth of 6 km (Fig. 5).

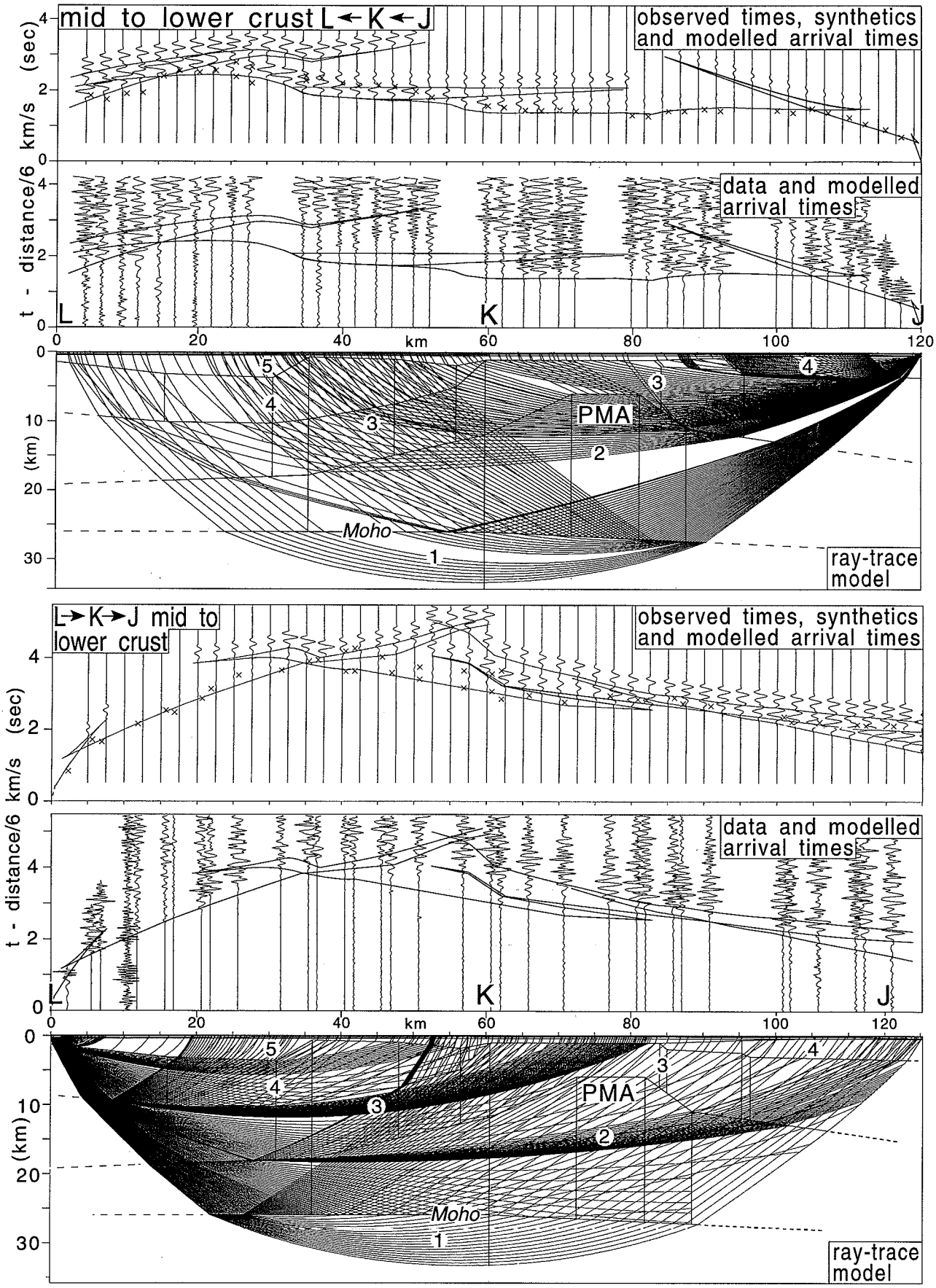

Fig. 7. Reversed ray-traced geometry of L-J lower crustal velocity structure. Moho depth is 26 km. The correlation of thinner crust with the apparent southwest dips of all the overlying velocity units is consistent with the entire crust being involved in the formation of the western limb of the Princess Margaret Arch (PMA).

Structure Normal to the Margin - Line O-R

A large basin containing some 5 km of Tertiary-Cretaceous unit 5 and 10 km of unit 4 marks the northern end of the Princess Margaret Arch offshore between O and P (Fig. 8). The linkage between the basin seen north of the Arch and that seen to the southwest of shotpoint K is not defined. Unit 5 includes a lower subdivision with a velocity of 3.4 km/s. This unit may also be present in the lower part of unit 5 beneath line N-I but is not sufficiently thick (less than a few hundred metres) to significantly affect the travel times. The 3.4 km/s unit thickens to the northeast beneath shotpoint R and thins to 1-2 km to the southwest on R-T (Fig. 9). The increased thickness of this slightly higher velocity sediment towards the Alpha Ridge may indicate early deposition of clastic sediments with a higher content of volcanic/mafic material.

The Franklinian basement (unit 3) and the overlying mainly Mesozoic section (unit 4) vary by several km in thickness over lateral distances of 7-20 km (Fig. 8) suggesting mid-crustal structures beneath the outer continental shelf. The relatively undisturbed thickness of the upper part of unit 5 may is in keeping with either a late Jurassic to Early Cretaceous period of deformation associated with the opening of the Canada Basin or developments related to the Alpha Ridge.

Outer Shelf Line R-T

Major changes in crustal structure are indicated beneath the outer shelf on line R-T (Figs. 9 and 10). To the northeast beneath shotpoint R, the outer shelf velocity structure indicates a relatively uniform 5 km thick unit 5, underlain by a thinner (2 km) unit 4 than seen in the other sections. The thinner unit 4 may indicate a seaward limit to Sverdrup Basin strata beneath the outer shelf. The Franklinian basement (unit 3), about 6 km thick, rests on an apparently thickened lower crustal unit 2 that, together with the thin unit 4, may reflect the proximity of the Alpha Ridge. To the southwest between shotpoints S and T a structural high on the Franklinian basement (unit 3) forms a margin to a basin containing some 10-12 km of unit 4 material. This basin continues beneath line T-B and may be part of the basins noted on lines M-K and O-P above. The Moho thins to a depth of 26 km beneath S-T. The thinner crust coincides with the northeasterly end of a classic continental margin elliptical gravity high (Fig. 11).

Velocity Structure Discussion

Fig. 10 shows an expanded fence diagram compilation of the individual 1986 model segments together with the 1985 results (Asudeh et al, 1989) to provide a three-dimensional picture of velocity structure beneath the continental shelf offshore of Ellef Ringnes and Axel Heiberg islands. The crustal model has been divided into five distinct velocity units (described earlier). Solid line model boundaries represent significant velocity changes derived from fitting ray-traced travel times and phase amplitudes to reversed observations from adjacent and offset shotpoints. Dashed and dotted interfaces represent boundaries estimated from partial or unreversed observations. Dashed lines with "?" marks are suggested but not modelled velocity changes indicated by the higher resolution 1986 data. Secondary arrivals including clear wide-angle reflections provide the main constraints for boundaries between velocity units 3 and 2 and between units 2 and 1. Refracted first arrivals provide the principal constraints for the overlying units.

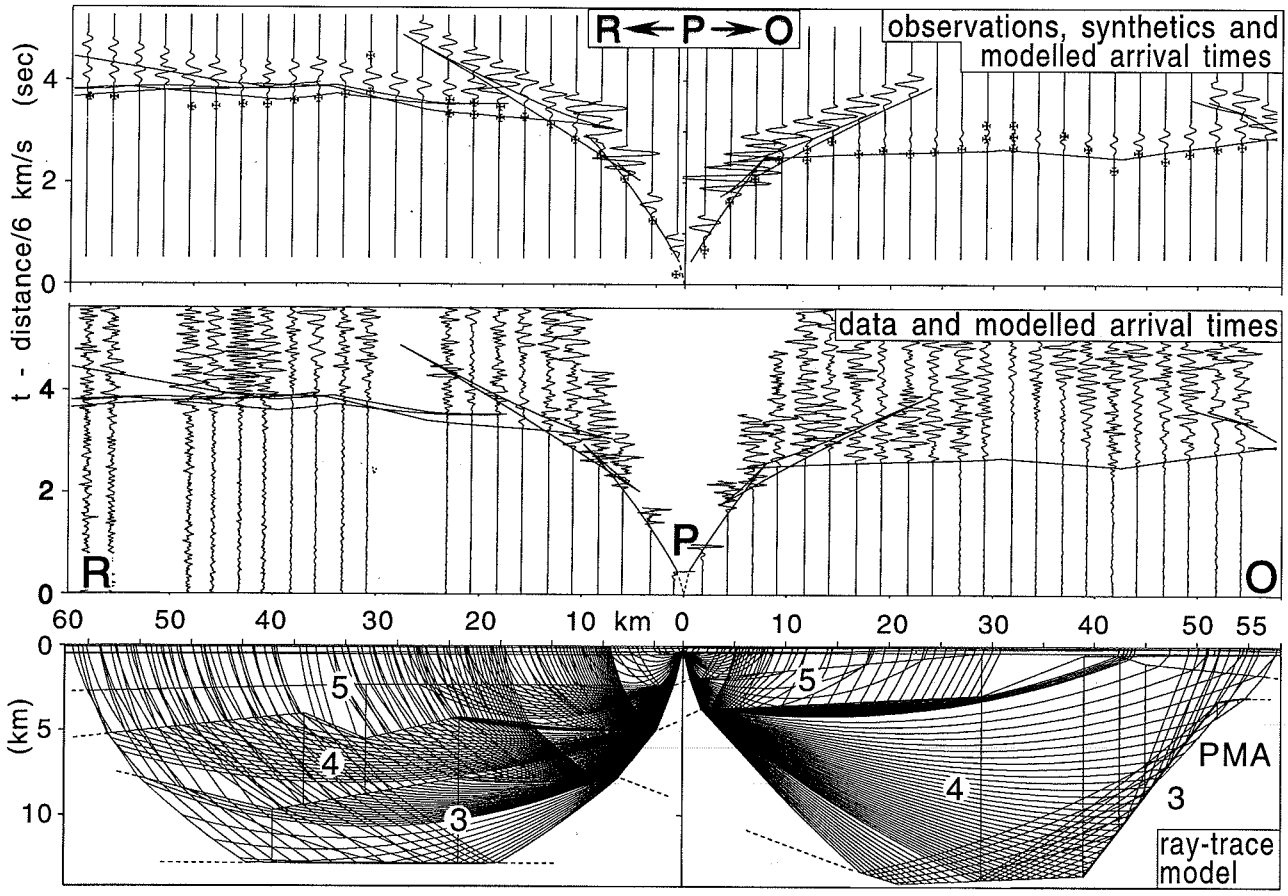

Fig. 8. Geometry of upper crustal velocity units normal to the margin on Line O-R. A 10 km-thick basin of mainly unit 4 marks the northern end of the Princess Margaret Arch (PMA). Between P and R the upper division of unit 5 (1.9-2.1 km/s) appears relatively uniform while the lower part appears to have been deposited on a structurally disturbed unit 4 and underlying Franklinian basement (unit 3).

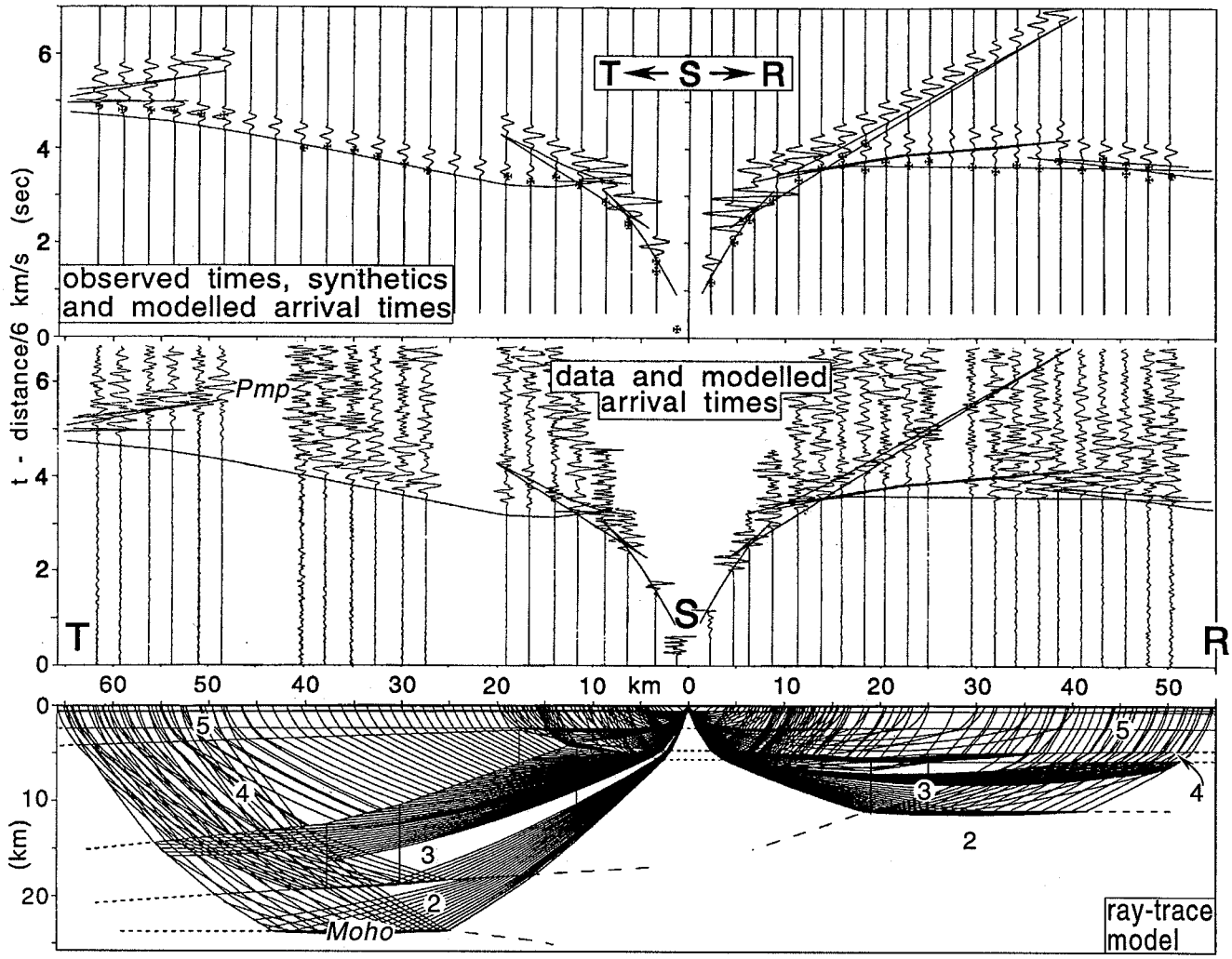

Fig. 9. Upper crustal velocity structure beneath outer shelf line T-R. The 10 km-thick basin of unit 4 underlying S-T thins to 2 km beneath R across a basement high of unit 3. The thickness of unit 4 under S-T is similar to that observed on lines M-K and O-P. Clear Moho reflections indicate a crustal thickness of 26 km (see also Fig. 4).

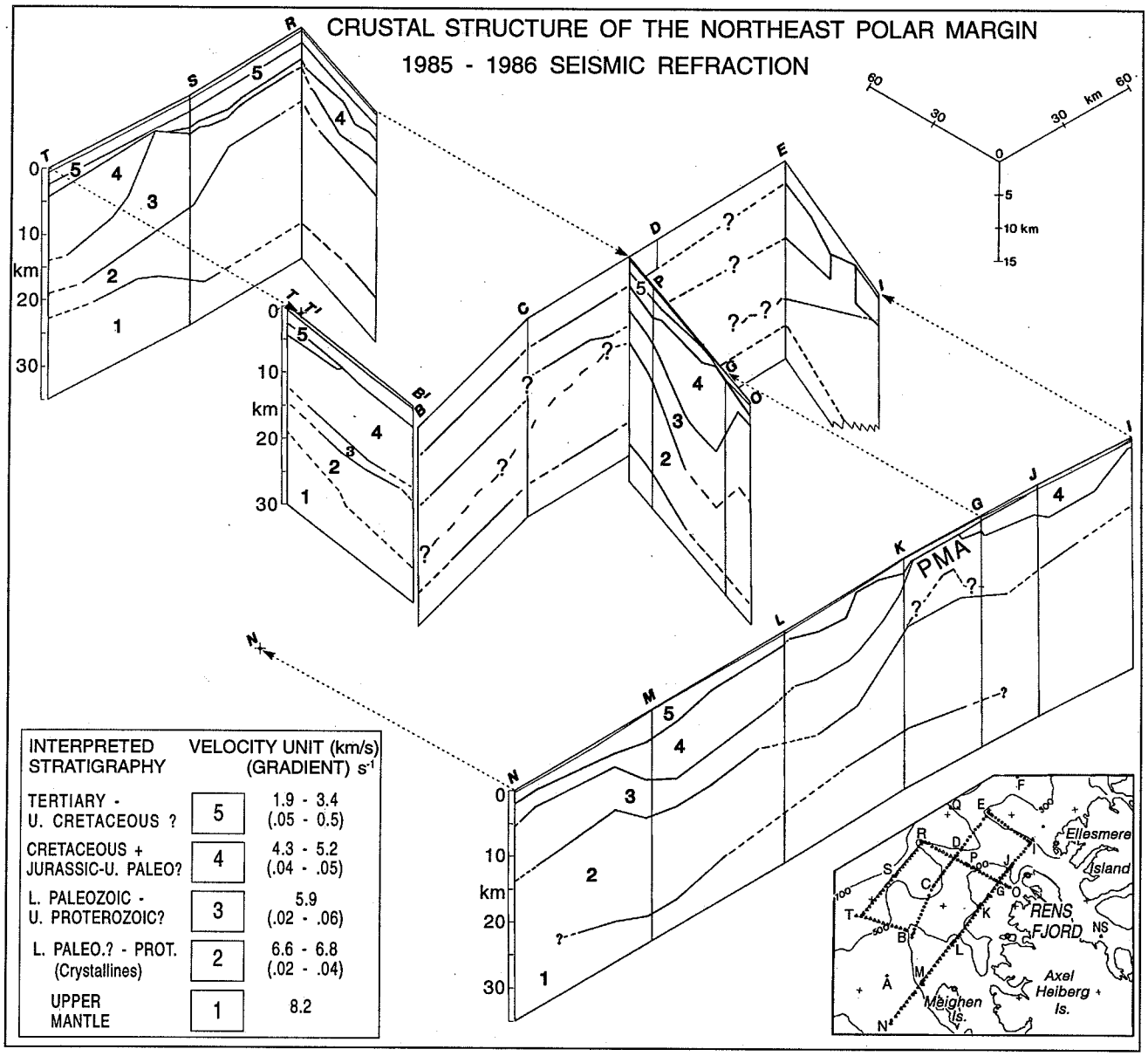

Fig. 10. Expanded fence diagram of velocity unit geometry from 1986 data and stratigraphic interpretation. structure on I-E and E-B from Asudeh et al, 1989. Lower division of unit 5 on R-T, R-G and T-B is 3.4 km/s. The basement high offshore of Rens Fjord corresponds to an extension of the Princess Margaret Arch bounded by complex basin margins both laterally (M-K and G-L) and seaward (G-P) beneath the shelf. Moho rises to 26 km to the northwest beneath shotpoint T. The thicker unit 2 and thinner unit 4 beneath R may represent the proximity of the Alpha Ridge nearby to the north (see Figs. 1 and 12).

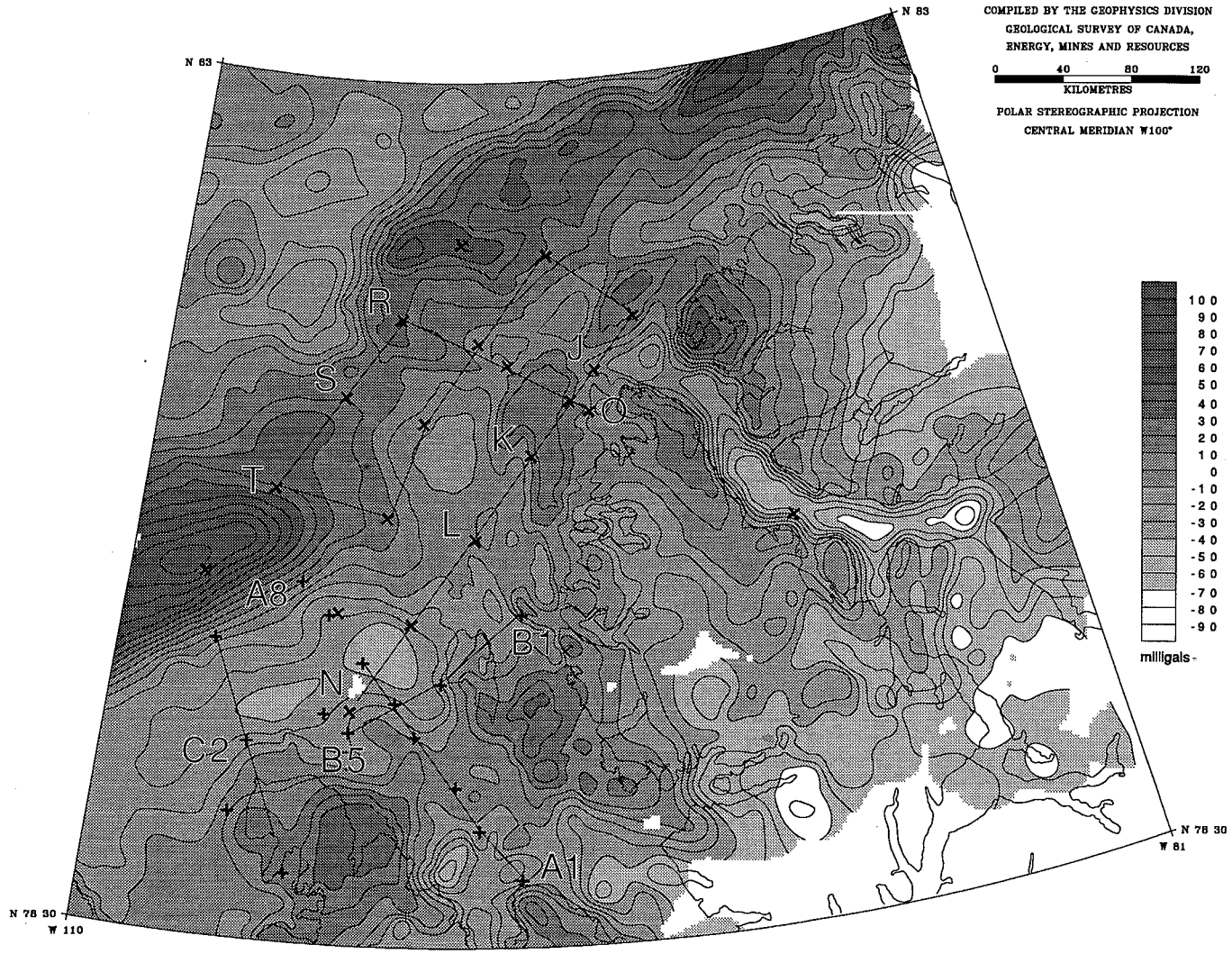

Fig. 11. Gravity (Bouguer on land, free-air offshore) map of the study area. Compiled by the Geophysics Division of the Geological Survey of Canada.

Variations in modelled velocities and gradients indicated by the ranges in Fig. 10 suggest that velocity contrasts between crustal units may vary along the profile sections. As the unit thickness increases, the velocity at the base of the unit increases according to the velocity gradient within the unit, and the velocity contrast with the underlying unit is reduced. For example, between shotpoints N and M, the velocity at the base of approximately 5 km of unit 4 is 4.6 km/s, while beneath shotpoints M and L, where unit 4 is approximately 9 km thick, it is 4.8 km/s. It follows that the models must be interpreted accordingly.

In addition to the regional velocity structure, the 1986 data provide limited resolution on several smaller scale structures including the core of the Princess Margaret Arch and the basement high beneath S-T. Except for general dip, the detailed nature of the lateral changes bounding these highs is not resolved and is probably much more complex than shown. Adjacent onshore structures include major north-trending, easterly vergent, thrust faults characterize the western part of the Princess Margaret Arch and trend normal to the seismic line. Field evidence (Ricketts, 1987) indicates that, at its northern end, the Princess Margaret Arch is cored by Lower Paleozoic strata (Rens Fiord Uplift, Trettin et al., 1972) and is flanked by progressively younger Sverdrup Basin rocks. This geological interpretation strongly resembles the new seismic model of the offshore basement high which brings 5.9 km/s material to within about 1 km of the surface and supports an interpretation of unit 3 as including Lower Paleozoic rocks. Although current evidence indicates a principal phase of Middle Eocene folding and faulting in the development of the Princess Margaret Arch, the Arch may have originated from an earlier Late Cretaceous-Early Paleocene compressional phase of the Eurekan orogeny (Ricketts, 1987).

Beneath the outer shelf between shotpoints S and T a structural high of Franklinian basement (unit 3) forms a margin to a basin containing some 10-12 km of unit 4 material. The similar total thickness of the combined units 5 and 4 on lines M-K, O-P, S-T and T-B suggests a major regional basin of Mesozoic and younger material north of Meighen Island. The basement ridge southwest of shotpoint S coincides with the change from longer wavelength, generally flat, negative magnetic anomalies to shorter wavelength, higher amplitude, positive anomalies that continues northeast to the Alpha ridge (Fig. 12). The basin north of Meighen Island correlates with the relatively flat, generally negative magnetic field. The northern end of Axel Heiberg Island and the immediate offshore extension of the Princess Margaret Arch identified seismically is characterized by a very distinctive short wavelength, high amplitude magnetic field (Fig. 12). Individual circular anomalies on northern Axel Heiberg Island correlate with diorite bodies of probable Devonian age suggesting that the short wavelength magnetic anomaly sources include near surface intrusive bodies that represent part of the Franklinian basement and provide additional support for the seismostratigraphic interpretation of velocity unit 3.

Summary of 1986 Models

The general crustal structure of the northeastern Canadian polar continental shelf consists of a complex network of thick sedimentary basins and basement arches. Crustal thicknesses generally less than 30 km indicate a thin continental or transitional crust underlies the margin, and that typical cratonic crustal thicknesses of 35 km or more lie farther south. Seismically identified basement highs that form margins to upper crustal sedimentary basins coincide with major changes in newly compiled magnetic anomaly data.

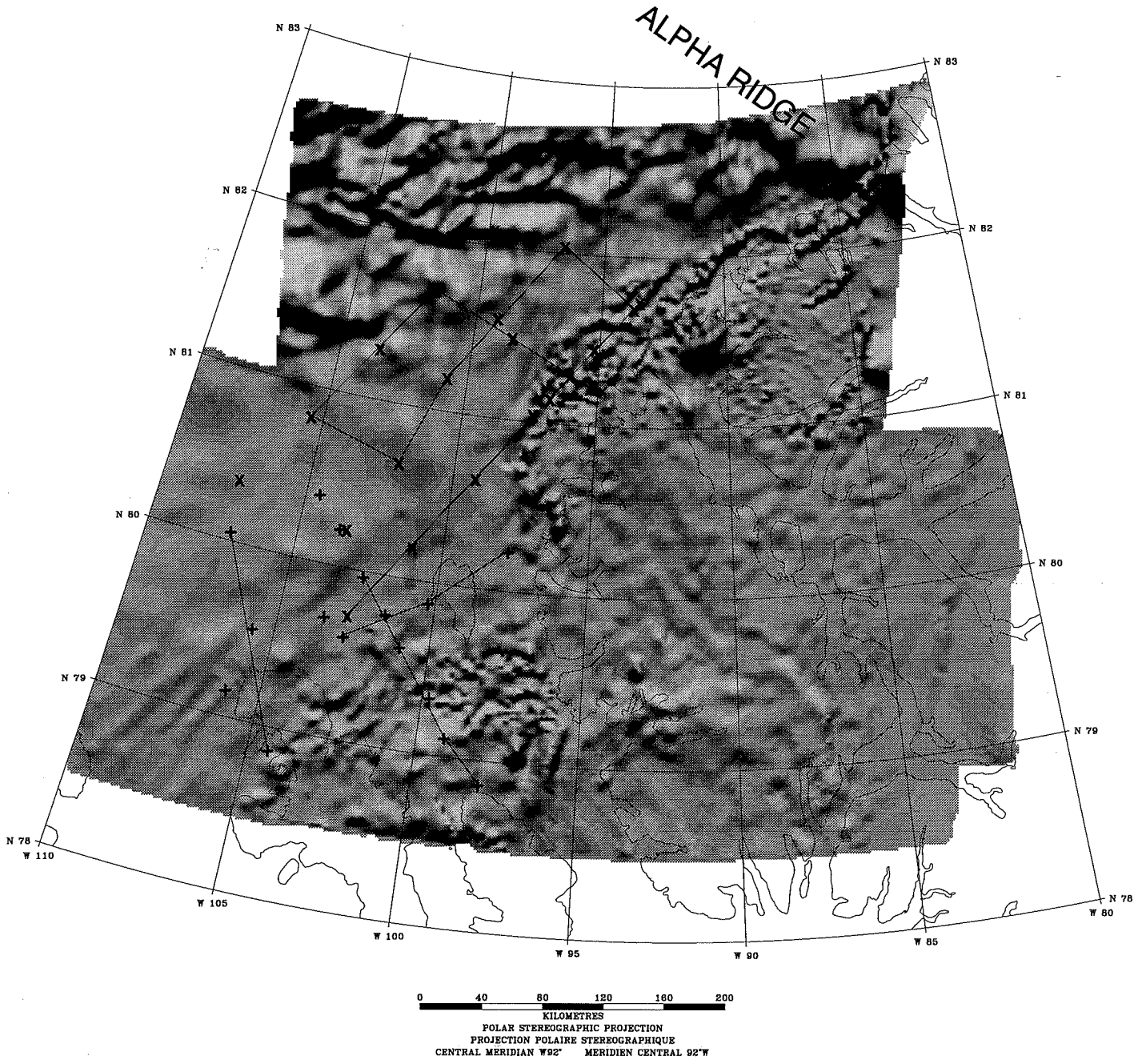

Fig. 12. Shaded relief map of newly compiled residual total field magnetic data. Illumination is from the north at 40 degrees inclination. Compiled by the Geophysics Division of the Geological Survey of Canada.

The seismic information provides new constraints on the crustal structure of the polar margin and by default, on the rifting associated with the formation of the adjacent Canada Basin. The seismic analysis has directly provided:

1) A new regional velocity structure of the continental shelf offshore of Ellef Ringnes to Axel Heiberg Island.
2) The first structural calibration for newly acquired and compiled magnetic data for the area.
3) New crustal evidence that documents both the apparent continuity and the changes in principal regional structures mapped onshore and clues to the nature of these structures at depth.
4) New parameters for resource assessments of Canada's polar margin.
5) New parameters to help define Canada's Arctic margin under the internationally ratified Law of the Sea agreement.

The newly compiled aeromagnetic data for the study area provide new supporting evidence for:

1) The offshore continuation and end of the Princess Margaret Arch.
2) A major basin north of Meighen Island.
3) A major change in crustal structure beneath the outer continental shelf that may be related to the proximity of the Alpha Ridge.

In the area between Ellef Ringnes and western Ellesmere Island and the adjacent offshore much conjecture surrounds the formation of multiple basins during Eurekan tectogenesis. To further quantify these linkages, a higher resolution integration of the seismic results with the new magnetic data and existing gravity data is required.

5.2 SEDIMENTARY BASIN ARCHITECTURE - DISCUSSION

The sedimentary basins delineated on the northeastern Canadian polar continental margin, defined by refraction velocity units 4 and 5, are interpreted to consist of strata from four of the inferred stratigraphic megasequences, (2) through (5), described earlier. The sequences include: syn-rift and thermally subsided Sverdrup Basin strata, syn-rift continental margin deposits, post-rift Sverdrup Basin and margin successions, and post-Eurekan deformation units of the continental margin. Asudeh et al. (1989), in their examination of the 1985 refraction data, suggested that the unit 4/unit 5 velocity boundary represented either the break-up unconformity between megasequences (3) and (4) (cf. Jackson, 1988) or the basal unconformity of the post-Eurekan megasequence (5).

The formation of the Princess Margaret arch appears to have taken place primarily during a mid-Eocene phase of the Eurekan Orogeny (Ricketts, 1987; McIntyre and Ricketts, 1989). If the basement uplift seen on profile L-K are Eurekan effects, it follows that the age of these structures is also primarily mid-Eocene. Within the resolution of the seismic model, the complex velocity boundaries underlying unit 5 may indicate mainly post-deformational deposition. Thus, the unit 4/unit 5 boundary may be inferred to be no older than Middle Eocene, perhaps corresponding to the Upper Cretaceous-Lower Tertiary/Upper Tertiary tectonic unconformity separating megasequences (4) and (5).

6. 1990 SEISMIC REFRACTION SURVEY

In 1990, three main refraction profiles and a test line were completed along the Canadian polar margin, using a fixed wing aircraft and three helicopters based at the Canadian Ice Island. Each of the main lines consisted of a 120 km reversed profile, with shots detonated every 30 km along the lines (Fig. 13). Shots were electronically detonated below the sea-ice, with charge weights ranging from 136 kg to 716 kg. Sixty vertical component digital refraction seismographs were deployed on the sea ice at a recorder spacing of 2 km. Offset shots at 30 km increments from the ends of the main profiles were recorded to distances of 200 km to provide information to the depth of the crust-mantle boundary. Seventeen shots were fired into 60 deployed recorders in the three main deployments, and two shots were fired into 15 recorders in the test line, producing a total of 1032 seismograms.

Line A is a 120 km long northwest-southeast trending line between Meighen and Ellef Ringnes islands, with five in-line shots (A2-A6) and three off-end shots (A1, A7 and A8). An initial 30 km test deployment (T1-T2) was recorded between the main line (A2) and the southern off- end shot (A1). Line B is a northeast-southwest trending line that crosses Meighen Island, with four in-line shots (B1, B3, B4 and B5) spread over its 120 km length. One off-line shot (B6) and one off-end shot (B7) were also recorded. Line C is a 120 km long northwest-southeast trending line crossing northern Ellef Ringnes Island, with two in-line shots (C2 and C4) and one shot off the southeastern end of the line (C1).

Three navigation systems were employed in the 1990 survey. Dynamic navigation was accomplished mainly using five Ultra High Frequency transmitters on the Ice Island, Meighen Island, Ellef Ringnes Island, Amund Ringnes Island, and on Axel Heiberg Island, with mobile receivers mounted in the aircraft. Global Positioning System (GPS) receivers were also used extensively in non-differential mode. In addition, the aircraft's Onboard Navigation System was available to complement the other more accurate systems.

The use of GPS receivers and the decreased shot and recorder spacing have made the 1990 data significantly higher resolution than the data from the adjacent 1985 and 1986 Ice Island refraction surveys (see Asudeh et al., 1985; and Asudeh et al., 1986). The refraction lines were positioned to take advantage of existing industry seismic reflection lines and boreholes (Fig. 13). The 1990 survey represents the first continuous detailed seismic refraction data across the transition from the hydrocarbon-rich Sverdrup Basin to the continental shelf.

6.1. SEISMIC REFRACTION RESULTS

Velocity Modelling

The velocity modelling involves matching calculated traveltimes and amplitudes to the observed values for all identified phases. The analysis differs from the modelling of the 1986 data that used the less sophisticated algorithm of Spence et al. (1984). Traveltimes are calculated based

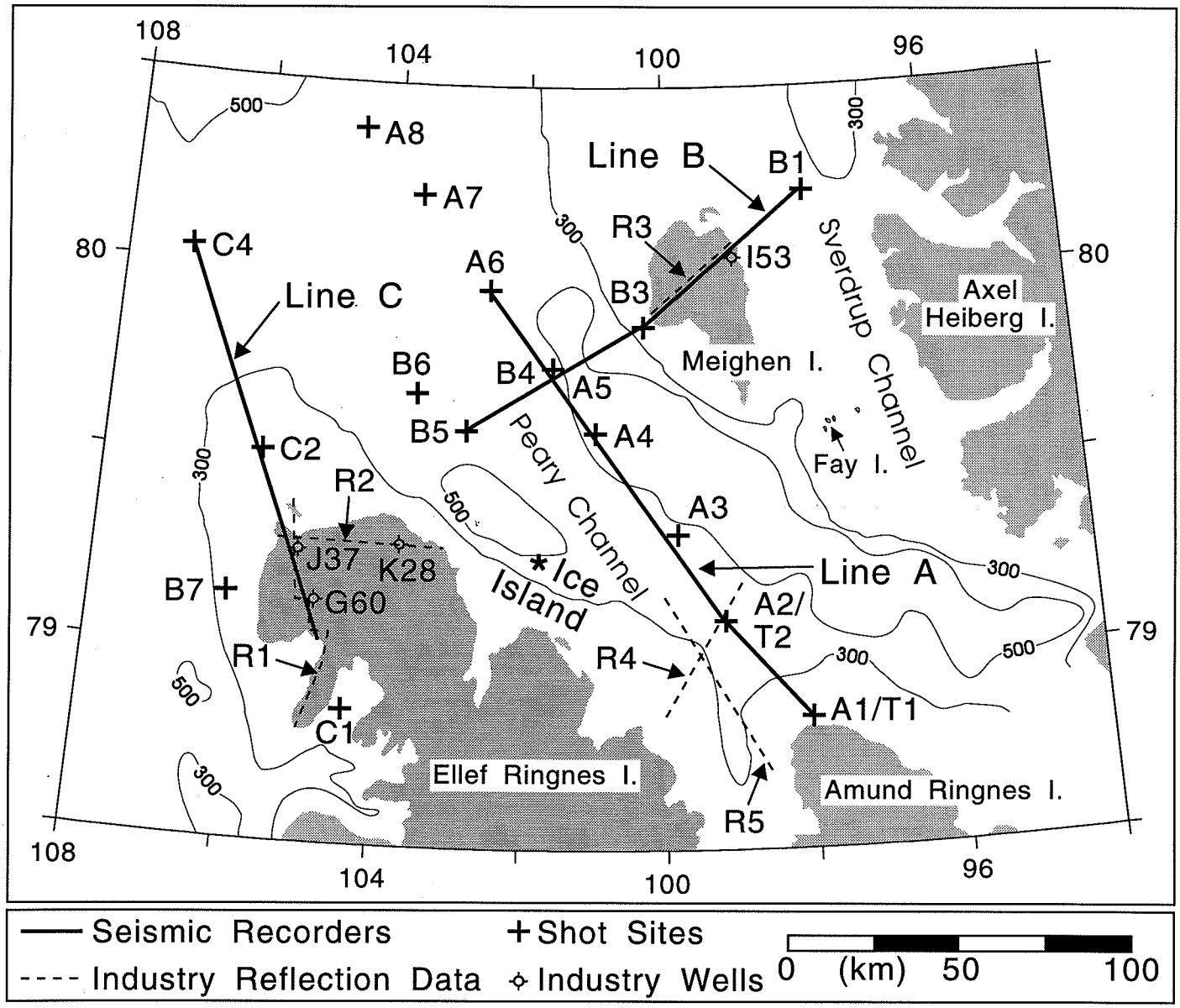

Fig. 13. Detailed location map of the 1990 survey area. Shown are the wide-angle seismic lines and shot sites, and the industry seismic reflection lines and well locations used for upper crustal control. The location of the Canadian Ice Island during the survey is also indicated.

on asymptotic ray theory through a 2-D, isotropic model, made up of velocity layers defined by an arbitrary number of boundary and velocity nodes (Zelt and Smith, 1992). Velocity nodes are defined within the model at arbitrary points along the top and bottom of each layer and a linear interpolation is performed between nodes, allowing both horizontal and vertical velocity gradients, and velocity discontinuities across layer boundaries. A simulation of smooth layer boundaries reduces shadow zones and ray focusing and scattering (Zelt and Smith, 1992). Observed traveltimes and amplitudes are then matched by an iterative combination of traveltime inversion and amplitude forward modelling to derive the P-wave velocity and interface geometry. Using a layer stripping approach, progressively deeper layers are modelled and then held fixed as greater offset data and the next deeper layer are modelled. Although amplitude modelling was used more extensively in the 1990 data analysis than in the 1986 analysis, greater emphasis was still placed on fitting traveltimes due to the sensitivity of amplitudes to small scale heterogeneities, differences in seismometer placements or shotpoints, and the limitation of ray theory (see eg. Mooney, 1983; Cerveny, 1985).

Water Wave Data

An independent check on positions was obtained by studying several seconds of water wave data recorded for each shot. Since the velocity of the water wave is uniform at about 1440 m/s, and the impulsive water wave arrivals can usually be picked to better than 50 ms, it was possible to identify and correct errors in position on the order of 75 m by using the reversed water wave arrival times. This verification was only required for 6 sites north of Ellef Ringnes Island on the final deployment when SYLEDIS reception was often weak.

Observation of the apparent velocity of the water wave on the various sections showed a small difference in velocity between portions of the survey, probably attributable to variations in salinity. The offshore areas covered by lines B and C, and the north end of line A, indicated a water wave velocity of 1.441 km/s, while the area within the islands north of Amundsen Island indicated a velocity of 1.442 km/s. This was confirmed by independent measurements made by R. Perkin, Institute of Ocean Sciences, Sidney, British Columbia during a survey conducted immediately following the refraction operation (R. Perkin, personal communication, 1990).

Features of the Data

In general, the 1990 data is high quality and the phase coherency can be followed confidently across the relevant parts of the sections. Using the procedure outlined above, a total of 1032 seismograms from 18 shots were used to derive the 2-D velocity models. Additional constraints on the shallow structure were provided by coincident industry seismic reflection data and borehole logs (described later), as well as the necessity for the models to agree at their intersection points .

Using both refracted first arrivals and later reflected events, six distinct phases were identified. Representative shots from all three lines are shown in Figs. 14-22 to illustrate a) ray coverage through the model, with every tenth ray shown for clarity; b) recorded seismic data in true relative amplitude with calculated traveltimes to match the identified phases; and c) synthetic amplitudes calculated for the derived model. Insets of specific features of the data are also

shown for some shots. The remainder of the modelled shots are included in Appendix 1. Note the reduction velocity of 6.5 km/s used on most shots, and the reduction velocity of 8.0 km/s used for shot B7 (Fig. 20). Distances used are model distances zeroed at the northern or westernmost shotpoint (ie., A8, B7 and C4 for Line A, Line B and Line C respectively), and offsets are distances relative to individual shotpoints.

The uniform, thin (3-4 m) ice layer introduces a constant and relatively insignificant time error of approximately 1 msec and was not included in the model. At offsets less than a few hundred meters the first arrival is the direct water wave. The water wave was only used to check relative positions, subsequently this high amplitude event was muted to allow resolution of lower amplitude arrivals. At offsets of up to 1-2 km the first arrival is a low amplitude event identified as a longitudinal plate wave generated within the sea ice (Hunkins, 1960). This event was not modelled. Between the water wave arrival and the ice wave arrival is the moderate amplitude refracted arrival from the ocean bottom sediments, identified as P_1. This event emerges as the first arrival beyond 2 km offset because of the rapid attenuation of the ice wave, but it is easily identified at nearer offsets behind the ice arrival due to its relatively high amplitude. At offsets of from 3 km on nearshore shots to 8 km on offshore shots P_2 appears as a moderate to low amplitude first arrival. The crossover to P_3, a generally low amplitude event, occurs at about 12 km offset on nearshore shots and 20 km on the furthest offshore shots. The arrival identified as P_g is an extremely variable amplitude event which is a first arrival from about 20 km to 110 km offset. P_1, P_2, P_3 and P_g together make up the refracted arrivals through the sediment and upper- and mid-crust. The reflection, $P_{lc}P$, from the top of the lower crust appears as a secondary arrival from some shots at about 50 km offset, but the associated refracted event is not evident as a first arrival. P_mP is the high amplitude reflection from the crust-mantle transition (Moho), and is evident on shots with offsets of greater than about 60 km. This arrival is fairly discontinous in nature and exhibits considerable lateral variation in amplitude, indicating that the transition is variable along the profiles. Arrivals from within the mantle, P_n, appear as low amplitude first arrivals beyond about 110 km offset. Following are features of the data specific to individual lines.

Line A

Line A (Figs. 14-17) has a generally high signal-to-noise ratio for all shots, except the two test shots (T1 and T2) which were smaller charges. The thickening of the upper layer from southeast to northwest is evident in the increasing crossover distance of P_1 to P_2 on Figs. 14 and 15 respectively. The P_2 arrival is only present on the southeastern portion of the line to about 100 km distance, beyond which P_1 crosses over to P_3 directly (Fig. 16). The P_g phase is generally coherent and easy to identify, but on shotpoint A6, between 75 and 110 km it is of very low amplitude (Fig. 17 box). When the section is muted and trace normalized (Fig. 17 upper left inset) P_g is resolved as a high frequency event that is of relatively high apparent velocity for this phase. The presence of local dikes or sills might account for these low amplitude, high frequency, early arrivals. A higher amplitude, later event is shown in Fig. 17 (lower right inset) to be well matched by a northerly dipping reflecting boundary at 69-79 km distance and 10.6-12.4 km depth (P_r) or possibly by an ocean bottom multiple of the P_g energy (P_g'). The inset in Fig. 16 indicates that the high amplitude events about 0.75 s behind Pg are probably not related to the $P_{lc}P$ phase, but are better modelled as an ice-seafloor multiple of the P_g phase (P_g'). The clear P_mP phase (Figs. 14 and 17) are well matched by the model.

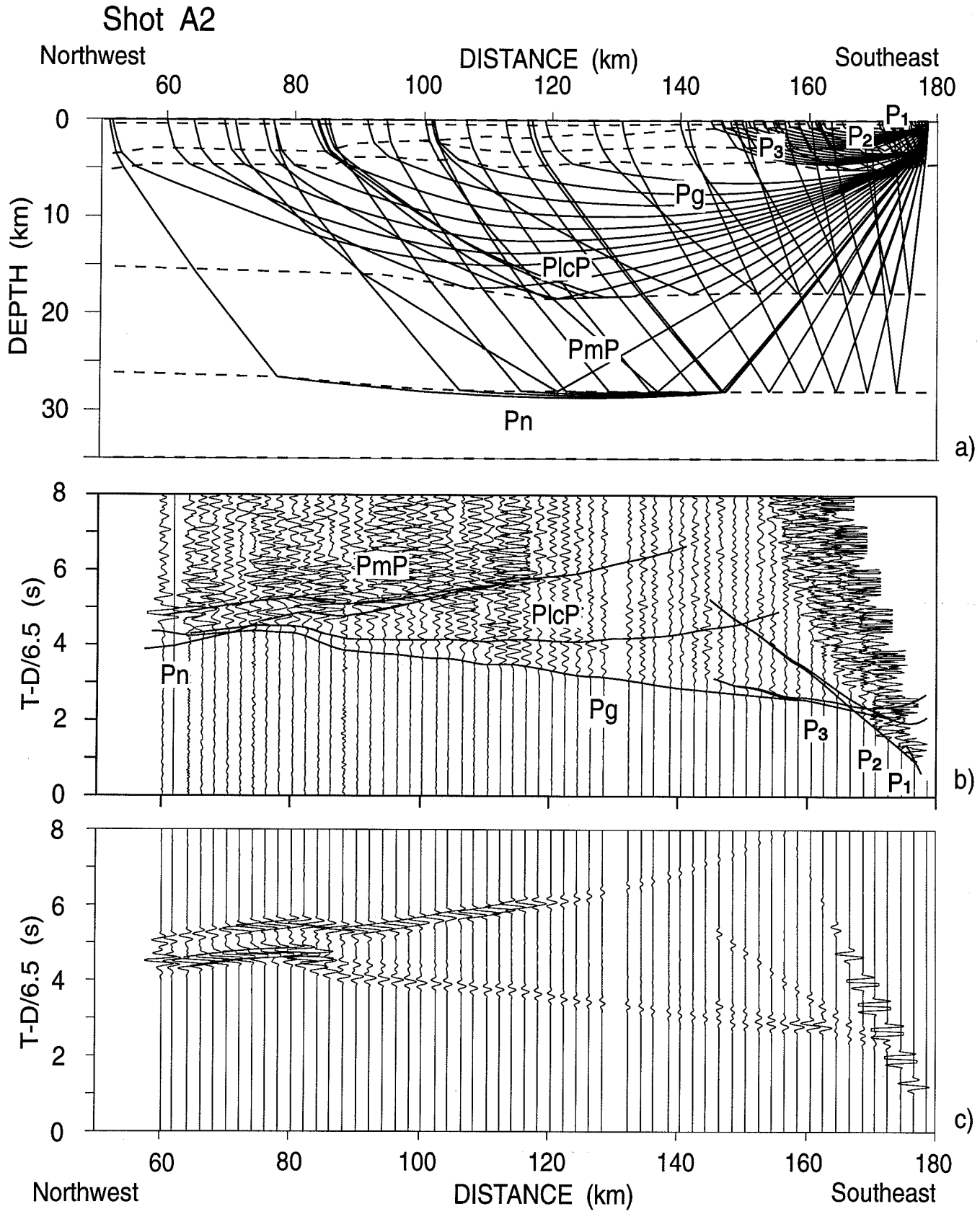

Fig. 14. Modelling results for Line A, shot A2. a) Velocity model with every tenth ray plotted to illustrate ray coverage; b) true amplitude recorded seismic data with traveltime curves calculated through the model (phases are as dicussed in the text); and b) true amplitude synthetic seismograms predicted by the modelling.

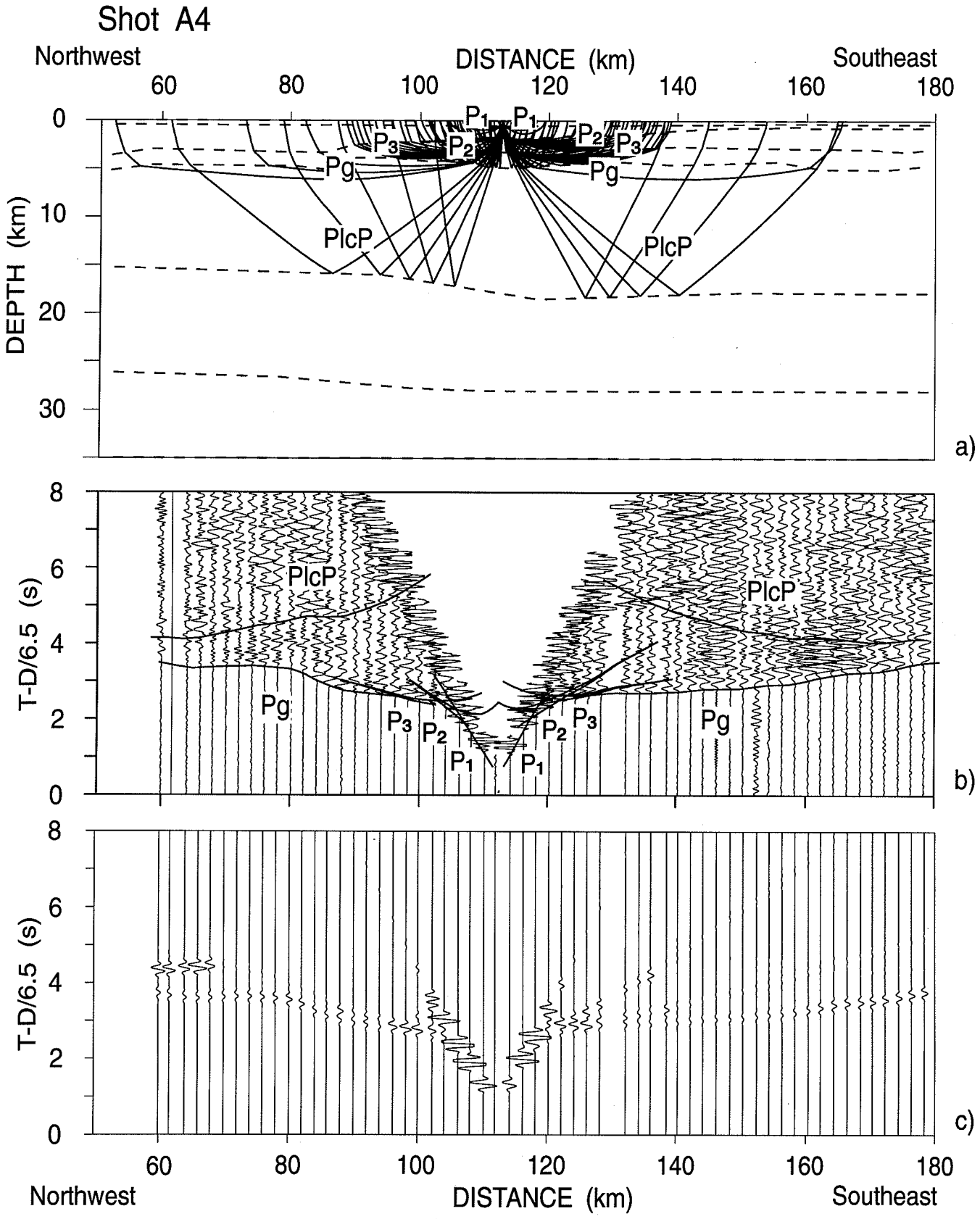

Fig. 15. Modelling results for Line A, shot A4. a) Velocity model with every tenth ray plotted to illustrate ray coverage; b) true amplitude recorded seismic data with traveltime curves calculated through the model (phases are as dicussed in the text); and b) true amplitude synthetic seismograms predicted by the modelling.

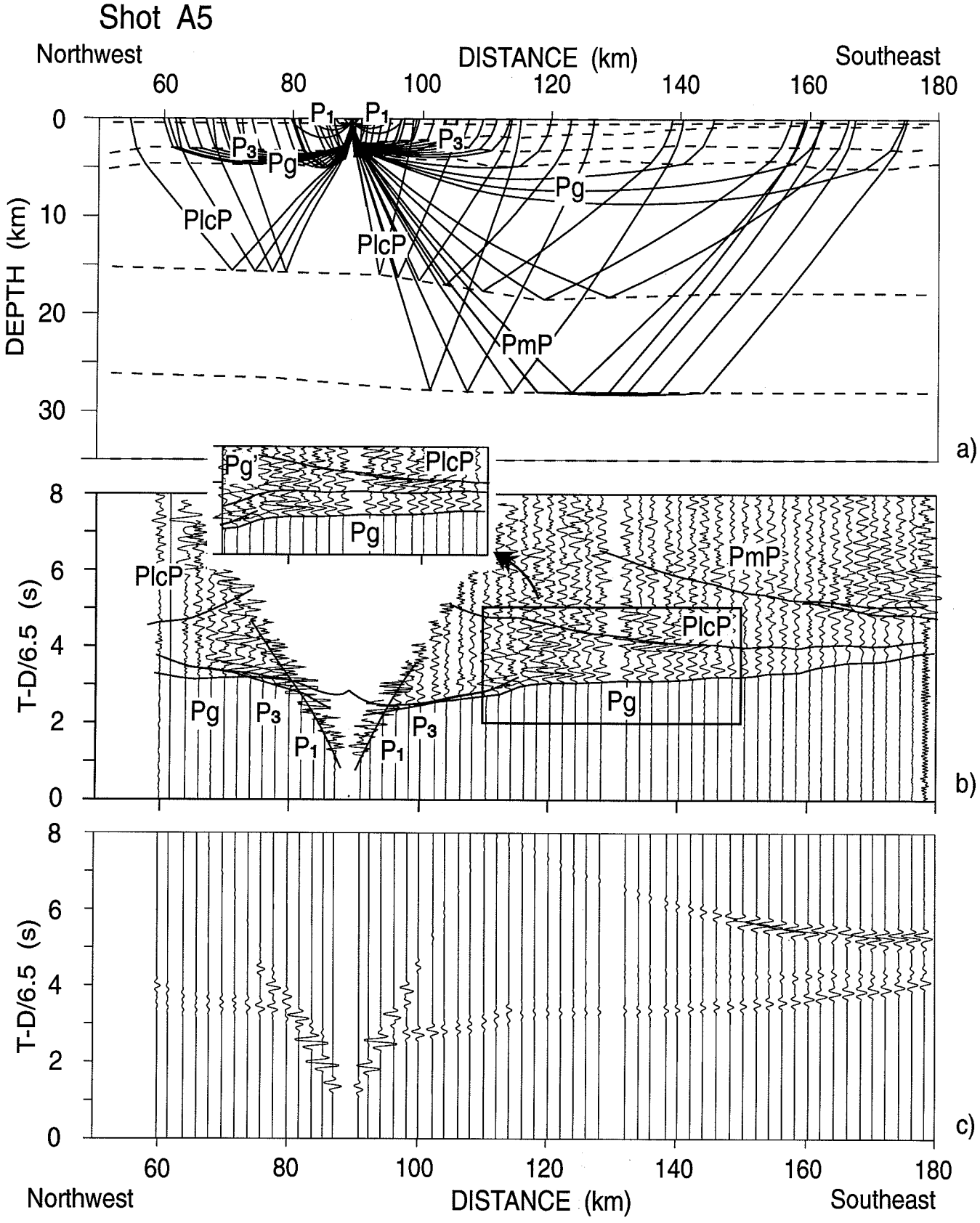

Fig. 16. Modelling results for Line A, shot A5. a) Velocity model with every tenth ray plotted to illustrate ray coverage; b) true amplitude recorded seismic data with traveltime curves calculated through the model (phases and inset are dicussed in the text); and b) true amplitude synthetic seismograms predicted by the modelling.

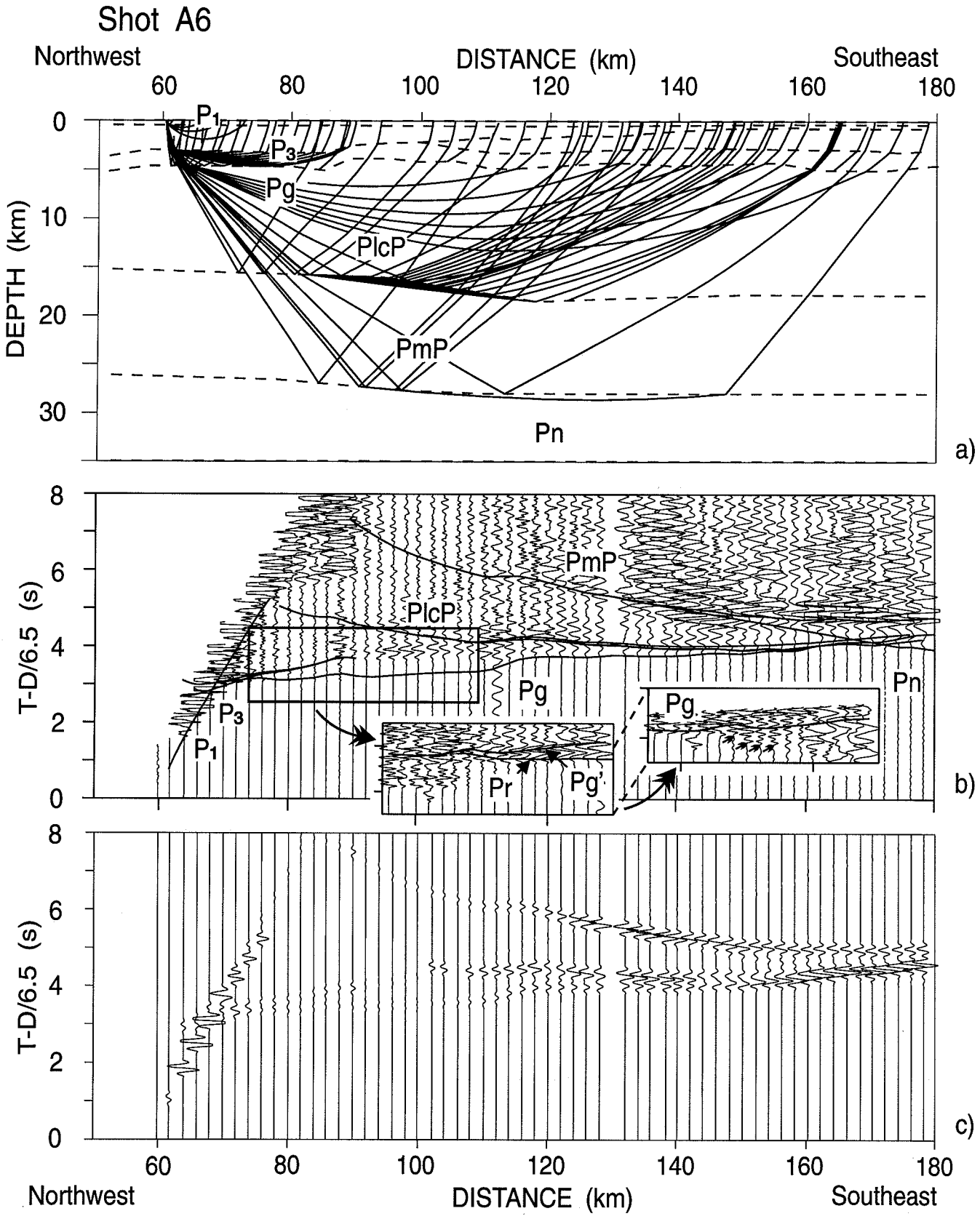

Fig. 17. Modelling results for Line A, shot A6. a) Velocity model with every tenth ray plotted to illustrate ray coverage; b) true amplitude recorded seismic data with traveltime curves calculated through the model (phases and insets are dicussed in the text); and b) true amplitude synthetic seismograms predicted by the modelling.

Line B

A general feature of Line B is the weak arrivals coincident with Meighen Island (Figs. 18-20). A portion of unusually low amplitude P_g is from shotpoint B1 (Fig. 18 box), shown in trace normalized form (Fig. 18 inset) to better illustrate the fit of the predicted traveltime curve to the observed data. These low amplitudes are not well matched by the synthetics, and may be due to a number of possible features that could attenuate energy, including the permafrost structure of the surficial material of Meighen Island. The local thickening of the upper sedimentary layer between 120 and 140 km is clearly shown by the time delay in onset of the P_2 phase in Fig. 19 towards the southwest relative to the northeast. The upper mantle arrival P_n is illustrated in trace normalized amplitude form in the large inset in Fig. 20. The small inset in Fig. 20 shows an interesting high amplitude event at about 10.5 s reduced time which may be due to up-going Moho reflected energy being reflected from the base of the permafrost layer on Meighen Island (P_mP'), but the event is also matched by energy reflected from a boundary within the upper mantle at about 80 km depth (P_1P). The high amplitude of the event and the proximity to Meighen Island suggest that it is more likely that the energy is some form of multiple related to the near surface properties of Meighen Island.

Line C

Line C exhibits a low signal-to-noise ratio for shot C2 (Fig. 21) relative to shot C4 (Fig. 22) due to a reduced charge size (163.2 kg and 380.8 kg respectively), while C1 (Appendix 1) is extremely low due to a possible partial detonation. These factors probably also account for the higher frequency content of C2 relative to C4. The difference in apparent velocity of P_g up-dip (southeast) versus down-dip (northwest) is clearly visible on shot C2 (Fig. 21). The increased thickness of low velocity sediments offshore is illustrated by the increased moveout of P_3 in Fig. 22 relative to Fig. 21. Clear Moho reflections (P_mP) and upper mantle refracted energy (P_n) are visible in Fig. 22.

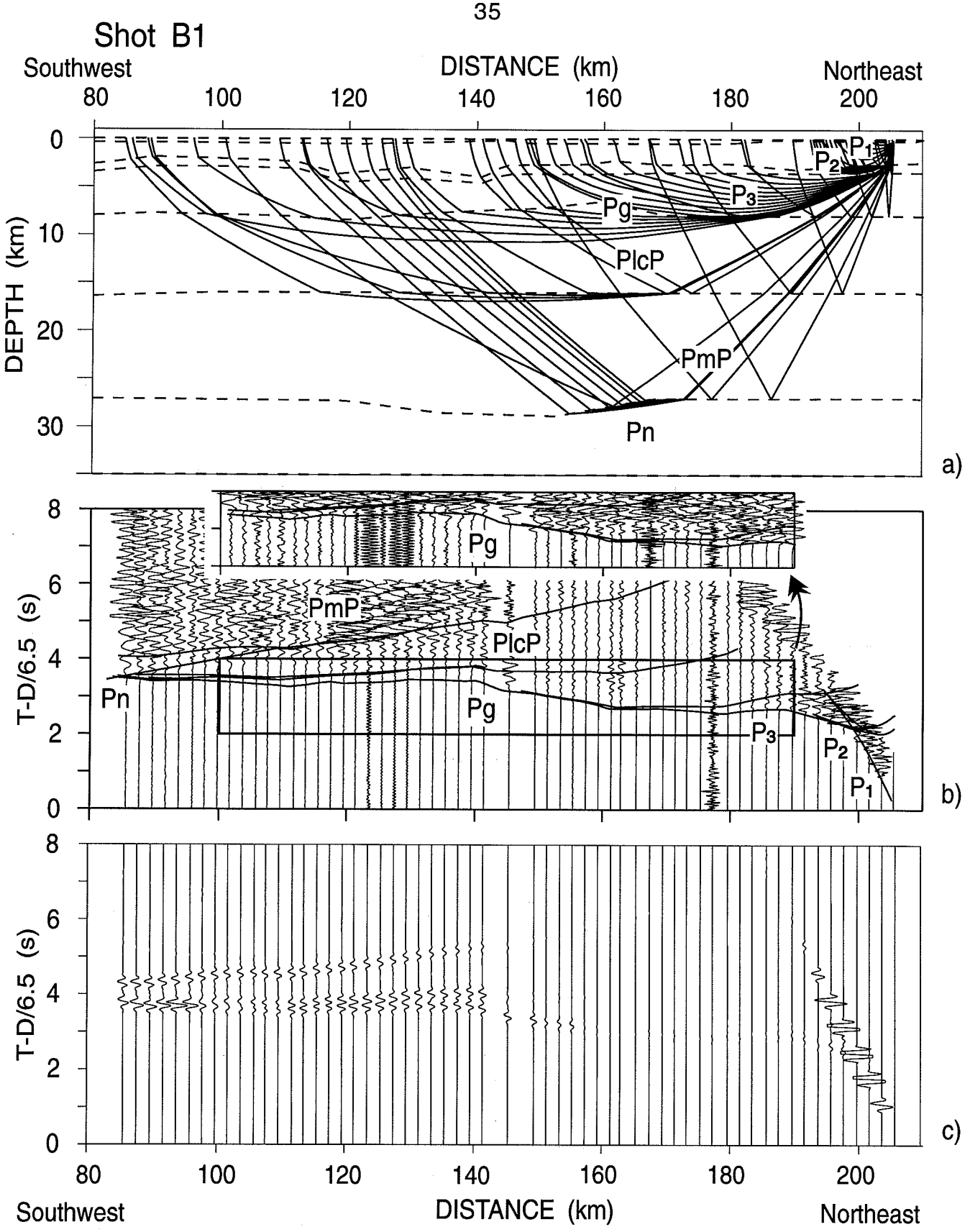

Fig. 18. Modelling results for Line B, shot B1. a) Velocity model with every tenth ray plotted to illustrate ray coverage; b) true amplitude recorded seismic data with traveltime curves calculated through the model (phases and inset are dicussed in the text); and b) true amplitude synthetic seismograms predicted by the modelling.

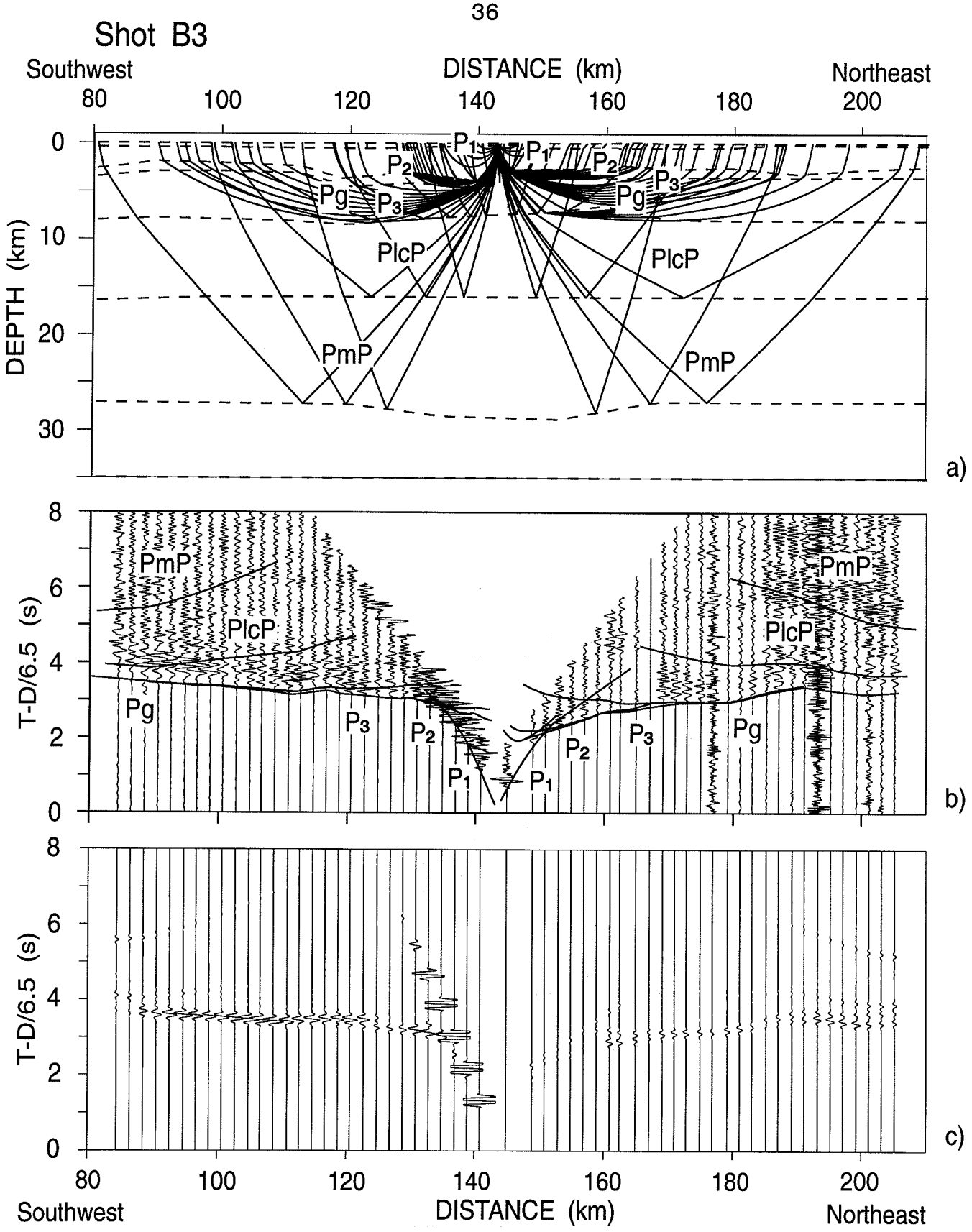

Fig. 19. Modelling results for Line B, shot B3. a) Velocity model with every tenth ray plotted to illustrate ray coverage; b) true amplitude recorded seismic data with traveltime curves calculated through the model (phases are as discussed in the text); and b) true amplitude synthetic seismograms predicted by the modelling.

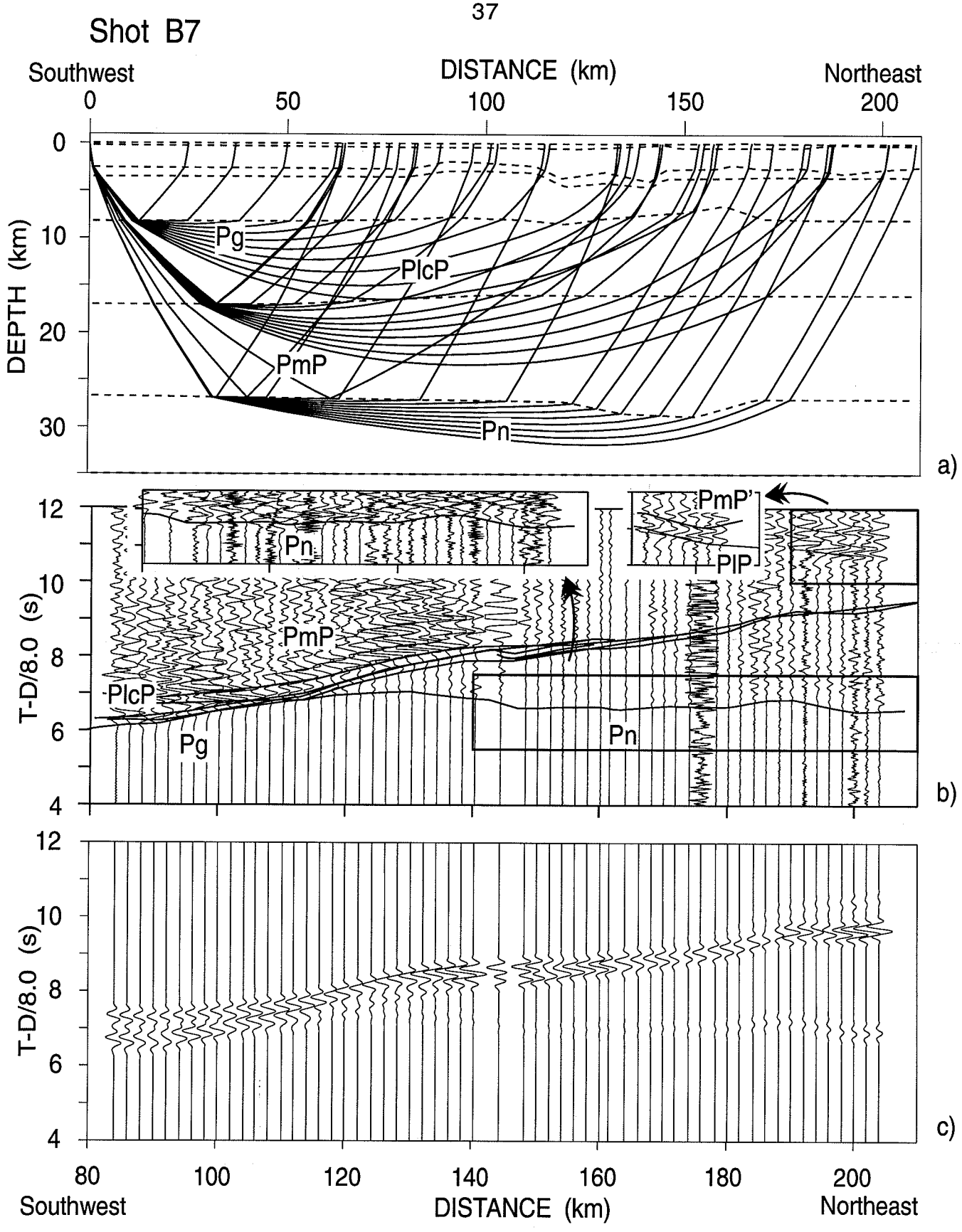

Fig. 20. Modelling results for Line B, shot B7. a) Velocity model with every tenth ray plotted to illustrate ray coverage; b) true amplitude recorded seismic data with traveltime curves calculated through the model (phases and insets are discussed in the text); and b) true amplitude synthetic seismograms predicted by the modelling.

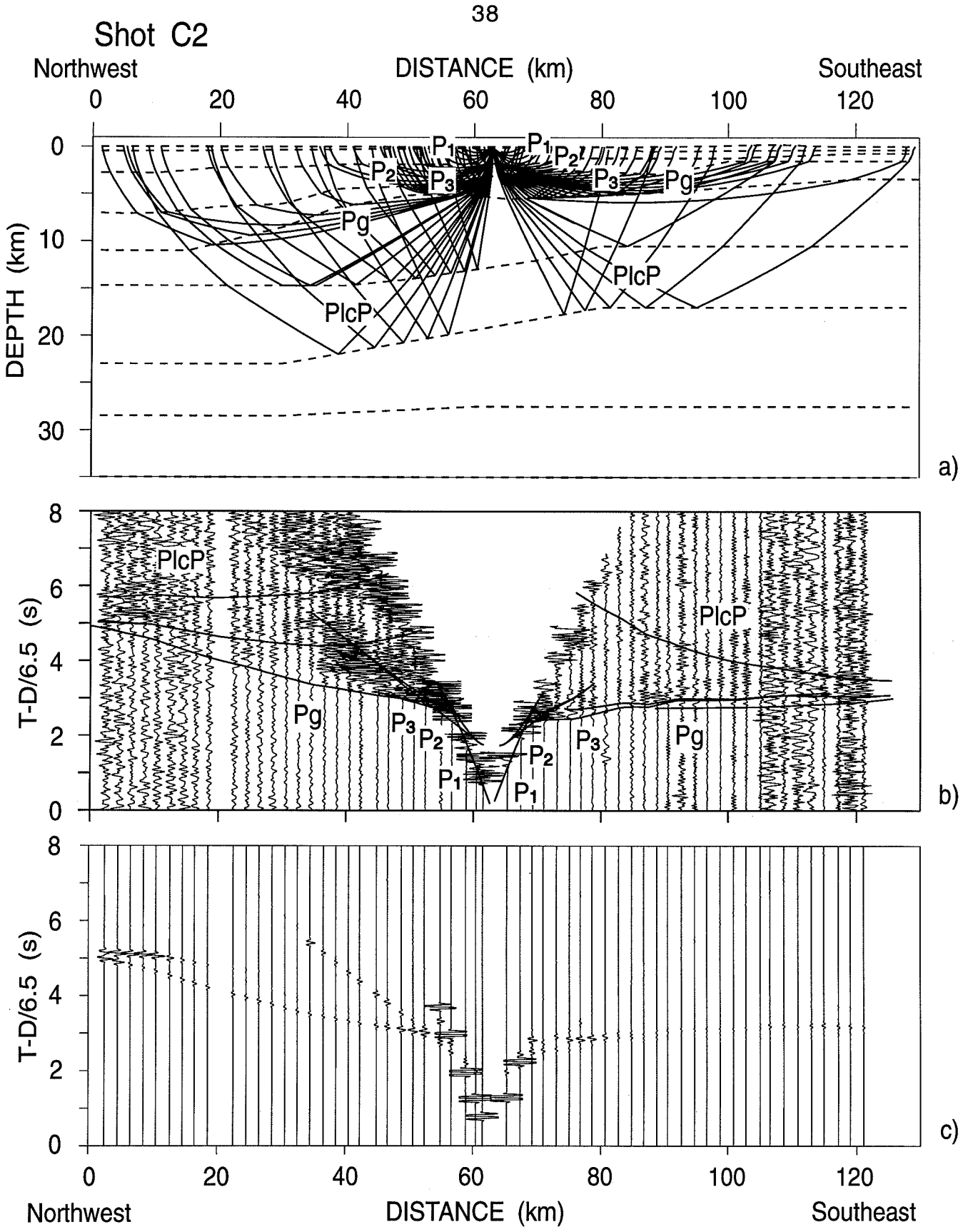

Fig. 21. Modelling results for Line C, shot C2. a) Velocity model with every tenth ray plotted to illustrate ray coverage; b) true amplitude recorded seismic data with traveltime curves calculated through the model (phases are as discussed in the text); and b) true amplitude synthetic seismograms predicted by the modelling.

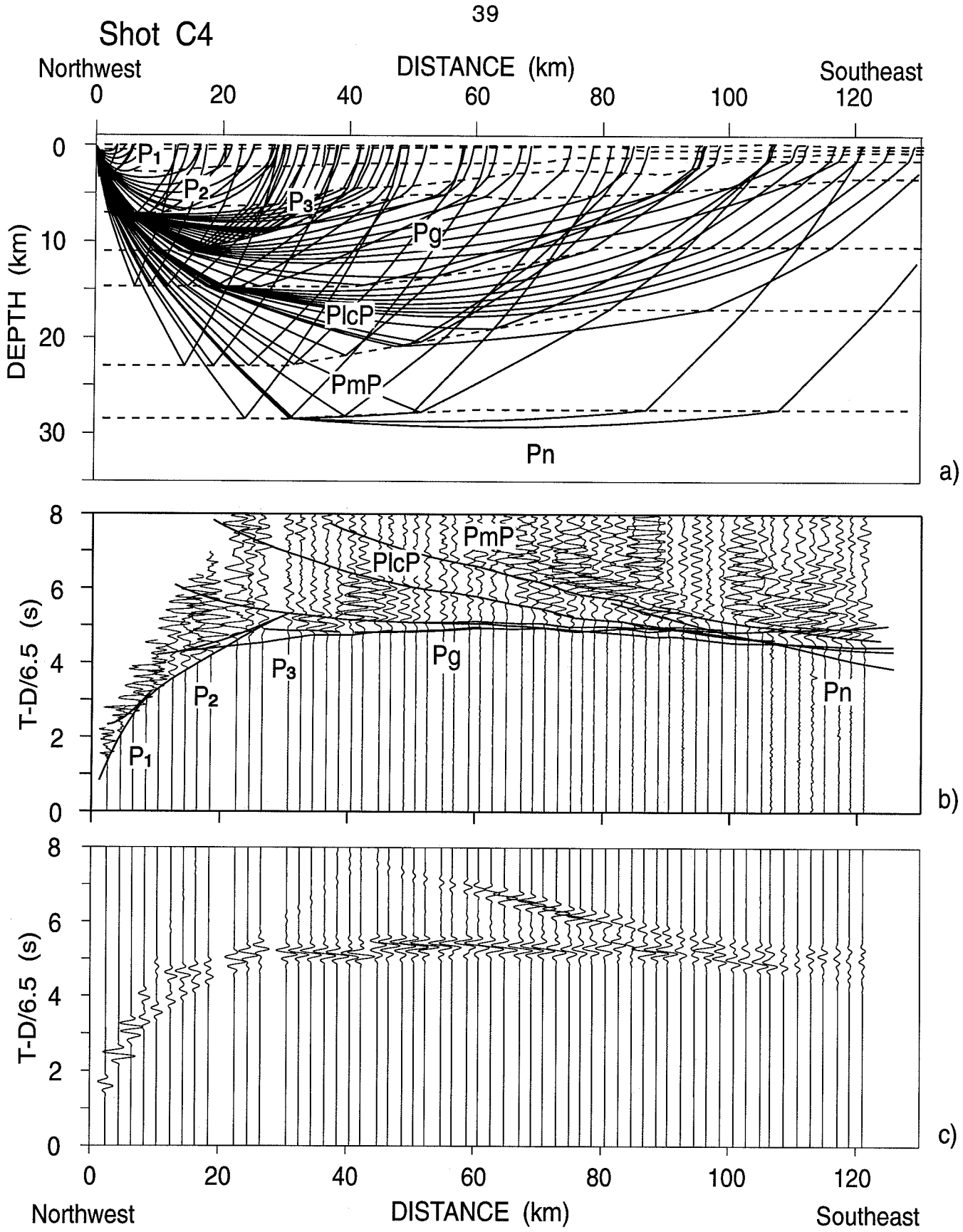

Fig. 22. Modelling results for Line C, shot C4. a) Velocity model with every tenth ray plotted to illustrate ray coverage; b) true amplitude recorded seismic data with traveltime curves calculated through the model (phases are as discussed in the text); and b) true amplitude synthetic seismograms predicted by the modelling.

Crustal Velocity Structure Models

Deriving a model to fit at the intersections of Line A and Line B, and of Line B and Line C provides additional constraints on the velocity structure (Fig. 23). The velocity-depth models derived from raytracing are shown in Fig. 24 and are discussed below for each line.

Line A

The velocity model for Line A is shown in Fig. 24 (top). The top layer in the model is a water unit with a velocity of 1.44 km/s and a thickness constrained by avaliable bathymetry information (CHS chart 7953). Below this is a high gradient (~0.5 s^{-1}) unit with a velocity of 1.8-2.2 km/s representing unconsolidated sediments. The sedimentary package thins from north to south, with a thickness of almost 8 km at the northern end of Line A and eventually pinching out near the southern end. A southward thickening wedge of sedimentary material with a velocity of 3.2-3.8 km/s pinches out at 100 km, creating an angular unconformity with the overlying unit. A thin 5.0-5.2 km/s layer underlies these sedimentary packages. The 5.0-5.2 km/s material overlies, and generally follows the structure of, a thicker unit with a velocity of 5.1-6.2 km/s. These units rise steeply towards the south, flattening out at about 60 km before rising again sharply at about 90 km. This second rise takes the form of a 20 km wide 2 km high arch, south of which the units are relatively flat. Underneath is a 6.4-6.6 km/s layer which rises towards the north from 17 to 15 km depth. The bottom layer of the model is an 8.1-8.2 km/s layer which is at about 28 km depth to the south and rises slightly towards the north to 26 km depth.

Line B

The velocity model for Line B is shown in Fig. 24 (middle). The uppermost model layer represents seawater with a velocity of 1.44 km/s and a thickness constrained by avaliable bathymetry information (CHS chart 7953 and unpublished CHS bathymetry information used by permission). Over Meighen Island the water layer gives way to a permafrost layer of 3.9 km/s, with velocities constrained by well logs and reflection data, but unconstrained by first arrival refraction data. Below this, lie unconsolidated sediments with a high gradient (~0.5 s^{-1}) and a velocity of 1.9-2.3 km/s, creating local low velocity zones beneath the higher velocity permafrost. Parallel to the shelf the 1.6-2.3 km/s material has a generally uniform thickness of about 2.5 km, with local deviations of +/- 1.5 km along Line B. No 3.2-3.8 km/s unit is apparent on Line B. A thin 5.0-5.6 km/s layer underlies these sedimentary packages. The 5.0-5.3 km/s material overlies, and generally follows the structure of, a thicker unit with a velocity of 4.9-6.1 km/s. This package has a broad arch from 80 to 120 km with about 1.5 km of relief. Further east the structure increases in complexity, but decrease in amplitude and wavelength, with a low occuring immediately west of Meighen Island. A layer of 5.9-6.5 km/s material lies below these two units. It is generally flat lying except for a 2 km high rise centred at 160 km. Below this unit is a 6.3-6.8 km/s layer which is essentially horizontal at 16-17 km depth. At the base of the model is a 7.9-8.2 km/s layer which is at about 28 km depth and is relatively flat except for a 40 km wide 1.5 km deep depression centred at about 140 km.

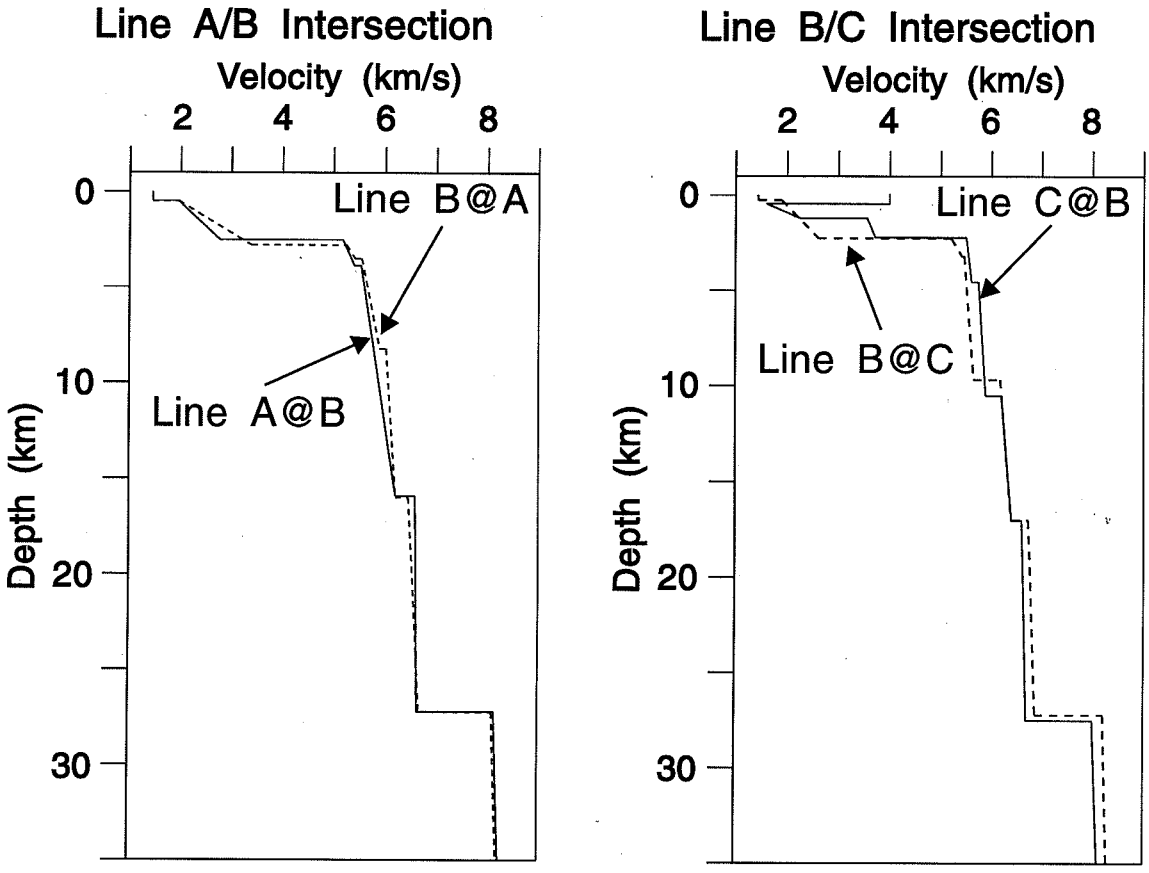

Fig. 23. Velocity-depth profiles of the models at the intersection of Line A and B and of Line B and C. The poor fit of the Line B and C profiles in the upper portion is due to the high velocity permafrost on Ellef Ringnes Island not being a modelled element on Line B because no seismic recorders were present in this region of the line.

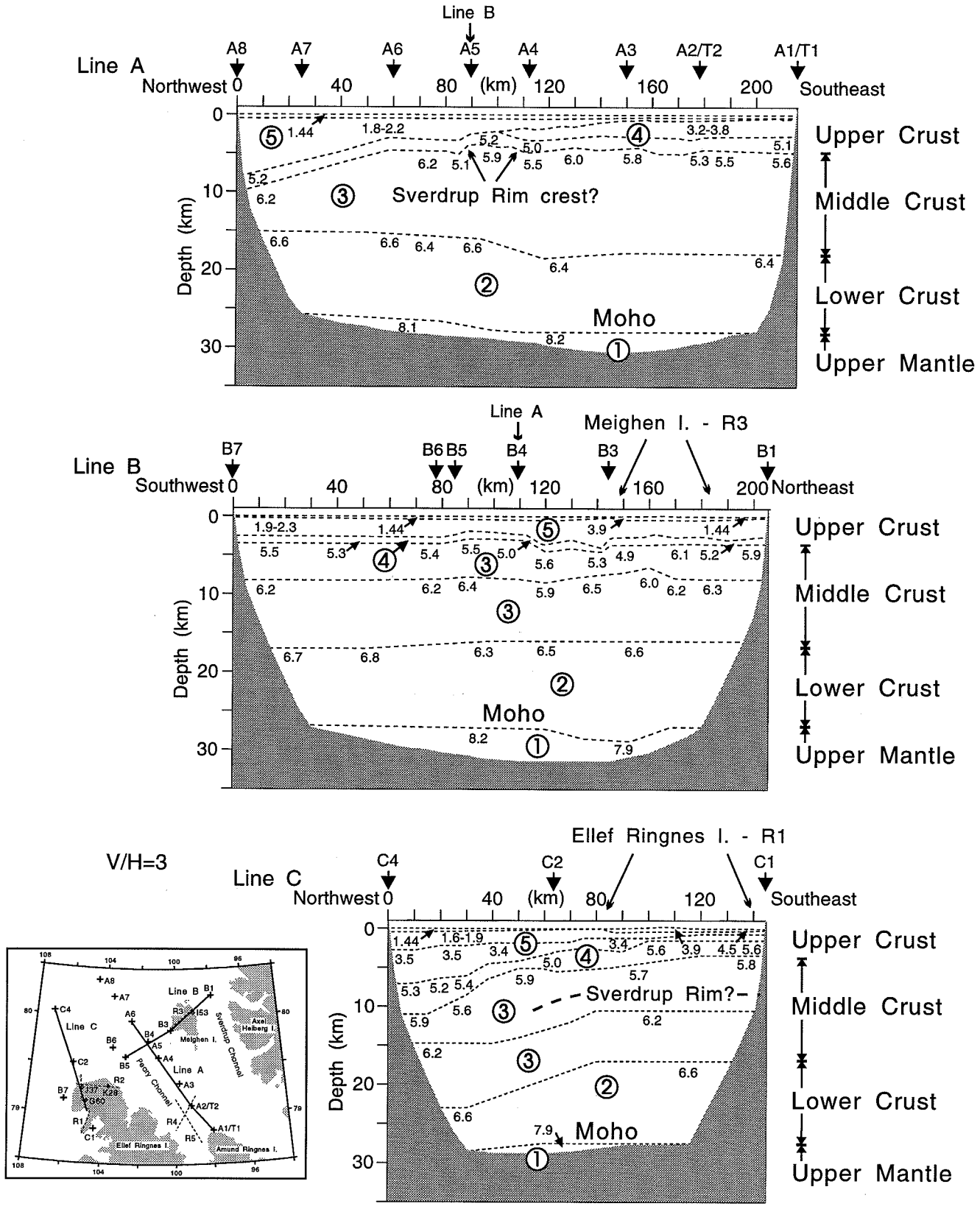

Fig. 24. Velocity-depth models for Line A, B and C derived from raytrace modelling of the wide-angle seismic data. Velocities in km/s are shown at their appropriate locations. Circled numbers represent interpreted stratigraphic units as discussed in the text. The model layers have been grouped into upper, mid, and lower crust, and the Moho marks the junction between crust and upper mantle. Note vertical exagerration of 3.

Line C

The velocity model for Line C is shown in Fig. 24 (bottom). A layer representing seawater with a velocity of 1.44 km/s and a thickness constrained by avaliable bathymetry information (CHS chart 7953) is at the surface. Over Ellef Ringnes Island the water layer gives way to a permafrost layer of 3.9-4.5 km/s, with velocities constrained by well logs and reflection data, but unconstrained by the refraction data because of the lack of any first arrivals from this layer. Below this is a high gradient (~0.5 s-1) unit with a velocity of 1.6-2.3 km/s representing unconsolidated sediments, creating local low velocity zones beneath the relatively high velocity permafrost. A local velocity discontinuity exists between the 1.6-2.3 km/s layer and the underlying 3.4-3.5 km/s unit, whereas on Lines A and B similar velocities are encountered at the base of the high gradient layer with no discontinuity suggested. The 1.6-2.3 km/s package thins from north to south, with a thickness of 7 km at the northern end of Line C, eventually pinching out near the southern end. A southward thickening of the 3.4-3.5 km/s unit, at 100 km, appears to correspond to the wedge of similar velocity material on Line A. Below is a thin 5.0-5.6 km/s layer. The 5.0-5.6 km/s material overlies, and generally follows the structure of, a thicker unit with a velocity of 5.6-5.9 km/s. These two units rise steeply towards the south, flattening out at about 60 km before rising again sharply at about 90 km and flattening out at the top of a 3 km rise. A layer of 6.2 km/s material lies below. It is horizontal at 15 km depth from 0 to 40 km and then rises steeply to flatten out at 11 km depth at 80 km. Below this unit is a 6.6 km/s layer which rises towards the south from 23 to 18 km depth. The deepest layer in the model is a 7.9 km/s layer which is at about 28 km depth and dips slightly towards the north to 29 km depth.

Velocity Interpretation

The velocity layers in Fig. 24 have been assigned to the tectonostratigraphic units in Table 1 based on available geological and geophysical information, including surface mapping, borehole logs, and interpreted seismic reflection data. The southward thinning wedge of 1.6-2.3 km/s material, as well as the 3.4-3.5 km/s material on Line C, are interpreted as Uppermost Cretaceous and Tertiary sediments of the Arctic Continental Terrace Wedge (unit 5). On Line A this gives way to the southward thickening wedge of 3.2-3.8 km/s sediment which comprises the Triassic section of the Sverdrup Basin deposits (unit 4). Below these on all three lines, Upper Paleozoic and Mesozoic material with a velocity of 5.0-5.6 km/s represents the remainder of the Sverdrup Basin sediments (unit 4). Underlying the sediments is the 4.9-6.2 km/s layer representing Lower Paleozoic Franklinian basement rocks (unit 3). The 5.9-6.5 km/s unit which occurs below on Lines B and C is also interpreted to be part of the Lower Paleozoic basement (unit 3). The 6.3-6.8 km/s layer is interpreted as Precambrian craton (unit 2). Below this, the Moho separates the crustal succession from the upper-mantle with a velocity of 7.9-8.2 km/s (unit 1).

In addition, the model layers have been subjectively grouped into upper, middle, and lower crust based on the velocity structure (Fig. 24). The seafloor sediments of the Arctic Terrace Wedge and the Sverdrup Basin together make up the upper crust. The middle crust is composed of the underlying Franklinian basement rocks. Below these, the Moho marks the transition from lower crust to upper mantle material.

TABLE 1 - 1990 Velocity Interpretation

Model Unit	Velocity (km/s)	Interpreted Stratigraphic Unit
5	1.6-3.5	Tertiary-U. Cretaceous
4	3.2-5.6	Cretaceous + Jurassic-U. Paleozoic
3	4.9-6.5	L. Paleozoic-U. Proterozoic
2	6.3-6.8	L. Paleozoic-Proterozoic (crystallines)
1	7.9-8.2	Upper Mantle

The velocity models in Fig. 24 illustrate the velocity-depth node structure used to model the interpreted phases. The velocity fields of the models were then sampled and isovelocity contours were plotted at 0.5 km/s intervals to better illustrate the nature of the 2-D velocity field along the lines (Fig. 25). The velocity contours may be better structural indicators than the velocityn ode structure, as the contours illustrate the lateral and vertical changes in velocity. Although the general features of the velocity node structure are maintained, significant velocity variation becomes immediately apparent from the contoured sections, especially in the mid to lower crust. Unfortunately, the contouring algorithm can not contour low velocity zones, which creates an artificial pull-up of contours and a masking of structure within low velocity regions, such as the local areas beneath permafrost. In the upper crust, short wavelength (~10 km) features are evident on the southern portion of Line A, as well as pull-up of contours below high velocity permafrost regions on Lines B and C (Fig. 25). In the mid to lower crust, extensive velocity structure is revealed, especially on Lines A and B where features with wavelengths of 20-30 km, and amplitudes of greater than 10 km, are indicated. A prominent velocity low is evident on Line A at 90 km distance, flanked on either side by local highs. This feature appears to penetrate to lower crustal depths. No significant Moho and upper mantle structure is apparent. The models for all three lines are shown in coloured contour format as a fence diagram in Fig. 26 to better illustrate the three dimensional nature of the velocity structure of the survey area.

A number of general statements can be made about the crustal structure (Figs. 24 and 25) within the study area. The upper crust has an average thickness of 4-5 km on the continental shelf, but thickens steeply to at least 10 km on the margin. Within the upper and middle crust there are a number of velocity features with wavelengths and amplitudes generally decreasing towards the east and south. The coincident reflection data indicates that these features are even more complex than the wide-angle models suggest. The base of the middle crust occurs at about 17 km on the shelf and 15 km northwest of Meighen Island (Line A), but reaches a depth of 23 km north of Ellef Ringnes Island (Line C). The contrasting character of these units, between Line A and Line C, suggests that a strong three dimensional component to the margin is present in this area. The structure of the middle and lower crust is followed in a muted fashion by the Moho and upper mantle as the total crustal thickness of about 28 km on the shelf thins to 26 km in the northeast, but thickens to 29 km in the northwest. The 1.5 km deep, 40 km wide, depression below Meighen Island is the only apparent structure on the Moho, and no crustal root is evident beneath the Sverdrup Rim. The minimum and maximum crustal thicknesses of 26 and 29 km, respectively, indicate that the surveyed area is transitional between continental and oceanic crust.

Model Limitations

The upper crust is well constrained by fully reversed first arrivals and reflected events, but with increasing depth and proximity to the ends of the lines the resolution decreases. For the off-end shots, in the regions beyond the recorder spread, no direct arrivals from the upper crust were recorded, so upper crustal velocities were held constant and layer depths were determined by

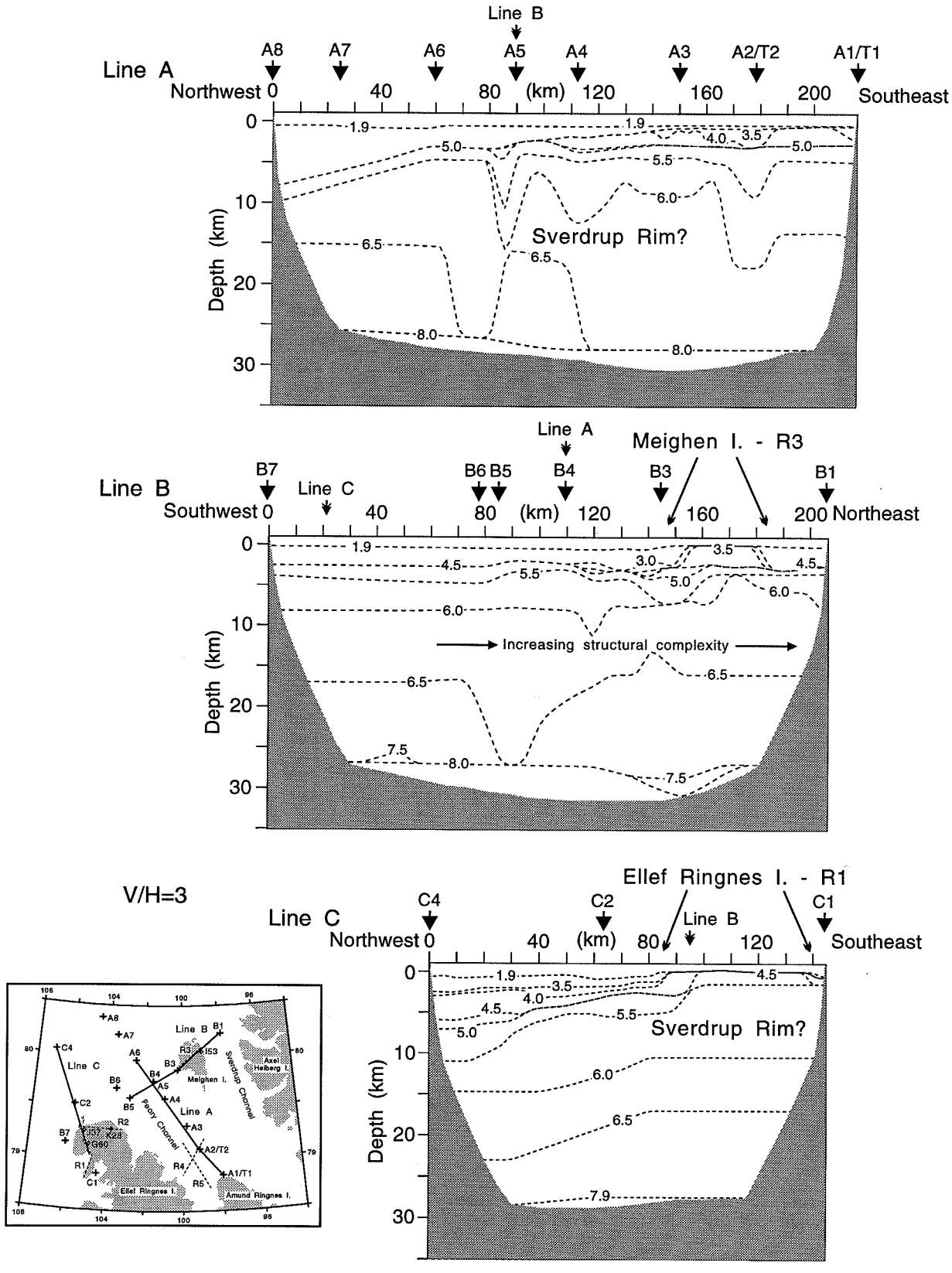

Fig. 25. Velocity-depth contoured models for Line A, B and C derived from raytrace modelling of the wide-angle seismic data. Contour velocities are shown in km/s. Note vertical exagerration of 3.

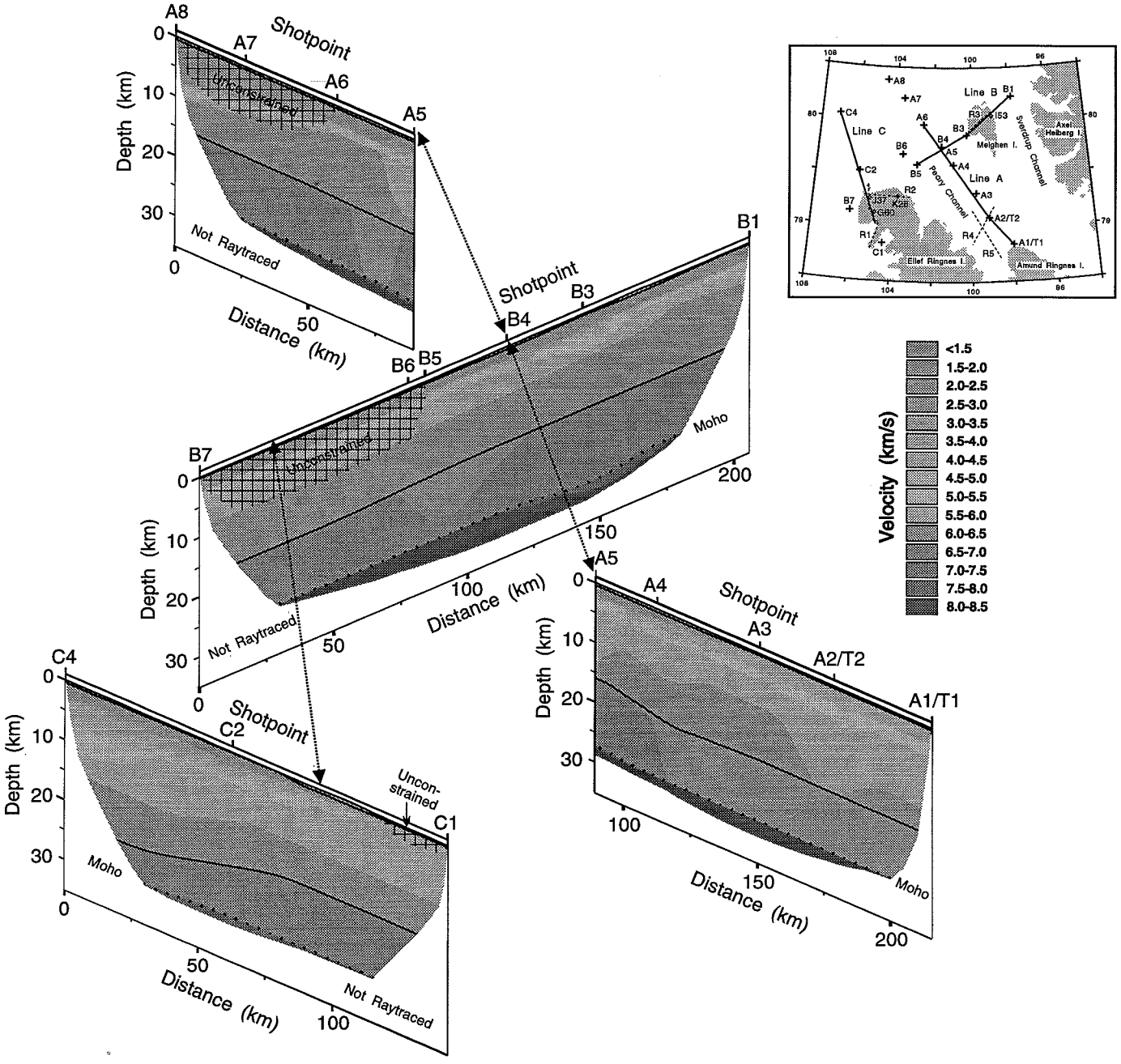

Fig. 26. Fence diagram of the 1990 wide-angle velocity models, contoured at 0.5 km/s intervals. Within the models the solid lines separate the middle and lower crust, and the dotted line represents the Moho, separating the lower crust and upper mantle. Both of these velocity discontinuities were identified by reflected energy within the wide-angle data. Unconstrained regions are areas of the model from which no direct arrivals were recorded, and regions identified as not raytraced were areas not sampled by any rays traced in the modelling process.

matching the observed delay in the middle and lower crustal arrivals. Tables 2-4 summarize the modelling results for all three lines. The uncertainties of the travel-time picks averages from +/- .03 s for the mainly first arrival upper crustal refracted phases to +/- .05 s to .10 s for later, often longer period, arrivals sampling lower midcrust to Moho depths. The RMS traveltime residual between the observed traveltime picks and the predicted times from the final model are similar in value or slightly higher than the average pick uncertainty. The corresponding chi-squared values (X^2) are greater than 1 indicating that, although the data are of high quality and the uncertainties are small, the model is underparameterized, i.e. the true nature of the crust is more complex than modelled and has shorter wavelength structural heterogeneities or lateral velocity changes that are not resolved by the data (Zelt and Smith 1992). This is particularly true for the upper mantle of Line B (Table 3) with a X^2=4. Together with the similar values for average uncertainty and RMS traveltime residuals, the X^2 values >1 indicate we have conservatively chosen a model that provides a reasonable trade-off between traveltime residual and parameter resolution that allows rays to be traced to all observations and simultaneously provides amplitude estimates. Tests of parameter consistency by perturbing velocity and depth values while retaining an acceptable fit to traveltime and amplitude estimates (Zelt and Smith 1992), suggest uncertainties that range from of 0.1-0.3 km/s for velocities and from +/- 0.2 km (upper crust) to 2.0 km (Moho) for depths. These values are typical for similar crustal profiles (Zelt et al. 1992; Zelt and Forsyth, 1994). Tables 2-4 provide a statistical measure of model fit, however, it is more difficult to quantify the uncertainty associated with the more subjective classification of arrivals from the lower crust. While the arrivals from the lower crust and Moho are more limited (Tables 2-4), the coherency of phases $P_{lc}P$ and P_mP (e.g., Fig. 14) and the better constrained overlying model suggest the depths are reasonable minima.

6.2. CONTINENTAL MARGIN CRUSTAL STRUCTURE

The continental margin crustal structure in the survey region has been influenced by four main episodes of uplift and deformation. The first is the Ellesmerian Orogeny during the Late Paleozoic; the second is the Late Cretaceous uplift that formed the Sverdrup Rim; the third is the Middle Jurassic-Early Cretaceous continental rifting that formed the Canada Basin; and the fourth is the Eurekan Orogeny during the Early Tertiary. The first two events were predominantly north-south directed compression, creating east-west striking structures, and the third event was north-south dilation. The fourth event - the Eurekan Orogeny - resulted from the impingement and consequent squeezing of Ellesmere Island by Greenland, forming northerly trending features, such as major thrusts on Axel Heiberg Island and Cornwall and Princess Margaret arches. The transition between these two trends appears to occur in the Meighen Island region, with the east-west trending structures dominating to the west and the northerly striking features dominating to the east, suggesting Eurekan deformation was effective westward to Meighen Island.

The presence of a complex crust is indicated on both lines A and B, while line C suggests a more uniform, gently seaward-dipping crust is present towards the west. This indication of increasing structural complexity towards the east is consistent with tectonic models for the region, which suggest that Eurekan (Tertiary) deformation diminishes westward from Ellesmere Island.

TABLE 2 - Line A Modelling Results

Phase	Number of picks	Average uncertainty (s)	RMS traveltime residual (s)	X^2 fit
P_1	14	0.021	0.028	1.915
P_2, P_3, and P_g	364	0.041	0.057	1.897
$P_{lc}P$	55	0.106	0.119	1.933
P_mP	111	0.092	0.101	1.781
P_n	58	0.066	0.083	2.029

TABLE 3 - Line B Modelling Results

Phase	Number of picks	Average uncertainty (s)	RMS traveltime residual (s)	X^2 fit
P_1	19	0.022	0.039	2.603
P_2, P_3, and P_g	221	0.038	0.053	2.579
$P_{lc}P$	32	0.070	0.080	1.865
P_mP	94	0.078	0.080	1.239
P_n	43	0.045	0.071	4.017

TABLE 4 - Line C Modelling Results

Phase	Number of picks	Average uncertainty (s)	RMS traveltime residual (s)	X^2 fit
P_1	16	0.024	0.039	1.669
P_2, P_3, and P_g	88	0.046	0.063	2.247
$P_{lc}P$	7	0.075	0.085	1.127
P_mP	50	0.072	0.072	1.717
P_n	5	0.060	0.059	1.648

6.3. SVERDRUP RIM - DISCUSSION

A dominant structural feature in the central portion of the eastern Arctic islands region is the Sverdrup Basin, a 1200 km long, 400 km wide, generally east-west trending structural depression. Hea et al. (1980) classify the Sverdrup Basin as a succesor basin based on the presence of the underlying pre-existing Franklinian Basin, and as a marginal basin due to its location on the edge of the craton. The basin was formed by thermal subsidence following Late Carboniferous to Early Permian continental rifting and contains up to 12 km of Upper Paleozoic and Mesozoic strata (Harbert et al., 1990). A major northeast trending system of dykes and normal faults that may characterize the development of an incipient rift during the Early Cretaceous, extends into the study area from the southwest (Forsyth et al., 1979; Balkwill, 1982).

The northern limit of the Sverdrup Basin is described by Sweeney et al. (1990) as a broad arch structure - the Sverdrup Rim - which trends east-west across northern Ellef Ringnes Island. Various northeastward extensions of the rim, past Meighen Island, have been proposed. The geological history of the structural arch that forms the rim itself is quite complex. Sweeney et al. (1990) suggest that regional uplift took place in latest Cretaceous time, but that uplift and subsequent erosion for Meighen Island probably occurred in pre-Late Cretaceous time. They postulate that the uplifted Sverdrup Rim began to collapse during the Late Maastrichtian, while coeval Eurekan tectonism was producing uplift and erosion of Sverdrup Basin and older material in the region. This material was predominantly transported northwestward where it was deposited and forms the seaward thickening Arctic Continental Terrace Wedge (Sweeney et al., 1990). Over the crest of the Sverdrup Rim, they note that the Upper Paleozoic and Mesozoic sediments (the Sverdrup Basin strata) overlie the older units (the Franklinian strata) unconformably, and appear to be less than 4 km thick.

The seismic refraction models support the presence of a structural high that is cored by Franklinian Basin (Lower-Middle Paleozoic) rocks, separating the Arctic coastal Basin and Sverdrup Basin, and interpreted to be the Sverdrup Rim. On Line C (Fig. 24) the structural high occurs at 100 km distance, 15 km south of the northern shore of Ellef Ringnes Island. It appears to have a steep northern flank, but Line C does not appear to cross the Rim's southern flank. On Line A the top of the Rim occurs at 90 km distance and is characterized by a local arch structure with a steep northern flank, a shallower southern flank and a flat crest of 10 km width. Total relief of the local high is 1.5 km on both lines. Line B appears to run along the general crest of the Sverdrup Rim and illustrates the lateral complexity approaching Axel Heiberg Island. The velocity structure indicates lateral variations with a typical wavelength of 10-20 km and topography of 2-3 km within the upper crust (Fig. 24). The Sverdrup Rim appears to commonly have a steep and complex northern flank, and a shallowly dipping, less complex southern flank. From west to east the Rim becomes increasingly complex, probably due to the increasing effects of Eurekan deformation towards Axel Heiberg Island, as the Rim becomes overprinted by other structures.

The velocity-depth profiles in Fig. 27 illustrate the transition along Line A from continental shelf structure to the north (a), across the Sverdrup Rim (b) to the Sverdrup Basin (c). The continental shelf at 30 km model distance is characterized by 5 km of low velocity sediment (Fig. 27a), while the Sverdrup Rim (Fig. 27b) has less than 3 km of 1.8-2.3 km/s material, and the Sverdrup Basin at 130 km model distance has less than 2 km (Fig. 27c). The Sverdrup Basin also has a 1 km thick layer of 3.4-3.8 km/s sediment which is not present on the other profiles. The Sverdrup Rim is thus differentiated seismically by the presence of velocities >5.0 km/s above 3 km depth, underlain by 5.9 km/s material at about 4.5 km depth.

It is important to clarify that the Sverdrup Rim is not necessarily coincident with the angularly unconformable junction of the Arctic Continental Terrace Wedge sediments (Late Cretaceous to Tertiary) and the Sverdrup Basin material (Mesozoic) (Fig. 1). Instead, the Sverdrup Rim divides the Arctic Coastal Basin to the north and the Sverdrup Basin to the south. Indeed, within the 1990 refraction survey area the junction of the two units is consistently south of the Rim. The junction passes just south of the Rim on northern Ellef Ringnes Island, diverges increasingly as it continues east and then, south of Meighen Island, curves north to pass between Meighen and Axel Heiberg islands. This region of curvature also appears to be a region of transition based on potential field data and onshore features (Forsyth et al., 1990b).

7. INTERPRETATION OF SEISMIC REFLECTION DATA

In 1990 Pan-Arctic Oil and Home Oil released to the Geological Survey of Canada previously proprietary industry reflection data and borehole logs from the Eastern Arctic Islands. A number of these lines and boreholes were either proximal or intersected the refraction lines, and can help to extend the refraction models. All reflection velocities below are average stacking velocities and are in general agreement with the wide-angle velocities.

Ellef Ringnes Island - Line C and reflection Lines R1 and R2

On Ellef Ringnes Island a composite reflection section (Line R1) was assembled from a number of lines running sub-parallel to refraction Line C (Fig. 28). Further constraints were provided by a perpendicular reflection line (Line R2) and three boreholes, Sirius K28, Isachsen J37 and Pollux G60 (Fig. 28). This data allowed a detailed upper crustal model to be constructed for the gap between shot C1 and the closest recorders, as well as to provide an accurate estimate of the velocity and thickness of the permafrost layer on northern Ellef Ringnes Island. The reflection model along Line R1 (parallel to Line C) indicates a 400 m thick 3.90-4.50 km/s permafrost layer that thins gradually towards the south and decreases to 3.33 km/s as it changes to a more consolidated host sediment. Below this, and forming the matrix for the permafrost, is sediment of the Eureka/Beaufort Formation (Upper Cretaceous/Tertiary) with a velocity of 2.20 km/s which pinches out towards the south and is underlain by a wedge of Triassic Pat Bay Formation sediment with a slightly higher velocity of 3.0 km/s. Underlying this are Permian sediments of the Trold Fiord/Degerbols Formation and the Belcher Channel Formation, with velocities of 3.82-4.08 km/s and 4.98-5.33 km/s respectively. These units appear to be down-faulted towards

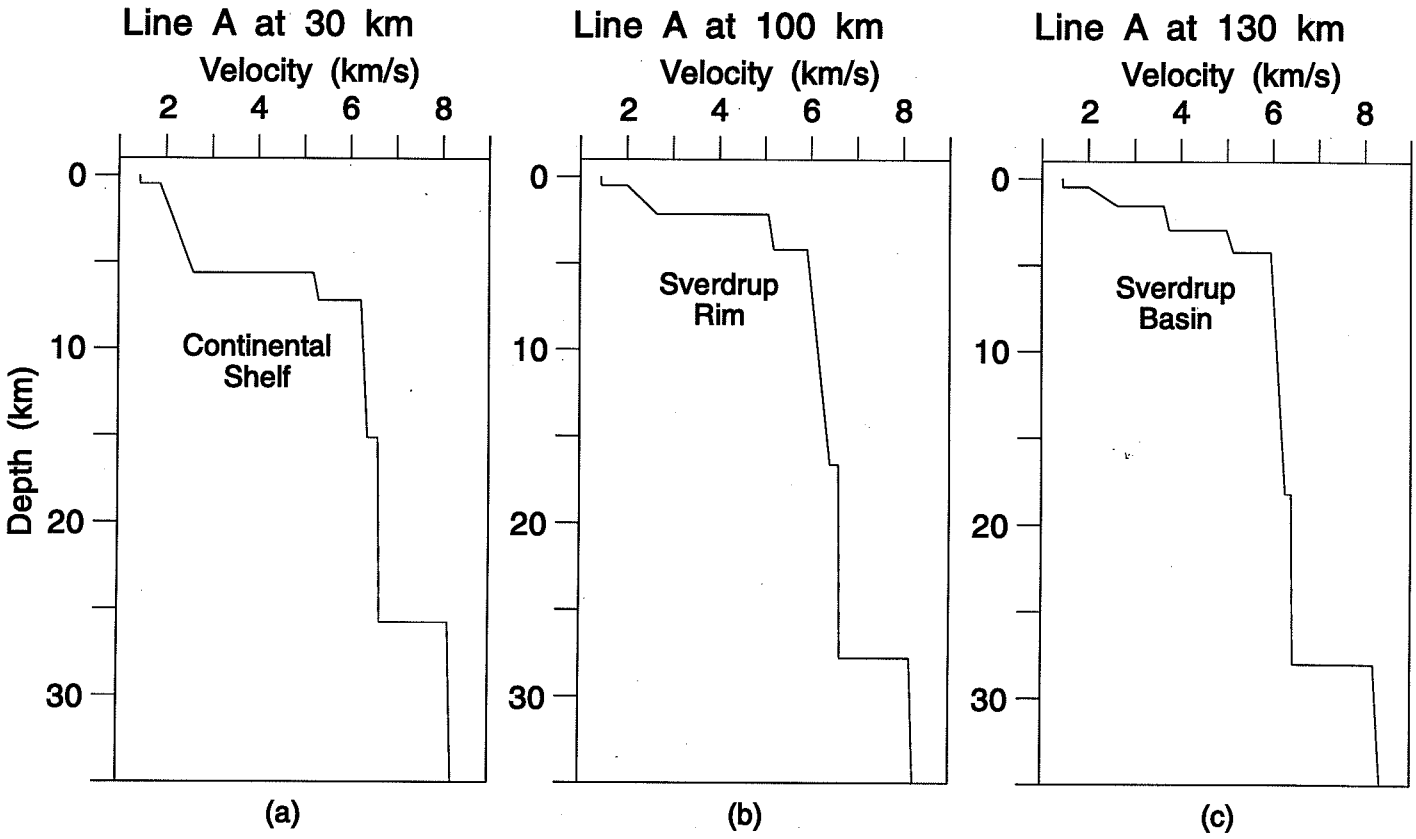

Fig. 27. Velocity profiles along Line A at model distances of 30 km (a; continental shelf), 100 km (b; Sverdrup Rim) and 130 km (c; Sverdrup Basin). The profiles illustrate the changes in crustal velocity structure along the line, as well as the velocity structure specifically associated with the Sverdrup Rim.

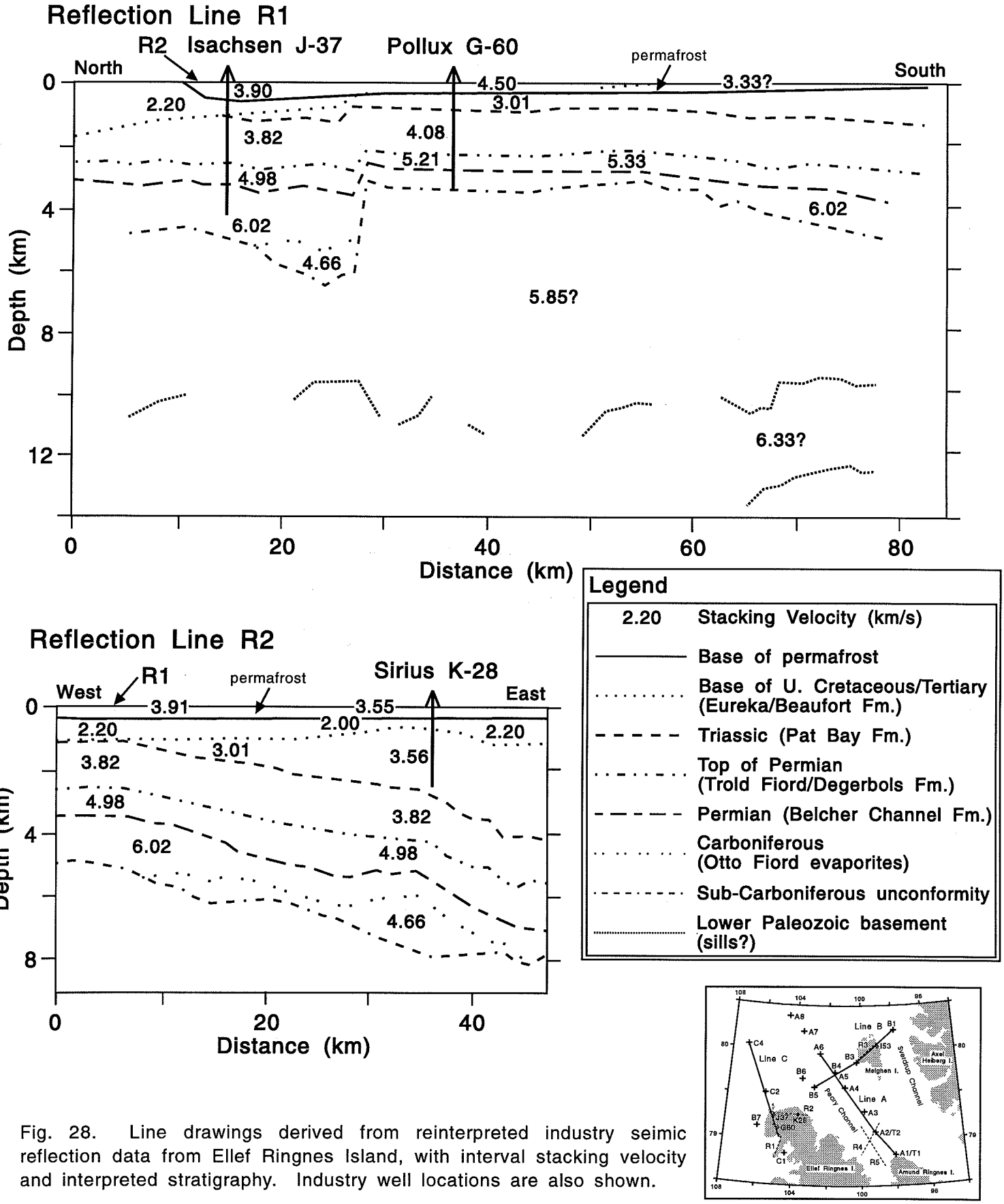

Fig. 28. Line drawings derived from reinterpreted industry seimic reflection data from Ellef Ringnes Island, with interval stacking velocity and interpreted stratigraphy. Industry well locations are also shown.

the north, between the Isachsen and Pollux wells. The underlying sub-Carboniferous unconformity, marking the bottom of a 6.02 km/s layer, is also faulted in the same location with a throw of about 3 km. Nestled against the fault wall is a 4.66 km/s Carboniferous evaporite body of the Otto Fiord Formation. A number of discontinous reflectors, that may be sills within the Lower Paleozoic basement, occur at about 10 km depth. The perpendicular Line R2 suggests that the Eureka/Beaufort Formation (Upper Cretaceous/Tertiary) is relatively flat towards the east, while all the underlying units dip at about 10^0 towards the east. In addition, the presence of a laterally extensive evaporite body of the Otto Fiord Formation (Carboniferous) is indicated at between 5.5 and 8 km depth in the central portion of the line.

Meighen Island - Line B and reflection Line R3

On Meighen Island several reflection lines that crossed refraction Line B were used to constrain a composite reflection model (Line R3) along Line B (Fig. 29). In addition, the Crocker I-53 borehole, only 5 km south of the refraction line, provided constraints on velocity and lithology to 3.1 and 3.5 km depth respectively (Fig. 29). This information was valuable to constrain the velocity and thickness of the high velocity permafrost layer on Meighen Island. The Line R3 and the Crocker I-53 well log indicate the presence of a 3.9 km/s permafrost layer below Meighen Island, with a uniform thickness of about 300 m. Below this, but not identified on the reflection model, is the Beaufort Formation (Tertiary) and the Eureka Sound Formation (Upper Cretaceous). Underlying these, the base of the Upper Cretaceous/Tertiary Eureka Sound Formation, which dips from 1.5 km depth in the southwest to over 2.5 km in the northeast, is indicated on the section. These three units have indicated average velocities of 2.4-3.1 km/s. It has been suggested by Sweeney et al. (1990) that Franklinian basement should lie at about 4 km depth, but the well only penetrated to 3.5 km within Triassic (Blaa Mountain Formation) sediments and, other than some southwest dipping reflectors at 6.5 and 8.5 km, nothing is indicated on the reflection model. The wide-angle interpretation suggests that velocities associated with Franklinian material may be found at about 5 km depth below Meighen Island.

Peary Channel - Line A and reflection Lines R4 and R5

Just north of Amund Ringnes Island, two reflection lines (Lines R4 and R5) that trend perpendicular and parallel to the refraction line respectively, were used to constrain the upper crustal model of Line A (Fig. 30). No borehole data is available. These lines, although not used directly to construct the model, provided additional evidence of the wavelength and amplitude of the large lateral velocity variations indicated in the refraction model. Both lines indicate a high degree of variability in both velocity and depth for the two units defined, the Isachsen Formation (Lower Cretaceous) with a velocity of 2.6-3.5 km/s and the King Christian Formation (Lower Jurassic) with a velocity of 3.5-5.4 km/s. Line R4 appears to have intersected a 5 km wide diapir, possibly evaporite, that has pierced the two sedimentary units to reach the seafloor. At the northeast end of Line R4 another diapir that reaches the seafloor is evident. Line R5 has imaged the edge of a diapir that has uplifted the overlying sediments.

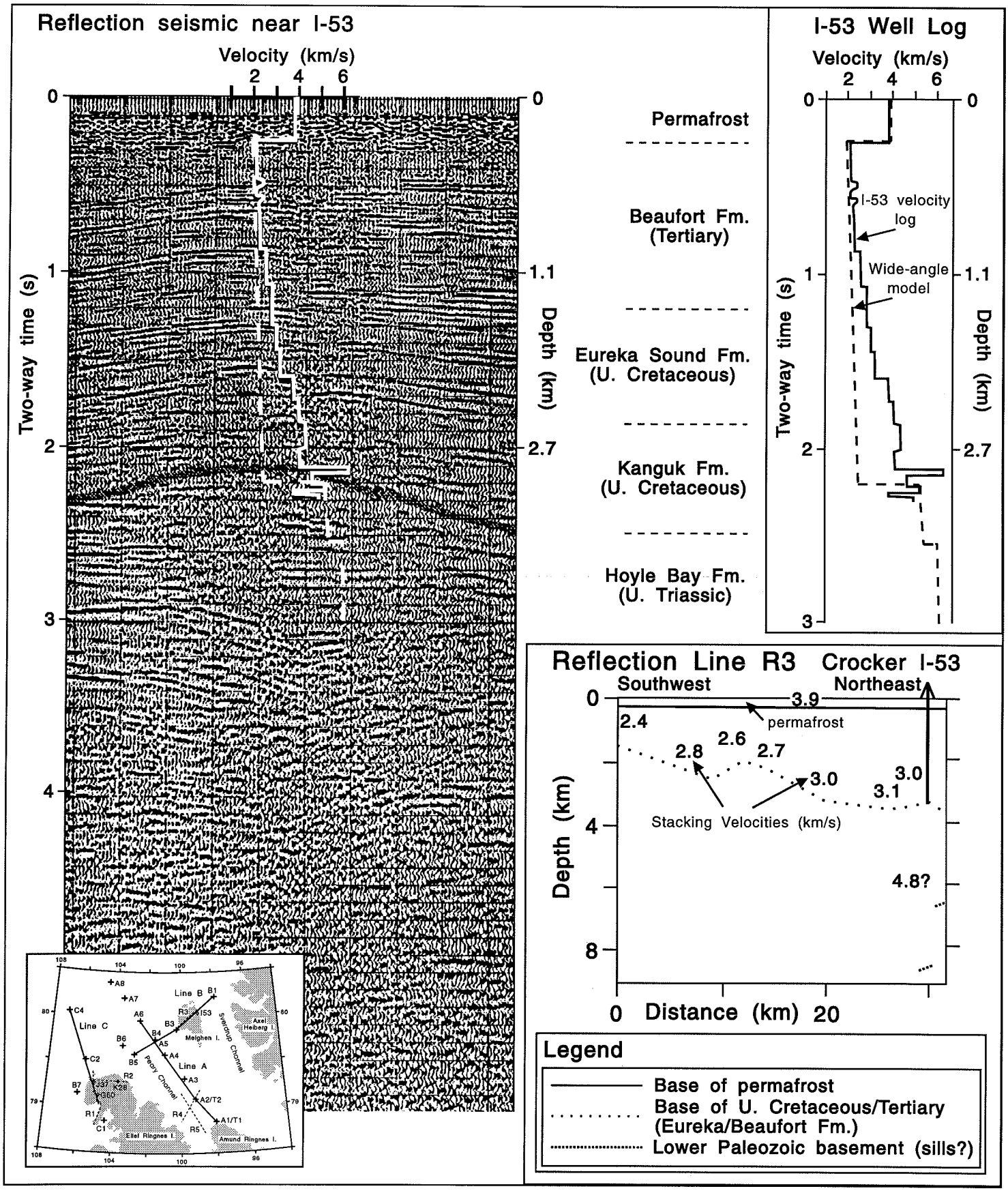

Fig. 29. Example section of reinterpreted industry seismic reflection data from Meighen Island, with velocity log from I-53 and wide-angle model. Line drawing derived from composite reflection section across Meighen Island, with interval stacking velocity and interpreted stratigraphy.

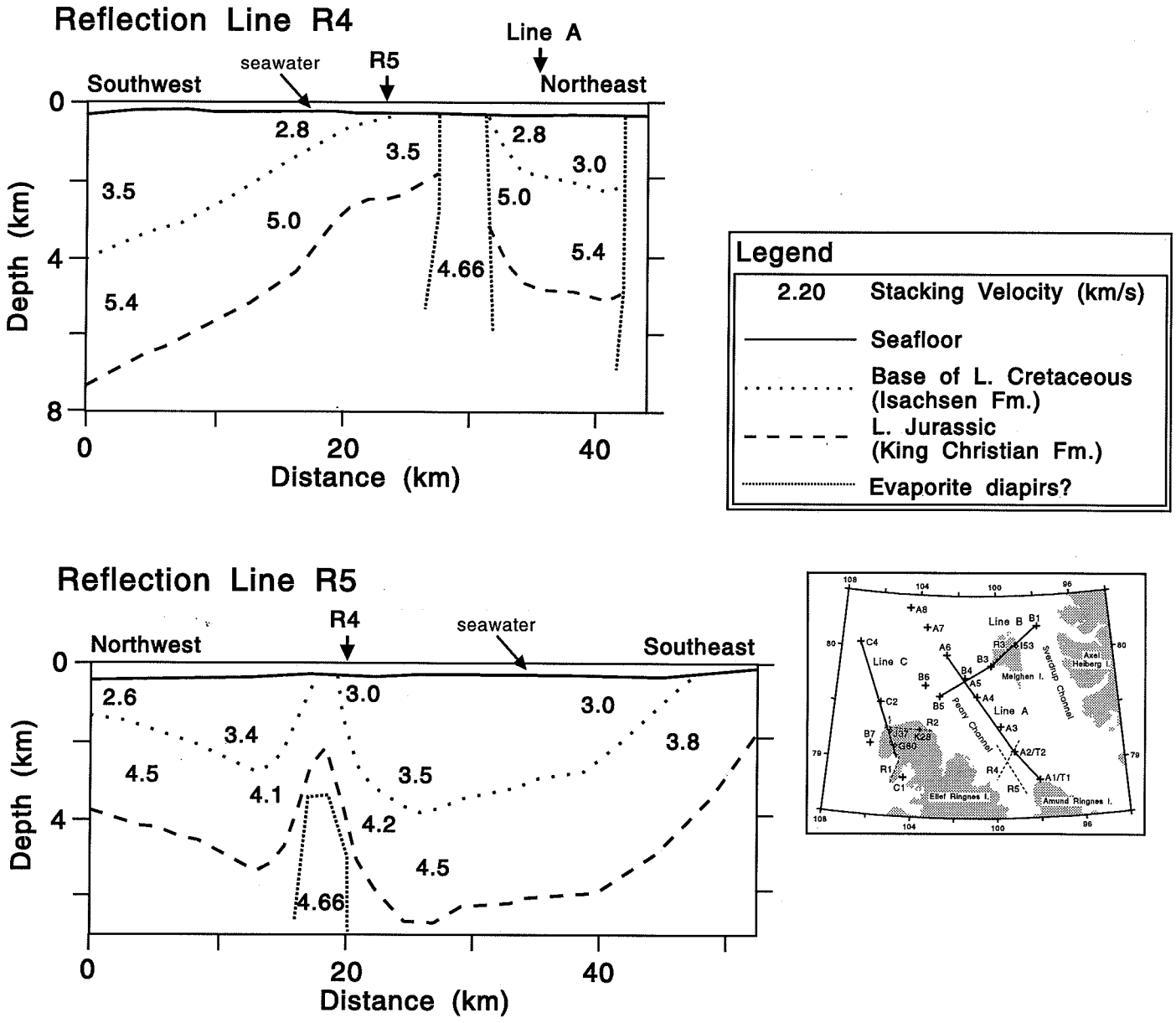

Fig. 30. Line drawings derived from reinterpreted industry seimic reflection data from north of Amund Ringnes Island, with interval stacking velocity and interpreted stratigraphy. Intersection of the two lines and the intersection of Line R4 with the wide-angle Line A are also shown.

8. MAGNETIC AND GRAVITY ANOMALIES

Magnetic

An enlarged segment of the new aeromagnetic data in Fig. 12 for the 1990 survey area is shown in Fig. 31. The study area encompasses the junction of three different magnetic anomaly patterns. To the west, the anomalies are, low amplitude, 10-20 km wavelength, northeast trending, en-echelon linear features, that represent the extension beneath the shelf of a system of linear anomalies identified as a northeast-trending incipient rift crossing the Sverdrup Basin (Forsyth et al., 1979; Balkwill, 1982). The anomalies trend across the NNW flight line direction and are not artifacts of the magnetic survey. Detailed seismic data from the central Sverdrup Basin and mapping indicates the anomaly sources are dykes and normal faults (Forsyth et al., 1990b). To the east the anomalies become higher amplitude and circular. Structural trends from the crests of the linear magnetic highs and prominent structures mapped on Ellef Ringnes Island are shown in Fig. 32. Here, as to the south, the agreement between fault and dike features and the linear anomalies is evident.

On central Ellef Ringnes Island and on northern Amund Ringnes Island circular anomalies characterize mapped diapiric structures containing evaporites and igneous material. Offshore, circular anomalies (near R4 and R5 in Fig. 32) correspond to 5 new diapiric features mapped seismically. Similar features are noted to the northeast south of Meighen Island. The northeast corner of the area is characterized by north-south trends of circular anomlies that generally parallel the regional structures of the Princess Margaret Arch. A complex merging of the trends described above characterizes the area of the Sverdrup Channel.

Farther to the north, the anomaly pattern over the continental shelf becomes relatively flat and generally negative, characteristic of the thick sedimentary cover described on the 1986 Line N-I. The low amplitude NNW trending linear anomalies in Fig. 32 are suspected flight line artifacts.

From Fig. 32 it is evident that the magnetic and mapped structures trend subparallel to refraction Line B and more normal to Lines A and C. The velocity structure in Fig. 25 indicates much stronger velocity variation on Line A than on Line B. The model velocity changes may be due in part to the differing transects of the intersection between the "incipient rift" and the Sverdrup Rim.

Gravity

A contoured map of the gravity field (Bouguer on land, free-air offshore) in the study area is shown in Fig. 33. Offshore the gravity field is dominated by the large (100 mGal) elliptical positive anomaly northwest of Ellef Ringnes Island. This anomaly marks the northeast limit to a series of similar anomalies that begin over the Beaufort Sea margin to the southwest. Beginning north of Axel Heiberg and continuing to the northeast the continental margin gravity high is offset seaward (Fig. 33) and is more linear, containing no elliptical highs on the scale seen to the southwest. The offset is marked by linear gravity highs that extend north from Sverdrup Channel, along the eastern margin of the offshore extension of the Princess Margaret Arch as modelled in the 1986 data, to the outer continental shelf (Fig. 33).

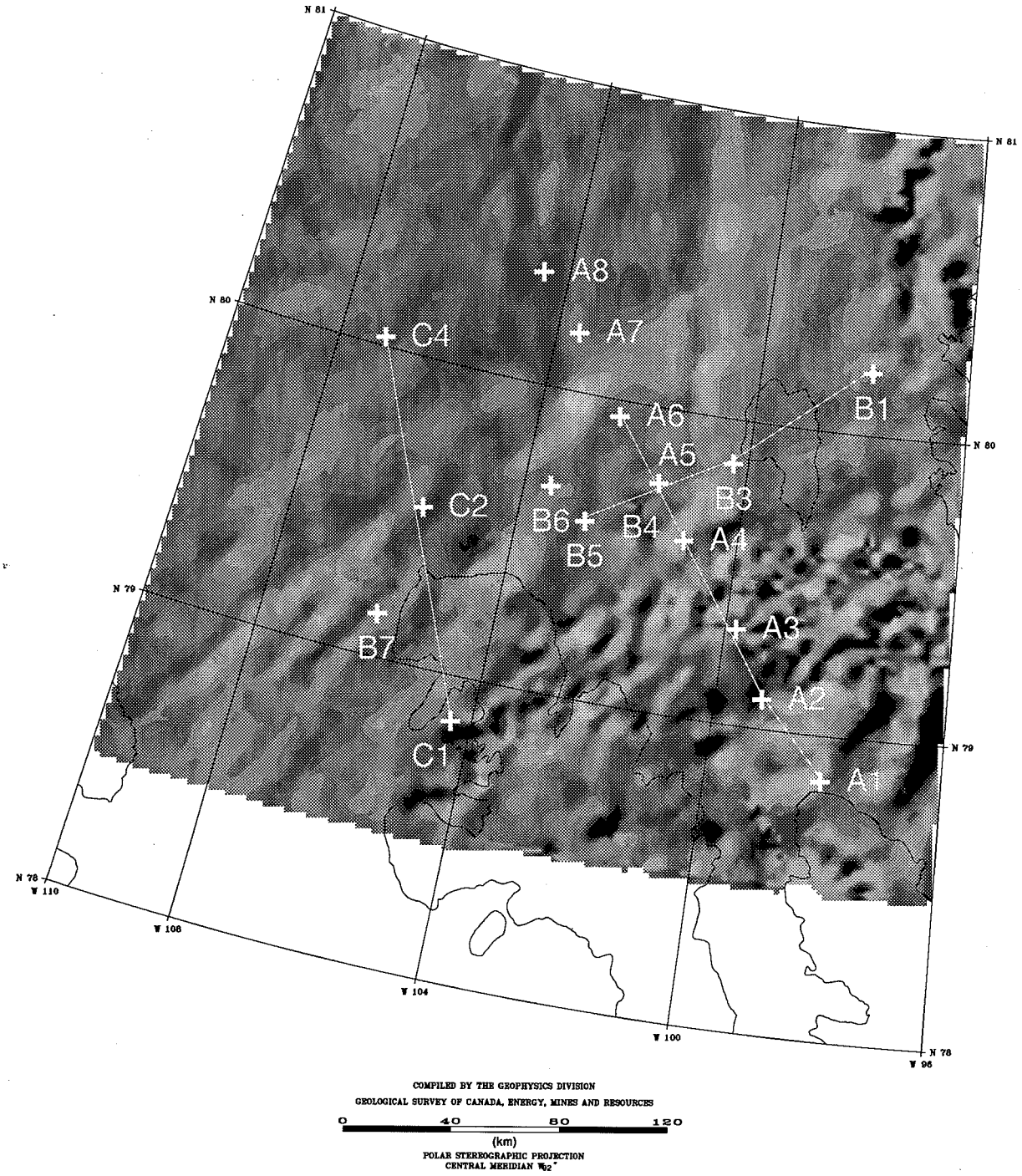

Fig. 31. Shaded relief map of newly compiled residual total field magnetic data. Illumination is from 135 degrees declination at 40 degrees inclination. Compiled by the Geophysics Division of the Geological Survey of Canada.

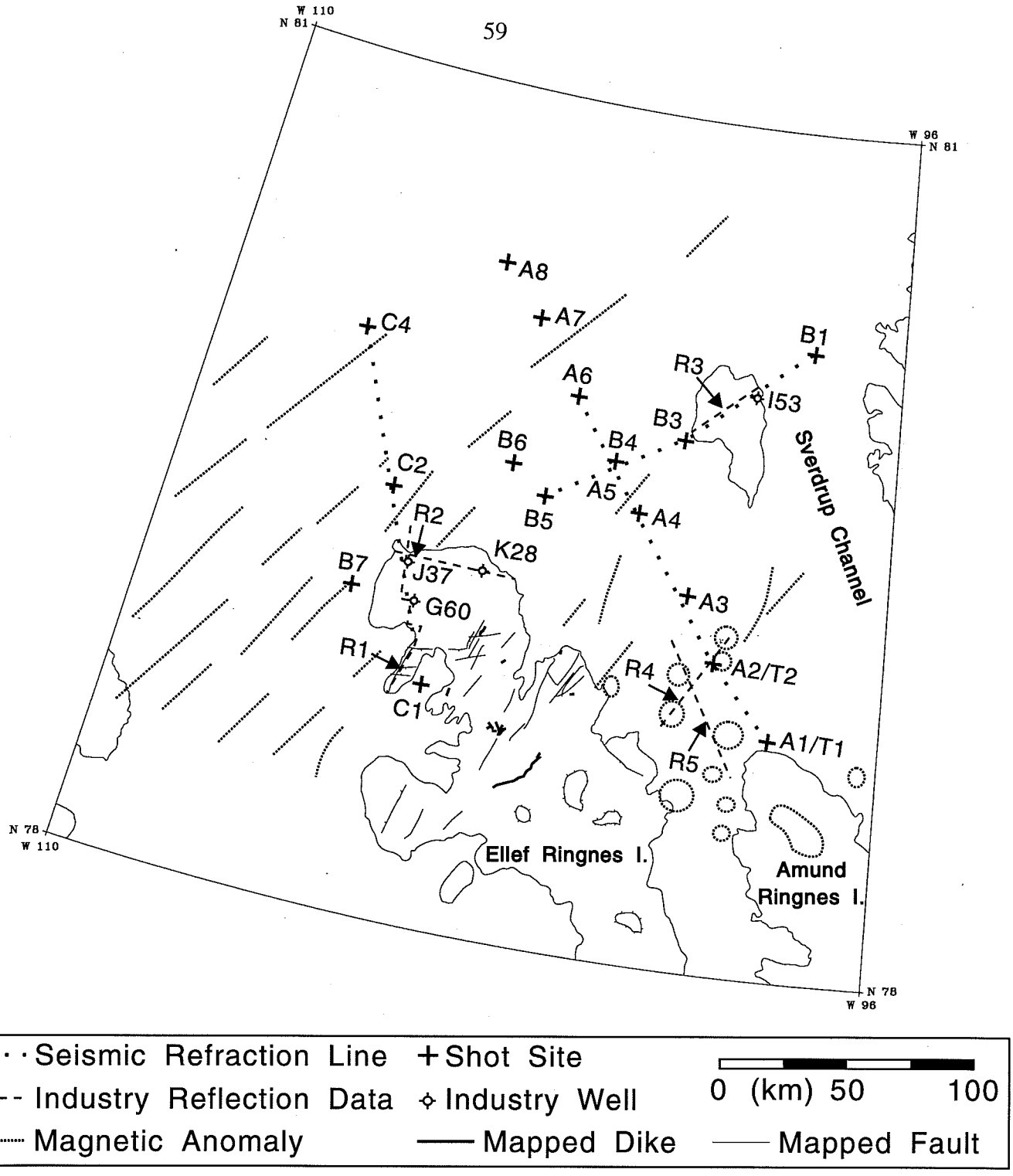

Fig. 32. Map of interpreted magnetic anomalies in the 1990 study area. Mapped onshore features on Ellef Ringnes Island are also shown. Circular features on land are related to evaporite diapirs.

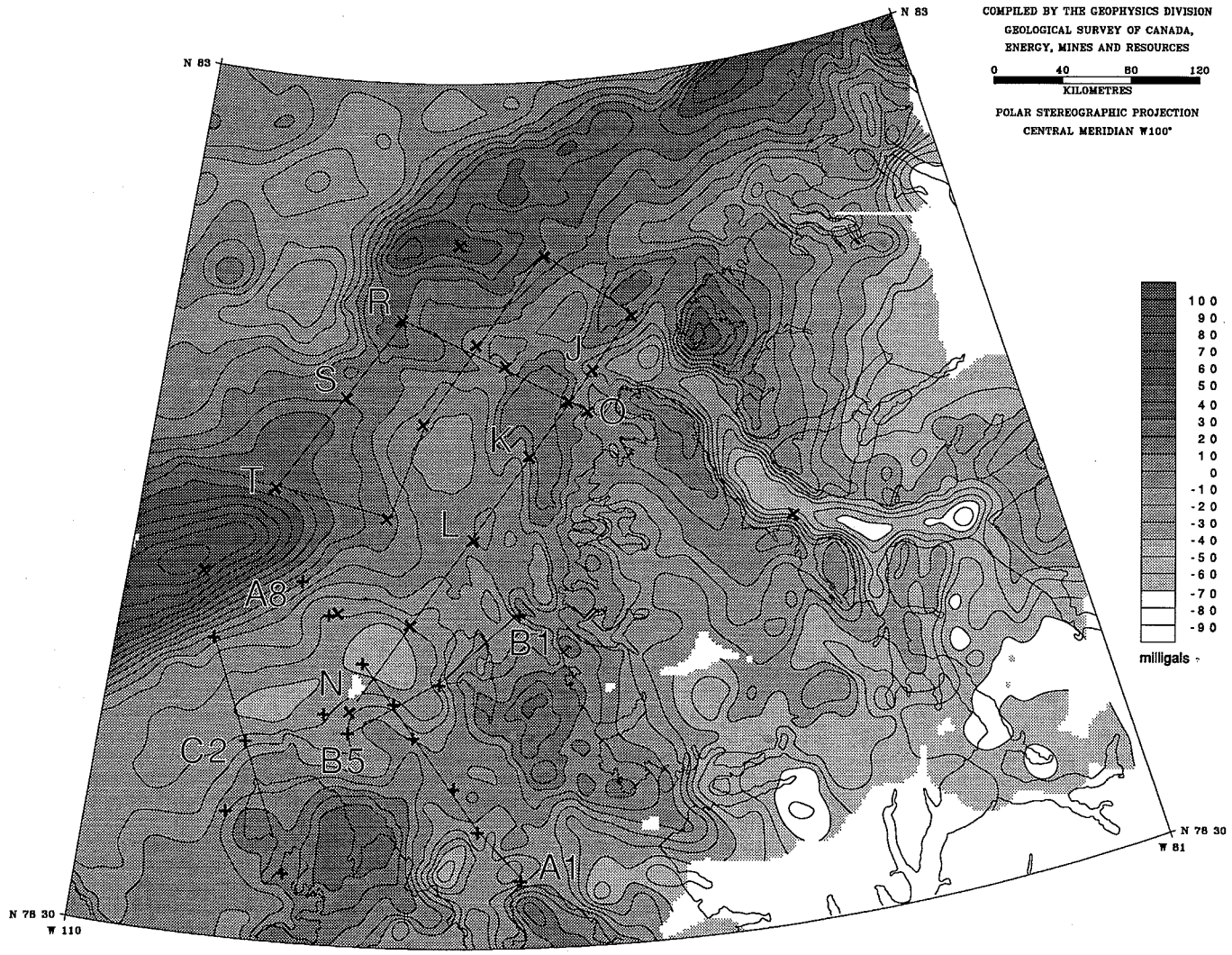

Fig. 33. Gravity (Bouguer on land, free-air offshore) map of the study area. Compiled by the Geophysics Division of the Geological Survey of Canada.

Although detailed modelling by Sobczak (1986) suggests that the elliptical high north of Ellef Ringnes Island is due to the composite effect of a thick sediment wedge which is not entirely isostatically compensated and an edge effect of the average density change and structure across the continent-ocean transition, the constraints provided by the present seismic data should be included in further studies. The high amplitude anomaly is bordered to the south by a low amplitude negative anomaly that trends along the northern side of the Sverdrup Rim and ends at the Sverdrup Channel. Further south, the positive anomaly over northern Ellef Ringnes Island follows the northeast trends seen in the magnetic data and mapped structures. The positive gravity high south of Meighen Island correlates with the zone of short wavelength, mainly circular highs in Fig. 31. A marked difference in character of the magnetic and gravity anomalies offshore and onshore occurs at Sverdrup Channel. The seismic results presented in this report have provided structural calibration for several parts of these differing anomaly patterns, however much remains to be done in this relatively small but remote and complex portion of Canada's polar margin

9. SEISMICITY

Another interesting geophysical data set that augments the regional features decribed above is provided by the better located recorded seismic events since 1962 (Fig. 34). The events include several earthquakes of magnitude >5. The offshore cluster of events begins at the elliptical gravity high and continues seaward but is enigmatic. The events on land, however, trend east-west south of the crest of the Sverdrup Rim as identified in this report, and intersect a north-south trend immediately east of the Sverdrup Channel. Events on western Axel Heiberg Island trend subparallel to the Princess Margaret Arch. In summary the main epicentre trends follow south and east of structral trends described by the Sverdrup Rim and a structural zone beneath the Sverdrup Channel.

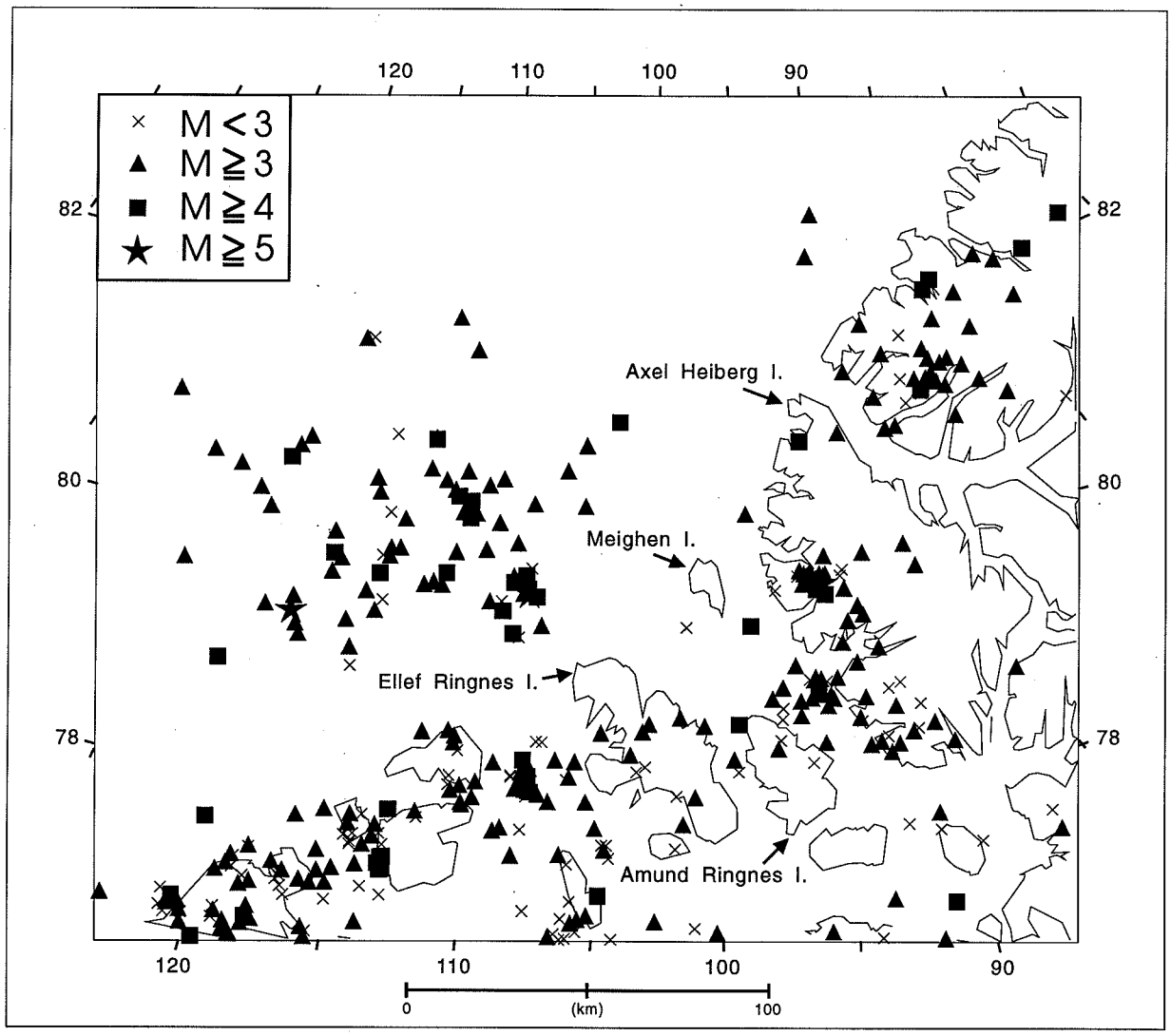

Fig. 34. Seismicity in the northeastern Canadian Arctic since 1962. Compiled by the Geophysics Division of the Geological Survey of Canada.

SUMMARY AND CONCLUSIONS

This report presents an integrated interpretation of the crustal structure of the northeast Sverdrup Basin and adjacent polar margin from new wide-angle seismic velocity models, newly interpreted industry reflection data, borehole data and newly compiled aeromagnetic data. The seismic information places new constraints on the crustal structure of a little known area of the polar margin and by default, on the rifting associated with the formation of the adjacent Canada Basin. The seismic data also provide the first structural calibration for the new magnetic data. The seismic analysis has directly provided:

1) A new regional velocity structure of the northeast Sverdrup Basin.
2) New crustal structure both along and across the transition from Sverdrup Basin to the adjoining continental shelf.
3) New crustal evidence beneath the continental shelf offshore of Axel Heiberg Island to document the continuity and changes in principal regional structures from those mapped onshore, and clues to the nature of these structures at depth.
4) New parameters for resource assessments of Canada's polar margin.
5) New parameters to help define Canada's Arctic margin under the internationally ratified Law of the Sea agreement.

Newly compiled aeromagnetic data for the study area provide new supporting evidence for:

1) The offshore continuation and termination of the Princess Margaret Arch.
2) A major sedimentary basin north of Meighen Island.
3) A major change in crustal structure beneath the outer continental shelf that may be related to the Alpha Ridge.
4) The northeast continuation of a suggested major mid-Cretaceous "incipient rift" that traverses the Sverdrup Rim and extends beneath the continental shelf north of Ellef Ringnes Island.
5) New seismically documented diapiric structures in Peary Channel.
6) A complex northerly merging of structural trends offshore from the area of Sverdrup Channel. Structural trends inferred from clear linear anomaly patterns in both the magnetic and gravity data are sub-parallel to major thrusts mapped on Axel Heiberg Island.

The wide-angle seismic data was recorded in 1986 northwest of Axel Heiberg Island, and in 1990 between Meighen Island and Ellef Ringnes Islands. Interpretation of the 1986 wide-angle data suggests that the regional crustal structure beneath the continental shelf consists of a complex series of basement arches separating sedimentary basins containing at least 12 km of strata with velocities less than 5.2 km/s. Crustal thickness is generally less than 30 km beneath the study area. The crust thins to about 26 km beneath the outer shelf in the area of a classic elliptical gravity high. The Princess Margaret Arch, a major Eurekan compressional structure extends offshore as a major basement high that bounds sedimentary basins in the wide-angle models. Strong reflections from the upper crust of the Princess Margaret Arch indicate a local discontinuity at a depth of 6 km and suggest a very complex structure along the flanks of the arch. Structural features modelled along the flanks appear compatible with major thrusts exposed on Axel Heiberg Island. A distinct velocity structure expression of the The Cornwall Arch is not

evident. Some of the major velocity units in the refraction models for the northeast margin are similar to those observed in the hydrocarbon-rich Beaufort Sea-Mackenzie Delta area 1500 km to the southeast. Basin formation apears to have been influenced by both structures predating the margin rifting and later compressional events.

Interpretation of the 1990 wide-angle data, together with industry reflection data, between Ellef Ringnes and Meighen islands shows that sediments of the mainly Mesozoic Sverdrup Basin section are characterized by velocities generally less than 5.2 km/s and a thickness of 5-6 km. The presence of several new diapiric structures are indicated by both seismic and magnetic data. The Sverdrup Rim - a local upper-mid crustal high, defined seismically by a 1.5 km high ridge of 5.2 km/s material overlying a 50 km wide basement high of 5.9 km/s material - is interpreted to be the northeastern boundary of the Sverdrup Basin. This Rim is imaged beneath Ellef Ringnes Island, on both the wide-angle and the reflection data, and is indicated beneath Peary Channel from the wide-angle interpretation. The structure of the Rim becomes increasingly complex to the northeast supporting an increase in regional deformation towards Axel Heiberg Island. A general thinning of low velocity sedimentary material from southwest to northeast, may be related to the change in character of the potential fields between Meighen Island and Axel Heiberg Island. The wide-angle model includes a sedimentary wedge, thickening offshore to 10 km, near the edge of the margin. Moho depths of less than 30 km indicate that thin continental, or transitional, crust continues beneath the shelf north of the Sverdrup Basin.

In the area between Ellef Ringnes and western Ellesmere Island and the adjacent offshore much conjecture surrounds the formation of multiple basins during Eurekan tectogenesis. The seismic results show clear evidence of a complex network of local basins separated by basement highs both within the Sverdrup Basin in the study area and beneath the adjacent continental shelf. To better quantify these linkages, further integration of the seismic reflection and refraction results with recently acquired magnetic data and existing gravity data is required.

ACKNOWLEDGEMENTS

The contributions made in the field and in the office by all of the PCSP officers and its contractors, is gratefully acknowledged. In particular, the authors thank Jay Ardai, Tim Cartwright, Tim Côté, Jim Craven, Jack Dearnley-Davison, Mike Gorveatt, Larry Johnson, Bob Schieman, Don White and Morley Wright, all of whom were actively involved in the refraction field programs. The ice island seismic surveys were funded as part of the Frontier Geoscience Program of the Geological Survey of Canada, and this report was produced under contract serial no. EMR-MMD-930294. The generous assistance and advice of C.A. Zelt with the Rayinvr algorithm and supplementary programs is greatly appreciated. The work would not have been completed without the encouragement and support of A. Embry. K. Andersen and W. Miles helped prepare aeromagnetic and gravity data, J.A. Drysdale prepared the seismicity map, and the Canadian Hydrographic service provided original copies of bathymetry charts.

REFERENCES

Argyle, M., D.A. Forsyth, A.V. Okulitch, and D. Huston, 1994. A New Crustal Model of the Lincoln Sea Polar Margin. In Thurston D. and K. Fujita, eds., Proceedings of the 1992 International Conference on Arctic Margins. United States Department of the Interior, Minerals Management Service, Outer Continental Shelf Report MMS 94-XXXX, in press.

Asudeh, I., D.A. Forsyth, R.A. Stephenson, A.F. Embry, H.R. Jackson and D. White, 1989. Crustal structure of the Canadian polar margin: results of the 1985 seismic refraction survey: Canadian Journal of Earth Sciences, v. 26, p. 853-866.

Asudeh, I., D.A. Forsyth, H.R. Jackson, R. Stephenson and D. White, 1986. 1986 Ice Island Refraction Survey Phase II report: Geological Survey of Canada, Open File No. 1511.

Asudeh, I., D.A. Forsyth, H.R. Jackson, R. Stephenson and D. White, 1985. 1985 Ice Island Refraction Survey, Phase I Report: Earth Physics Branch, Open File No. 85-23; Geological Survey of Canada, Open File No. 1196, 25 p.

Balkwill, H.R., 1982. Incipient rift zone, Western Sverdrup Basin, Arctic Canada. In: A.F. Embry and H.R. Balkwill (Editors), Arctic Geology and Geophysics. Bulletin of the Canadian Society of Petroleum Geologists, v. 8, p. 171-188.

Balkwill, H.R., 1978. Evolution of Sverdrup Basin, Arctic Canada: American Association of Petroleum Geologists, Bulletin, v. 62, p. 1004-1028.

Cerveny, V., 1985. Gaussian beam synthetic seismograms. Journal of Geophysics, v. 58, p. 44-72.

Cerveny, V., I. Molotkov, and I. Psencik, 1977. Ray Method in Seismology: Charles University Press, Prague, 214 p.

Dearnley-Davison, J. and D.A. Forsyth, 1989. Radio-positioning for Arctic seismic surveys: Engineering Digest, v. 35, p. 18-24.

De Paor, D.G., D.C. Bradley, G. Eisenstadt, and S.M. Phillips, 1989. The arctic Eurekan orogen: a most unusual fold-and-thrust belt: Geological Society of America Bulletin, v. 101, p. 952-967.

Dixon, J., and J.R. Dietrich, 1990. Canadian Beaufort Sea and adjacent land areas. In Grantz A., L. Johnson and J.F. Sweeney, eds., The Decade of North American Geology, vol. L: The Arctic Ocean Region, Geological Society of America, Boulder, Colorado, p. 239-256.

Embry, A.F., 1990. Geological and geophysical evidence in support of the hypothesis of anticlockwise rotation of northern Alaska. Marine Geology, v. 93, p. 317-329.

Embry, A.F., 1989. Correlation of Upper Paleozoic and Mesozoic sequences between Svalbard, Canadian Arctic Archipelago, and northern Alaska. Correlation in Hydrocarbon Exploration, Norwegian Petroleum Society, p. 89-98.

Embry, A.F., T.G. Powell and U. Mayr, 1991. Petroleum resources, Arctic Islands; In Trettin, H.P., ed., Geology of the Innuitian Orogen and Arctic Platform of Canada and Greenland, Chapter 20. Geological Survey of Canada, Geology of Canada, no. 3, p. 517-525.

Forsyth, D.A., T. Côté, J. Craven, M. Argyle, R.A. Stephenson, H.R. Jackson, L. Johnson, J. Dearnley-Davison, M. Wright, R.C. Schieman and T. Cartwright, 1990a. 1990 Ice Island Refraction Survey, Phase 1 Report, Geological Survey of Canada Open File No. 2273, 19 p.

Forsyth, D.A., J. Broome, A.F. Embry and J. Halpenny, 1990b. Features of the Canadian polar margin: Marine Geology, v. 93, p. 147-177.

Forsyth, D.A., I. Asudeh, A.G. Green, and H.R. Jackson, 1986. Crustal structure of the northern Alpha Ridge beneath the Arctic Ocean. Nature, v. 322, p. 349-352.

Forsyth, D.A., and J.A. Mair, 1984. Crustal Structure of the Lomonosov Ridge and Fram and Makarov Basins near the North Pole. Journal of Geophysical Research, v. 89, p. 473-481.

Forsyth, D.A., J.A. Mair and I. Fraser, 1979. Crustal structure of the central Sverdrup Basin: Canadian Journal of Earth Sciences, v. 16, p. 1581-1598.

Haimila, N.E., Kirschner, C.W., Nassichuk, W.W., Ulmichek, G., and Proctor, R.M., 1990. Sedimentary Basins and Petroleum Resource Potential of the Arctic Ocean Region. In Grantz, A., L. Johnson and J.F. Sweeney, eds., The Geology of North America, v. L: The Arctic Ocean Region. Boulder, Colorado, Geological Society of America.

Hajnal, Z., M.J.A. Burianyk, I. Kesmarky and A. Overton, 1990. Reflection Survey on Hobson's Choice Ice Island, Arctic Ocean. Marine Geology, v. 93, p. 211-224.

Harbert, W., L. Frei, R. Jarrard, S. Halgedahl, and D. Engrebreison, 1990. Paleomagnetic and Plate-Tectonic Constraints on the Evolution of the Alaskan-Eastern Siberian Arctic. In: The Decade of North American Geology, vol. L, The Arctic Ocean Region, edited by A. Grantz, L. Johnson, and J.F. Sweeney, Geological Society of America, Boulder, Colorado, p. 239-256.

Hea, J.P., J. Arcuri, G.R. Campbell, I. Fraser, M.O. Fuglem, J.J. O'bertos, D.R. Smith and M. Zayat, 1980. Post Ellesmerian Basins of Arctic Canada: their depocentres, rates of sedimentation and petroleum potential. In Miall, A.D., ed., Facts and Principles of World Petroleum Occurence. Memoir 6, Canadian Society of Petroleum Geologists, p. 447-488.

Hobson, G.D., 1962. Seismic exploration in the Canadian Arctic Islands. Geophysics, v. 27, p. 253-273.

Hunkins, K., 1960. Seismic Studies of Sea Ice. Journal of Geophysical Research, 65, 10, p. 3459-3472.

Jackson, H.R., 1988. A seismic stratigraphy for the polar margin (abstract): Geological Association of Canada, Program with Abstracts, v. 13, p. A60.

Jackson, L., 1989. Ice Island - an ideal platform. Canadian Geographic, Dec. 1988-Jan. 1989.

Jeffries, M.O., 1992. Arctic Ice Shelves and Ice Islands: origin, growth and disintegration, physical characteristics, structural-stratigraphic variability, and dynamics. Reviews of Geophysics, 30, 3, p. 245-267.

Mair, J.A. and J.A. Lyons, 1981. Crustal structure and velocity anisotropy beneath the Beaufort Sea: Canadian Journal of Earth Sciences, v. 18, p. 724-741.

McIntyre, D. and B.D. Ricketts, 1989. New palynological data concerning Cornwall Arch from Cornwall and Admund Ringnes Islands, District of Franklin: Geological Survey of Canada, Paper 89-1G, p. 199-202.

Miall, A.D., 1984. Sedimentation and tectonics of a diffuse plate boundary: the Canadian Arctic islands from 80 Ma B.P. to the present: Tectonophysics, v. 107, p. 261-277.

Mooney, H.M., 1983. Synthetic seismograms for body waves: an overview. First Break, v. 1, p. 9-20.

Nassichuk, W.W., 1987. Forty years of northern non-renewable natural resource development. Arctic, v. 40, p. 274-284.

Overton, A., 1970. Seismic refraction surveys, western Queen Elizabeth Islands and Polar continental margin. Canadian Journal of Earth Sciences, v. 7, p. 346-365.

Overton, A. and A.F. Embry, 1989. Seismic reflection profiling from an ice island along the continental shelf of the Canadian Arctic Archipelago: Geological Survey of Canada, Paper 89-1G, p. 257-265.

Ricketts, B.D., 1987. Princess Margaret Arch: re-evaluation of an element of the Eurekan Orogen, Axel Heiberg Island, Arctic Archipelago: Canadian Journal of Earth Sciences, v. 24, p. 2499-2505.

Sander, G.W., and A. Overton, 1965. Deep Seismic Refraction Investigation in the Canadian Arctic Archipelago. Geophysics, v. XXX, No. 1, p. 87-96.

Sobczak, L.W., U. Mayr and J.F. Sweeney, 1986. Crustal section across the polar continent-ocean transition in Canada: Canadian Journal of Earth Sciences, v. 23, p. 608-621.

Spence, G.D., K.P. Whittall and R.M. Clowes, 1984. Practical synthetic seismograms for laterally varying media calculated by asymptotic ray theory: Bulletin of the Seismological Society of America, v. 74, p. 1209-1223.

Stephenson, R.A., A.F. Embry, S.M. Nakiboglu and M.A. Hastaoglu, 1987. Rift-initiated Permian to Early Cretaceous subsidence of the Sverdrup Basin. In C. Beaumont and A.J. Tankard, eds., Sedimentary Basins and Basin-forming Mechanisms: Canadian Society of Petroleum Geologists, Memoir 12, p. 213-231.

Stuart Smith, J.H. and J.H.N. Wennekers, 1977. Geology and Hydrocarbon Discoveries of Canadian Arctic Islands. The American Association of Petroleum Geologists Bulletin, v. 61, no. 1, p. 1-27.

Sweeney, J.F., 1985. Comments about the age of the Canada Basin: Tectonophysics, v. 114, p. 1-10.

Sweeney, J.F., L.W. Sobczak and D.A. Forsyth, 1990. The Continental Margin Northwest of the Queen Elizabeth Islands. In Grantz, A., L. Johnson and J.F. Sweeney, eds., The Geology of North America, v. L: The Arctic Ocean Region. Boulder, Colorado, Geological Society of America, p. 227-238.

Trettin, H.P., 1987. Pearya: a composite terrane with Caledonian affinities in northern Ellesmere Island: Canadian Journal of Earth Sciences, v. 24, p. 224-245.

Trettin, H.P., T.O. Frisch, L.W. Sobczak, J.R. Weber, E.R. Niblett, L.K. Law, J. DeLaurier and K. Whitham, 1972. The Innuitian Province. In Price, R.A. and R.J.W. Douglas, eds., Variations in tectonic styles in Canada. Geological Association of Canada, Special Paper 11, p. 83-179.

Vogt, P.R., Taylor, P.T., Kovacs, L.C. and Johnson, G.L., 1982. The Canada Basin: Aeromagnetic constraints on structure and evolution. Tectonophysics, v. 89, p. 295-336.

Zelt, B.C., R.M. Ellis, R.M. Clowes, E.R. Kanasewich, I. Asudeh, J.H. Leutgert, Z. Hajnal, A. Ikami, G.D. Spence and R.D. Hyndman, 1992. Crust and upper mantle velocity structure of the Intermonatine belt, southern Canadian Cordillera. Canadian Journal of Earth Sciences, v. 29, p. 1530-1548.

Zelt, C.A. and D.A. Forsyth, 1994. Modelling wide angle seismic data for crustal structure: southeastern Grenville Province. Journal of Geophysical Research, in press.

Zelt, C.A., and R.B. Smith, 1992. Seismic traveltime inversion for 2-D crustal velocity structure. Geophysical Journal International, v. 108, p. 16-34.

APPENDIX 1

MODELLED 1990 WIDE-ANGLE DATA NOT SHOWN IN FIGURES

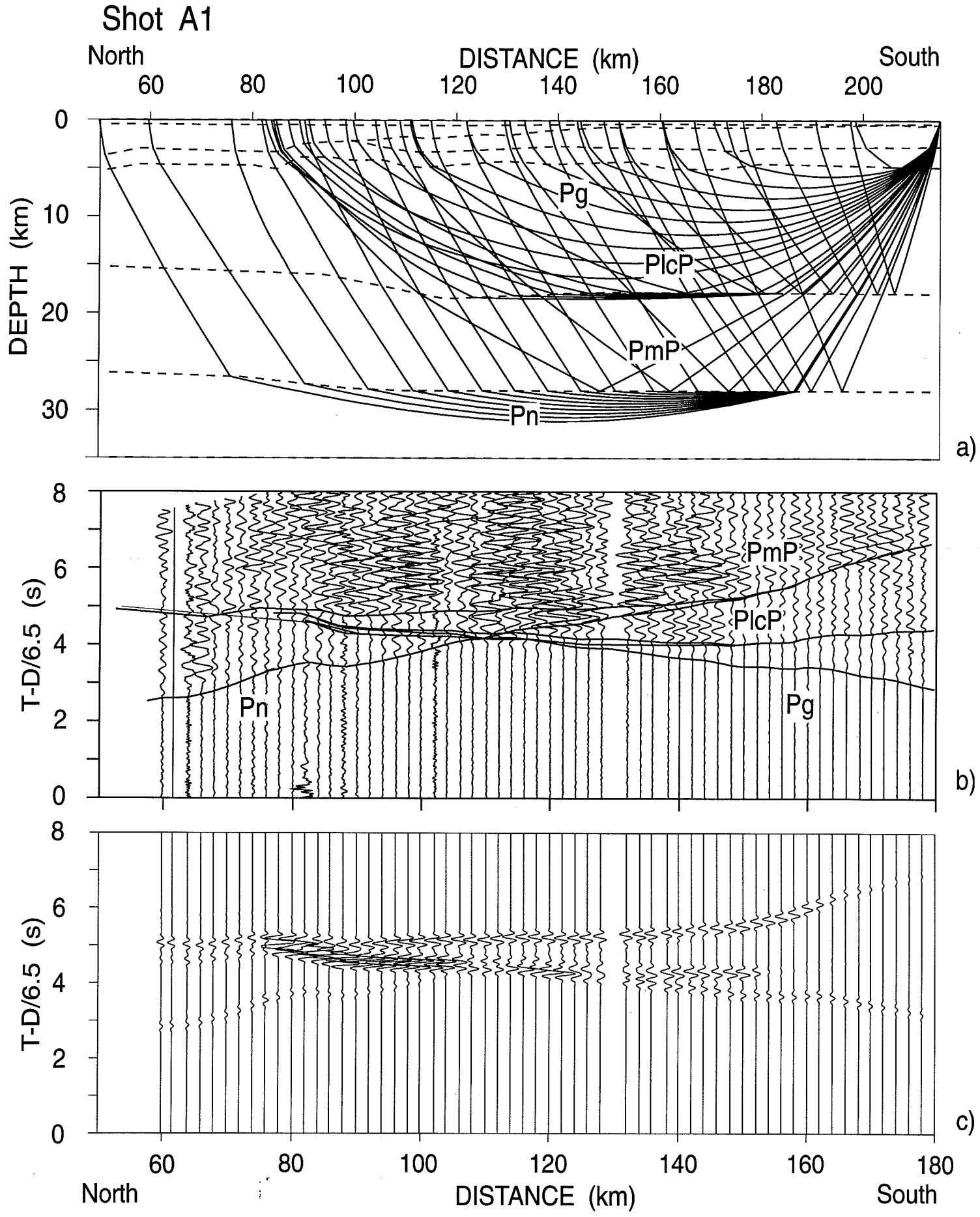
Shot A1
North
DISTANCE (km)
South
60
80
100
120
140
160
180
200
0
10
20
30
DEPTH (km)
Pg
PlcP
PmP
Pn
a)
8
6
4
2
0
T-D/6.5 (s)
PmP
PlcP
Pn
Pg
b)
8
6
4
2
0
T-D/6.5 (s)
c)
60
80
100
120
140
160
180
North
DISTANCE (km)
South

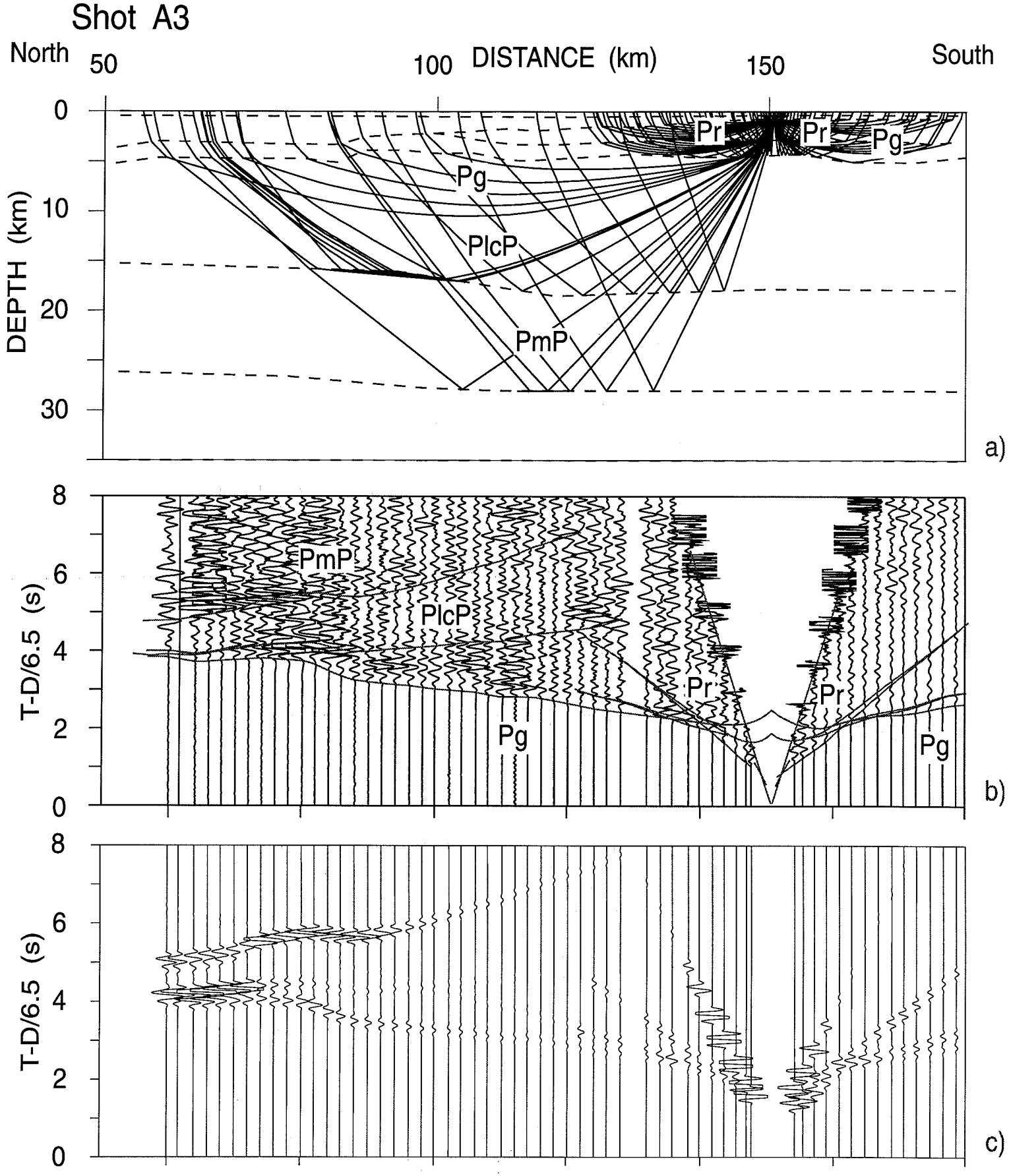
Shot A3
North
50
100
DISTANCE (km)
150
South
DEPTH (km)
0
10
20
30
Pr
Pr
Pg
Pg
PlcP
PmP
a)
T-D/6.5 (s)
8
6
4
2
0
PmP
PlcP
Pg
Pr
Pr
Pg
b)
T-D/6.5 (s)
8
6
4
2
0
c)

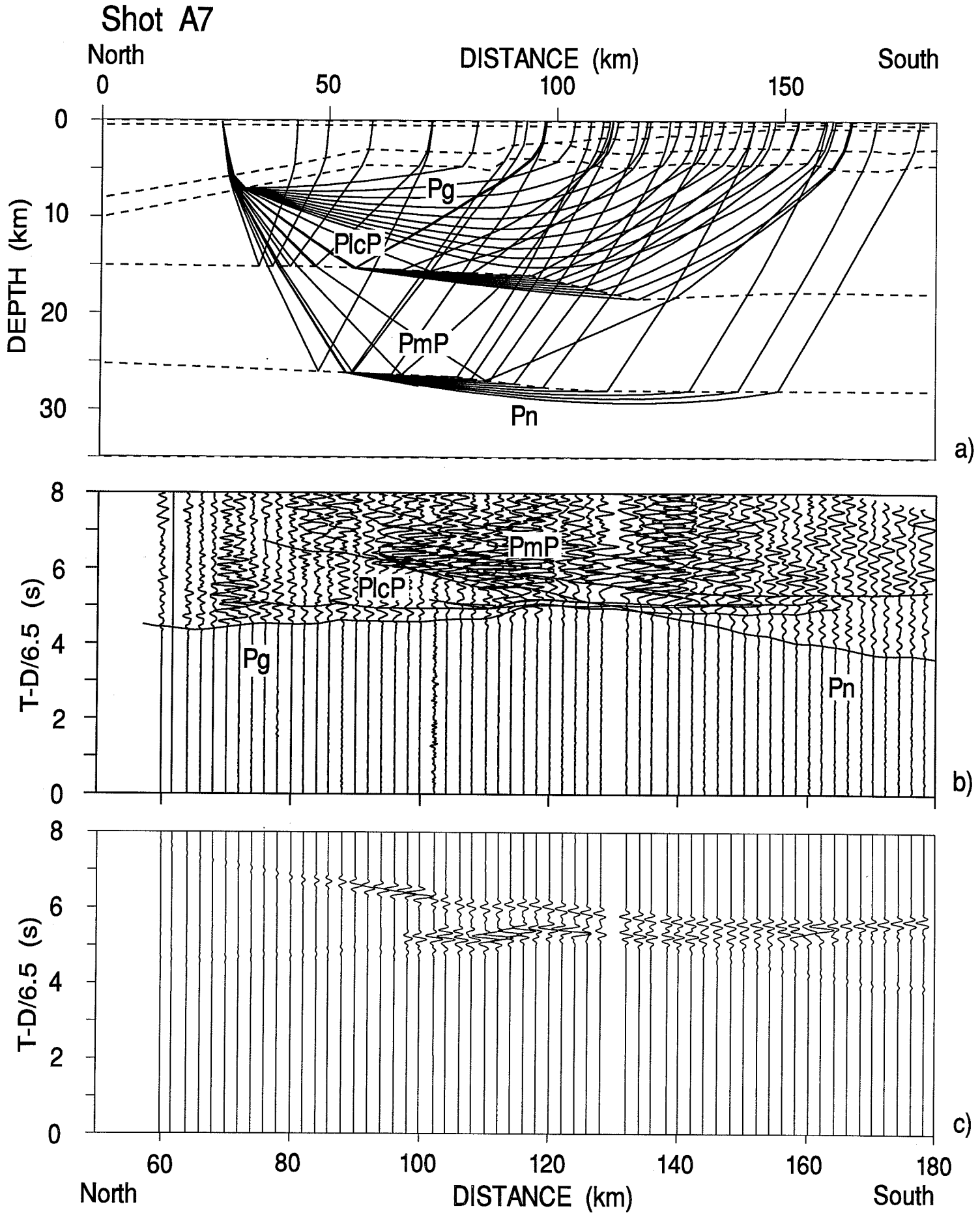
Shot A7
North
DISTANCE (km)
South
0
50
100
150
DEPTH (km)
0
10
20
30
Pg
PlcP
PmP
Pn
a)
T-D/6.5 (s)
8
6
4
2
0
PmP
PlcP
Pg
Pn
b)
T-D/6.5 (s)
8
6
4
2
0
c)
60
80
100
120
140
160
180
North
DISTANCE (km)
South

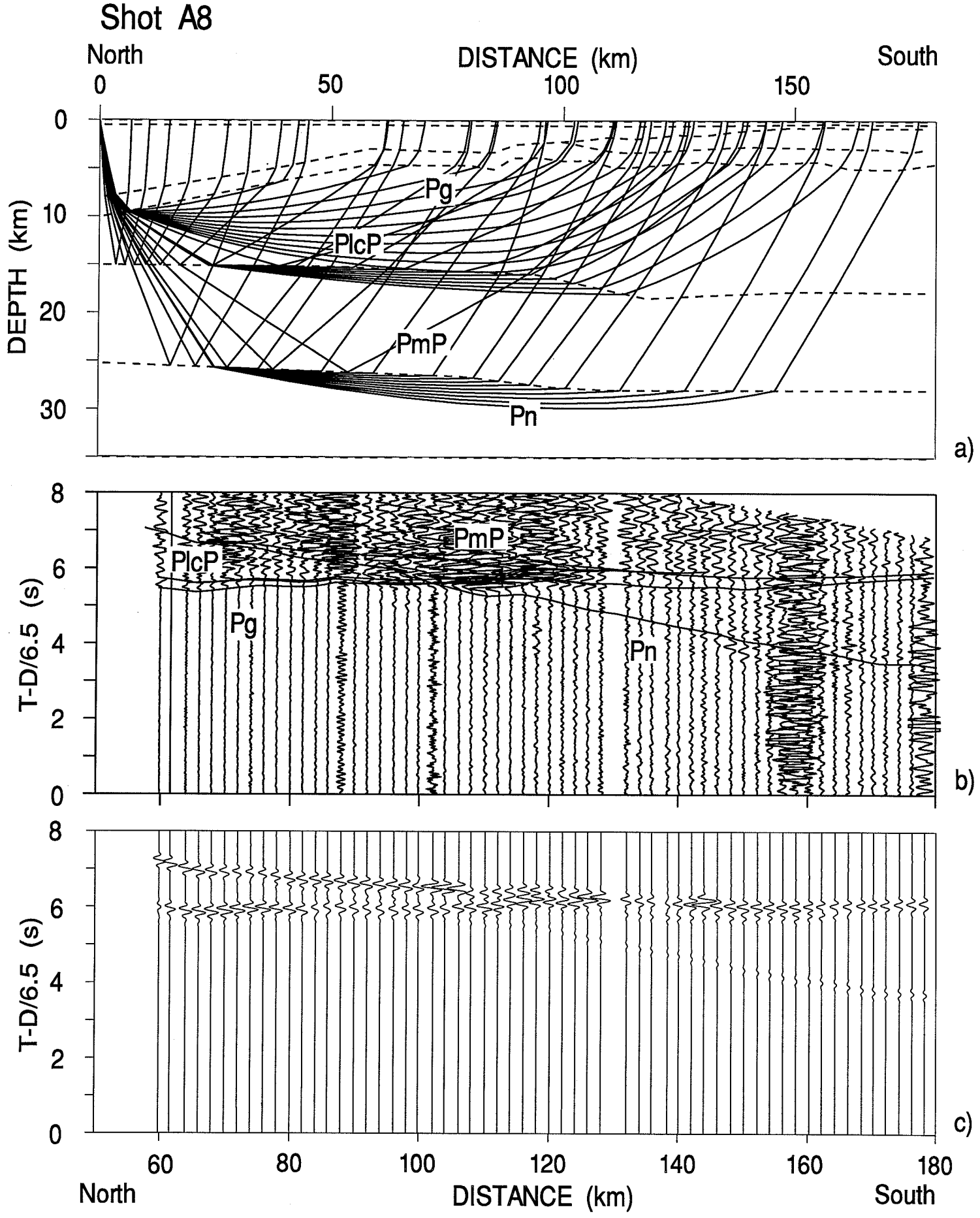
Shot A8
North
DISTANCE (km)
South
0
50
100
150
DEPTH (km)
0
10
20
30
Pg
PlcP
PmP
Pn
a)
T-D/6.5 (s)
8
6
4
2
0
PlcP
PmP
Pg
Pn
b)
T-D/6.5 (s)
8
6
4
2
0
c)
60
80
100
120
140
160
180
North
DISTANCE (km)
South

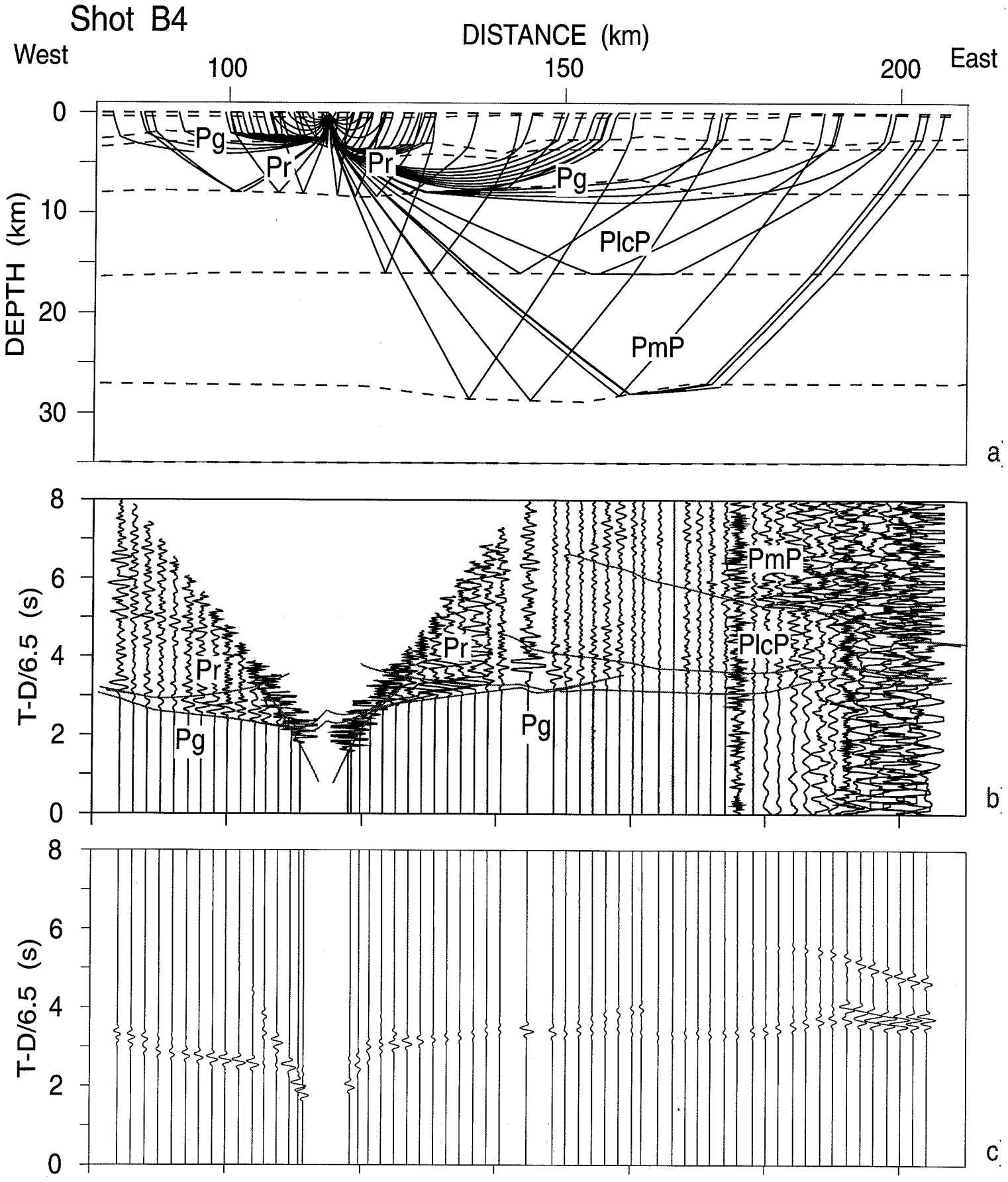
Shot B4
West
DISTANCE (km)
100
150
200
East
DEPTH (km)
0
10
20
30
Pg
Pr
Pr
Pg
PlcP
PmP
a
T-D/6.5 (s)
8
6
4
2
0
Pg
Pr
Pr
Pg
PmP
PlcP
b
T-D/6.5 (s)
8
6
4
2
0
c

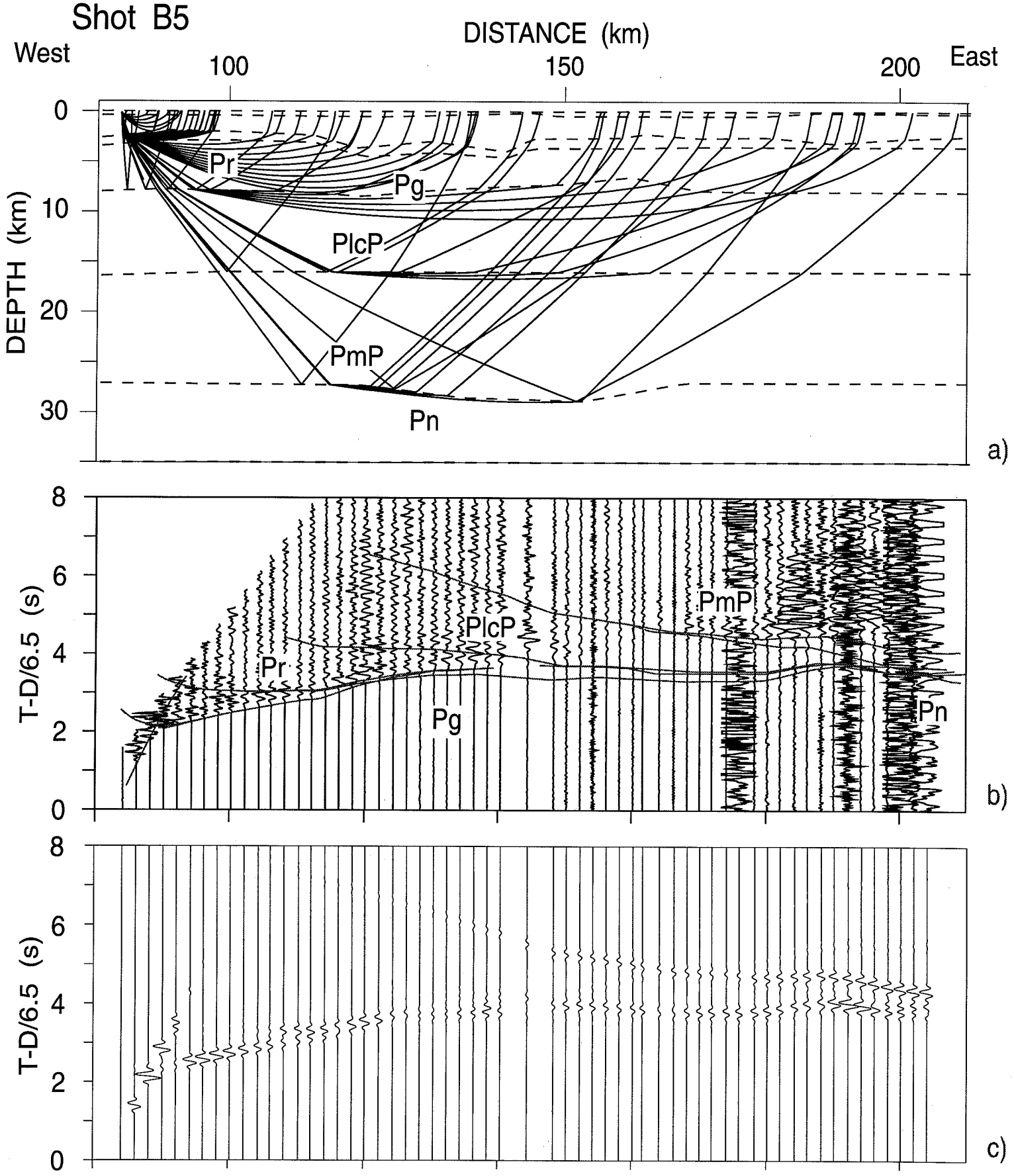
Shot B5
West
DISTANCE (km)
100
150
200
East
0
10
20
30
DEPTH (km)
Pr
Pg
PlcP
PmP
Pn
a)
8
6
4
2
0
T-D/6.5 (s)
Pr
PlcP
PmP
Pg
Pn
b)
8
6
4
2
0
T-D/6.5 (s)
c)

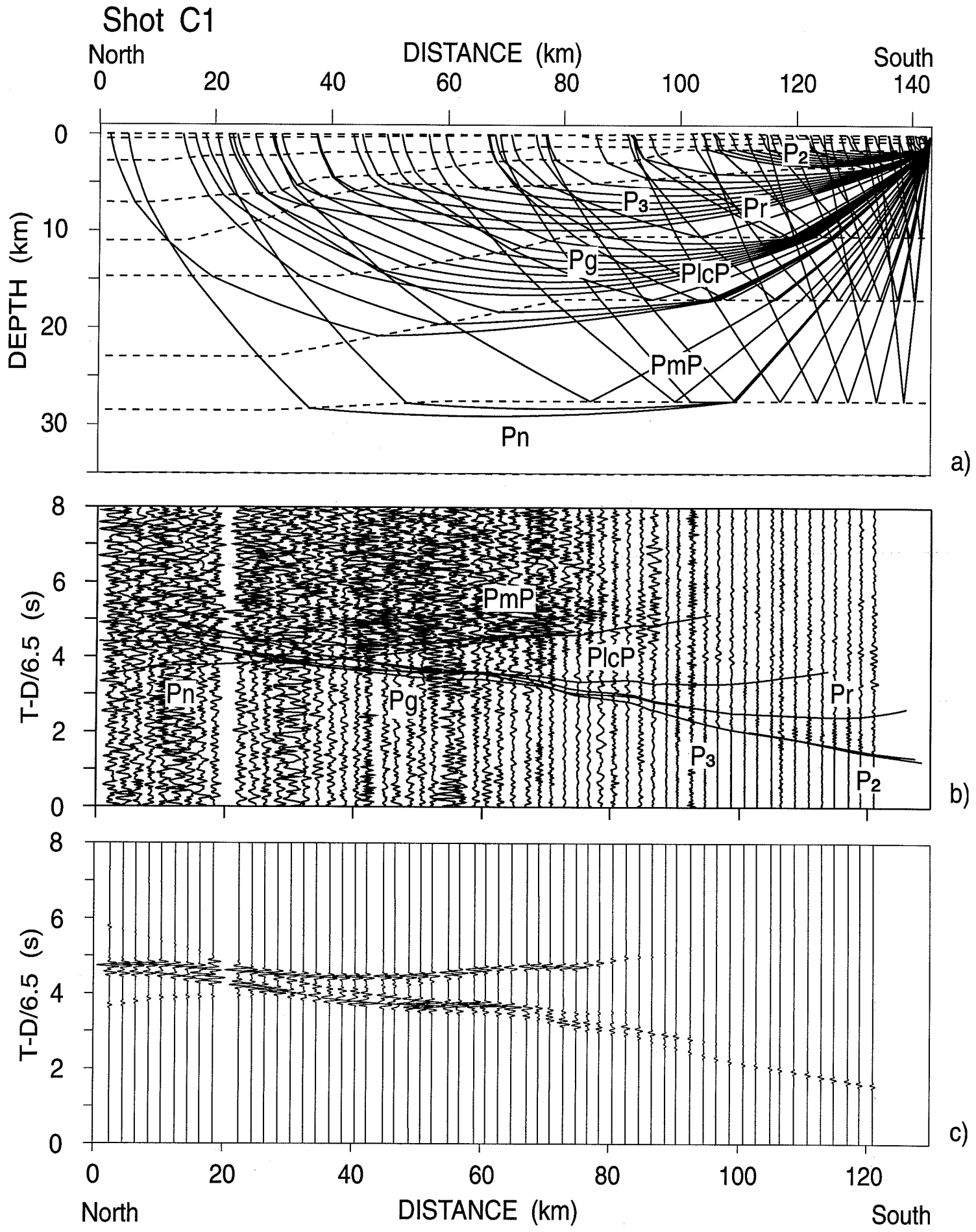
Shot C1
North
DISTANCE (km)
South
0
20
40
60
80
100
120
140
DEPTH (km)
0
10
20
30
P2
P3
Pr
Pg
PlcP
PmP
Pn
a)
T-D/6.5 (s)
8
6
4
2
0
PmP
PlcP
Pn
Pg
Pr
P3
P2
b)
T-D/6.5 (s)
8
6
4
2
0
c)
0
20
40
60
80
100
120
North
DISTANCE (km)
South

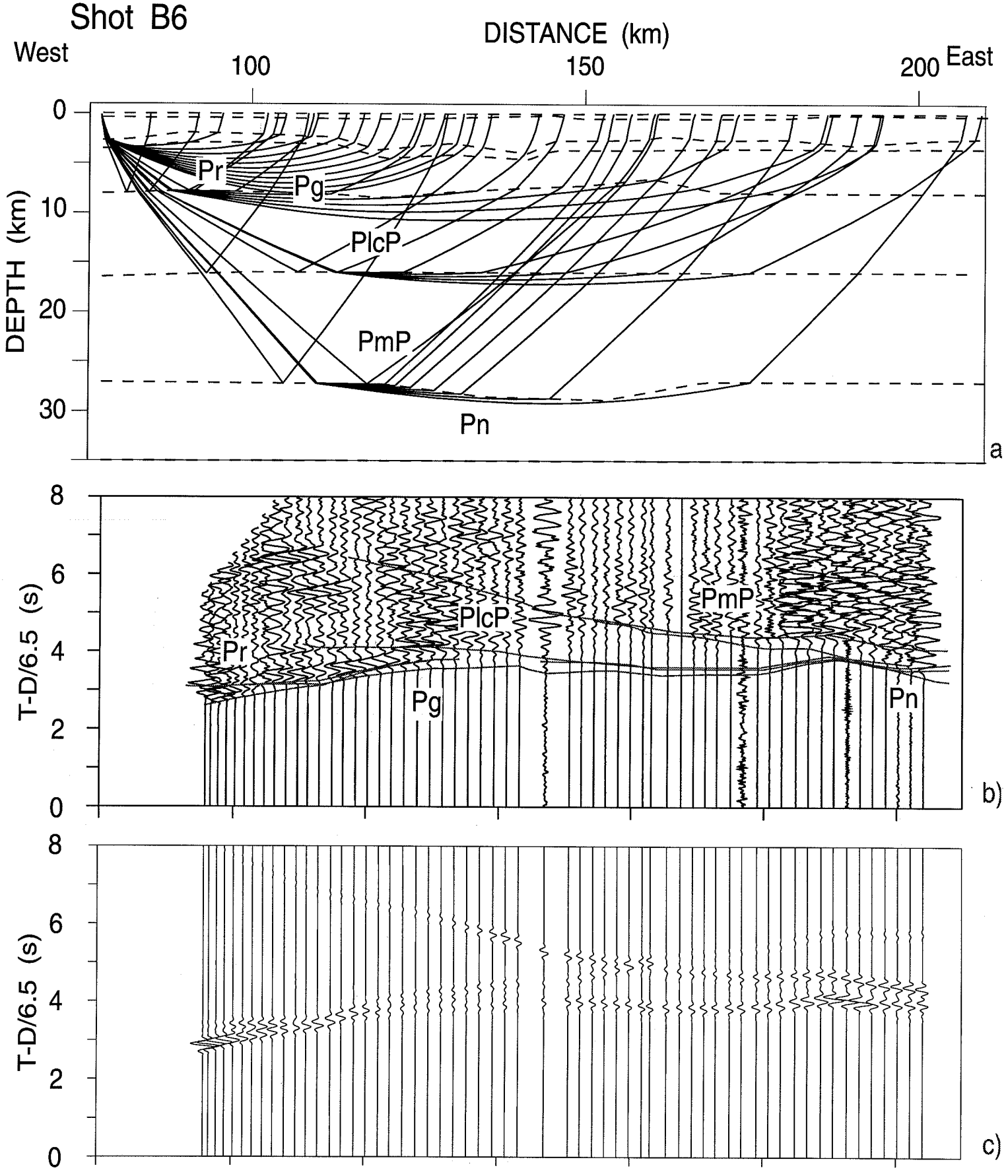
Shot B6
West
DISTANCE (km)
100
150
200
East
0
10
20
30
DEPTH (km)
Pr
Pg
PlcP
PmP
Pn
a
8
6
4
2
0
T-D/6.5 (s)
Pr
PlcP
PmP
Pg
Pn
b)
8
6
4
2
0
T-D/6.5 (s)
c)